



# Late-Stage Fluorination With $^{19}\text{F}$ - and $^{18}\text{F}$ - via Concerted Nucleophilic Aromatic Substitution

## Citation

Neumann, Constanze N. 2016. Late-Stage Fluorination With  $^{19}\text{F}$ - and  $^{18}\text{F}$ - via Concerted Nucleophilic Aromatic Substitution. Doctoral dissertation, Harvard University, Graduate School of Arts & Sciences.

## Permanent link

<http://nrs.harvard.edu/urn-3:HUL.InstRepos:33840664>

## Terms of Use

This article was downloaded from Harvard University's DASH repository, and is made available under the terms and conditions applicable to Other Posted Material, as set forth at <http://nrs.harvard.edu/urn-3:HUL.InstRepos:dash.current.terms-of-use#LAA>

## Share Your Story

The Harvard community has made this article openly available.  
Please share how this access benefits you. [Submit a story](#).

[Accessibility](#)

# Late-stage Fluorination with $^{19}\text{F}^-$ and $^{18}\text{F}^-$ *via* Concerted Nucleophilic Aromatic Substitution

A dissertation presented

by

Constanze Nicole Neumann

to

The Department of Chemistry and Chemical Biology

In partial fulfillment of the requirements

for the degree of

Doctor of Philosophy

in the subject of

Chemistry

Harvard University

Cambridge, Massachusetts

May 2016

© Constanze Nicole Neumann

All Rights Reserved.

Late-stage Fluorination with  $^{19}\text{F}^-$  and  $^{18}\text{F}^-$  *via* Concerted Nucleophilic Aromatic Substitution**Abstract**

The formation of C–F bonds has long been considered a challenging transformation and C–F bonds commonly had to be formed early on in a synthetic sequence towards complex organofluorides. Late-stage fluorination reactions are reactions with a broad substrate scope and extensive functional group tolerance that can be performed on complex molecules. Many classic fluorination reactions fail to qualify as late-stage transformations either due to severe limitations in their substrate scope or because the required reaction conditions are incompatible with many functional groups.

Nucleophilic aromatic substitution ( $\text{S}_{\text{N}}\text{Ar}$ ) is widely used for the aromatic functionalization with  $^{19}\text{F}$  and by far the most common method to introduce  $^{18}\text{F}$  fluoride into aromatic molecules. Classic  $\text{S}_{\text{N}}\text{Ar}$  reactions proceed with the formation of a negatively charged Meisenheimer intermediate upon fluoride attack on the aromatic nucleus. Because only arenes with electron-withdrawing substituents can sufficiently stabilize the Meisenheimer intermediate to allow nucleophilic substitution to proceed efficiently,  $\text{S}_{\text{N}}\text{Ar}$  is restricted to electron-deficient arenes.

In Chapter 1 of this work an unusual concerted mechanism for nucleophilic aromatic substitution with fluoride is presented. Unlike the classic two-step mechanism, the concerted ( $\text{CS}_{\text{N}}\text{Ar}$ ) mechanism does not proceed *via* a Meisenheimer intermediate, and build-up of negative charge on the arene ring is minimized. For the deoxyfluorination reaction with the PhenoFluor reagent a concerted mechanism is favored over a stepwise displacement and the resultant minimization of negative charge build-up over the course of the reaction allows deoxyfluorination to take place on

electron-rich arene substrates. Based on detailed mechanistic studies a functional-group tolerant deoxyfluorination reaction with  $^{18}\text{F}$ -fluoride for the synthesis of high specific activity  $^{18}\text{F}$ -PET probes was developed. Chapter 2 of this work describes attempts to develop novel deoxyfluorination reagents with reduced reaction barriers guided by mechanistic insights into the deoxyfluorination. Computational results indicate that the introduction of substituents that are capable of forming hydrogen bonds to fluoride at specific positions on the reagent can reduce the activation barrier for deoxyfluorination through transition state stabilization.

## TABLE OF CONTENTS

<b>Introduction</b> .....	<b>10</b>
<b>Late-stage Fluorination</b> .....	<b>10</b>
<b>Late-stage fluorination with <sup>18</sup>F</b> .....	<b>19</b>
Nucleophilic late-stage fluorination reactions .....	20
Electrophilic aromatic fluorination reactions.....	24
<b>Late-stage deoxyfluorination</b> .....	<b>29</b>
<b>Chapter 1: Concerted nucleophilic aromatic substitution (C<sub>N</sub>Ar) with <sup>19</sup>F<sup>-</sup> and <sup>18</sup>F<sup>-</sup></b>	<b>35</b>
<b>Mechanism Experiments</b> .....	<b>48</b>
Hammett Plot.....	48
Eyring Plots .....	49
Isokinetic Relationship.....	57
<sup>16</sup> O/ <sup>18</sup> O Kinetic Isotope Effect.....	61
<b>Tetrahedral adduct 6</b> .....	<b>68</b>
<b>Role of added CsF</b> .....	<b>73</b>
Fluoride versus bifluoride pathway.....	73
Entry points to a fluoride pathway.....	81
Introduction of <sup>18</sup> F fluoride .....	85
<b>Boundaries of a concerted mechanism</b> .....	<b>88</b>
Transition state structures .....	88
Internal Reaction Coordinates .....	91
<b>Chapter 2: A computational approach towards an improved deoxyfluorinating reagent</b> .....	<b>95</b>
<b>Computational reaction barriers for modified PhenoFluor scaffolds</b> .....	<b>95</b>
Controlling the equilibrium between tetrahedral adduct and uronium bifluoride .....	96
Controlling the energy difference between the tetrahedral adduct and the transition state....	102
Controlling the equilibrium between the tetrahedral adduct and the cyclized product .....	111
<b>Chapter 3: Experimental methods</b> .....	<b>122</b>
<b>General methods</b> .....	<b>122</b>
Preparation of labeling precursors .....	123
Labeling precursors bearing additional hydroxyl groups .....	123

<sup>18</sup> F-Fluorination of the labeling precursor .....	125
Specific Activity .....	126
<b>References .....</b>	<b>129</b>

## List of Abbreviations:

DFT ..... Density functional theory

Dipp.....diisopropylphenyl

F-TEDA.....1-Chloromethyl-4-fluoro-1,4-diazoniabicyclo[2.2.2]octane bis(tetrafluoroborate)

KIE .....Kinetic isotope effect

RCC.....Radiochemical conversion

RCY.....Radiochemical yield

TOI.....Time of injection



## Publications:

Portions of the introduction have been reproduced, with permission, from the following publication:

**C. N. Neumann**, D. S. Edwards, T. Ritter "Late-Stage Fluorination Advances PET Tracer Development." *MI Gateway* **2013**, 7, 1.

**C. N. Neumann**, T. Ritter "Late-Stage Fluorination: Fancy Novelty or Useful Tool?" *Angew. Chem. Int. Ed.* **2015**, 54, 3216. Copyright © 2015, Angewandte Chemie International Wiley, Wiley-VCH.

The work in chapter 1 and 3 has been reproduced, with permission, from the following publication:

**C. N. Neumann**, J. M. Hooker, T. Ritter "Concerted Nucleophilic Aromatic Substitution ( $CS_NAr$ ) with  $^{19}F^-$  and  $^{18}F^-$ ." *Nature* **2016**, 534, 369.

In addition to the work presented in this thesis, additional investigations conducted during my Ph.D. studies have been published as contributions to the following publications:

E. Lee, A. S. Kamlet, D. C. Powers, **C. N. Neumann**, G. B. Boursalian, T. Furuya, D. C. Choi, J. M. Hooker, T. Ritter "A Fluoride-Derived Electrophilic Late-Stage Fluorination Reagent for PET Imaging." *Science* **2011**, 334, 639.

A. S. Kamlet, **C. Neumann**, E. Lee, S. Carlin, C. Moseley, N. Stephenson, J. Hooker, T. Ritter "Application of Palladium-Mediated  $^{18}F$ -Fluorination to PET Radiotracer Development: Overcoming Hurdles to Translation" *PLOS one* **2013**, 8, e59187.

T. Liang, **C. Neumann**, T. Ritter "Introduction of Fluorine and Fluorine-Containing Functional Groups" *Angew. Chem. Int. Ed.* **2013**, 52, 8214-8264.

X. Shen, **C. N. Neumann**, C. Kleinlein, N. W. Goldberg, T. Ritter "Alkyl Aryl Ether Bond Formation with PhenoFluor" *Angew. Chem. Int. Ed.* **2015**, 54, 5662.

E. M. D'Amato, **C. N. Neumann**, T. Ritter "Selective Aromatic C–H Hydroxylation Enabled by  $\eta^6$ -Coordination to Iridium(III)" *Organometallics* **2015**, 34, 4626.

**C. N. Neumann**, T. Ritter "Deoxyfluorination of Electron-poor Phenols with  $^{18}\text{F}$ -Fluoride."  
Submitted.

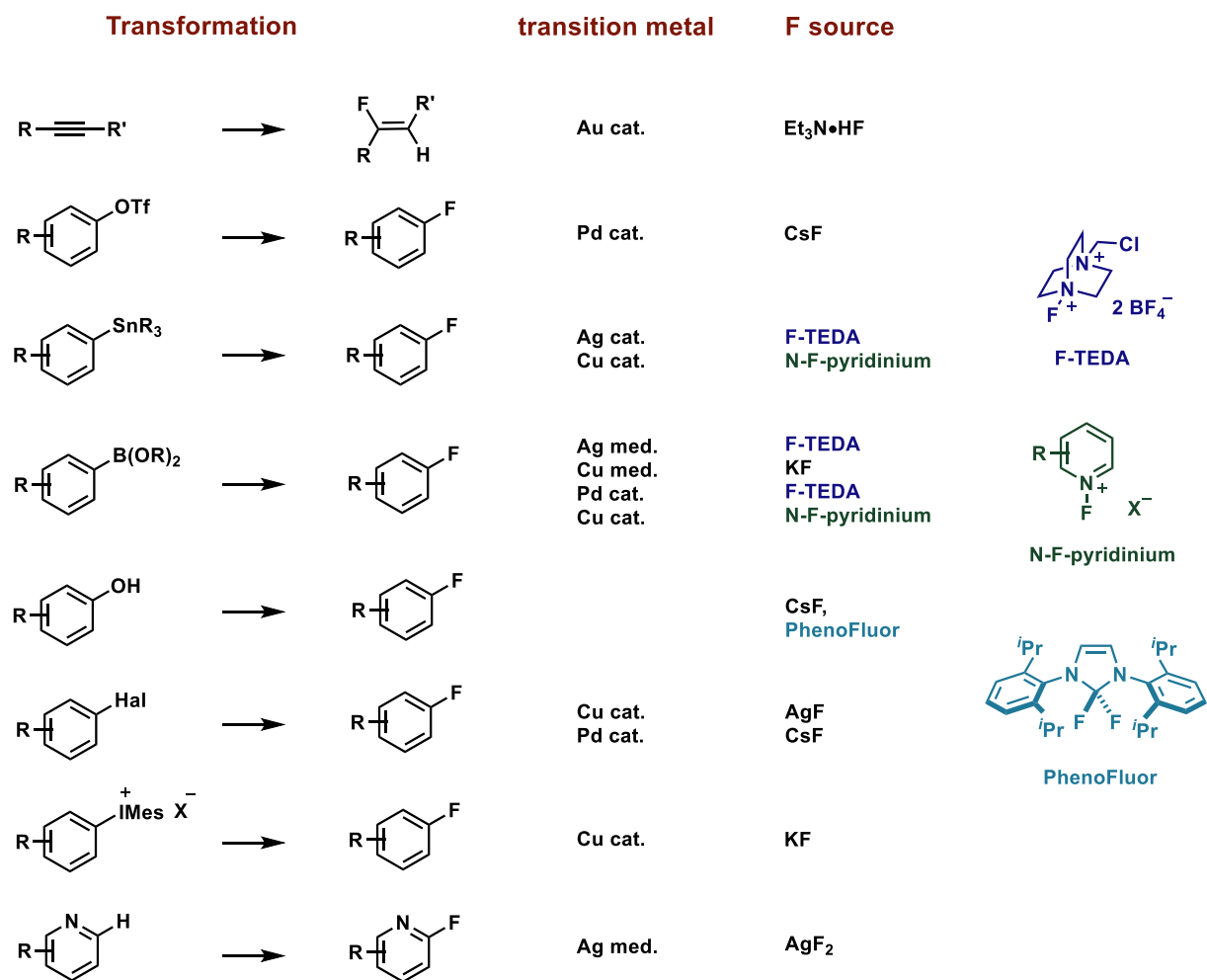
## INTRODUCTION

### Late-stage Fluorination

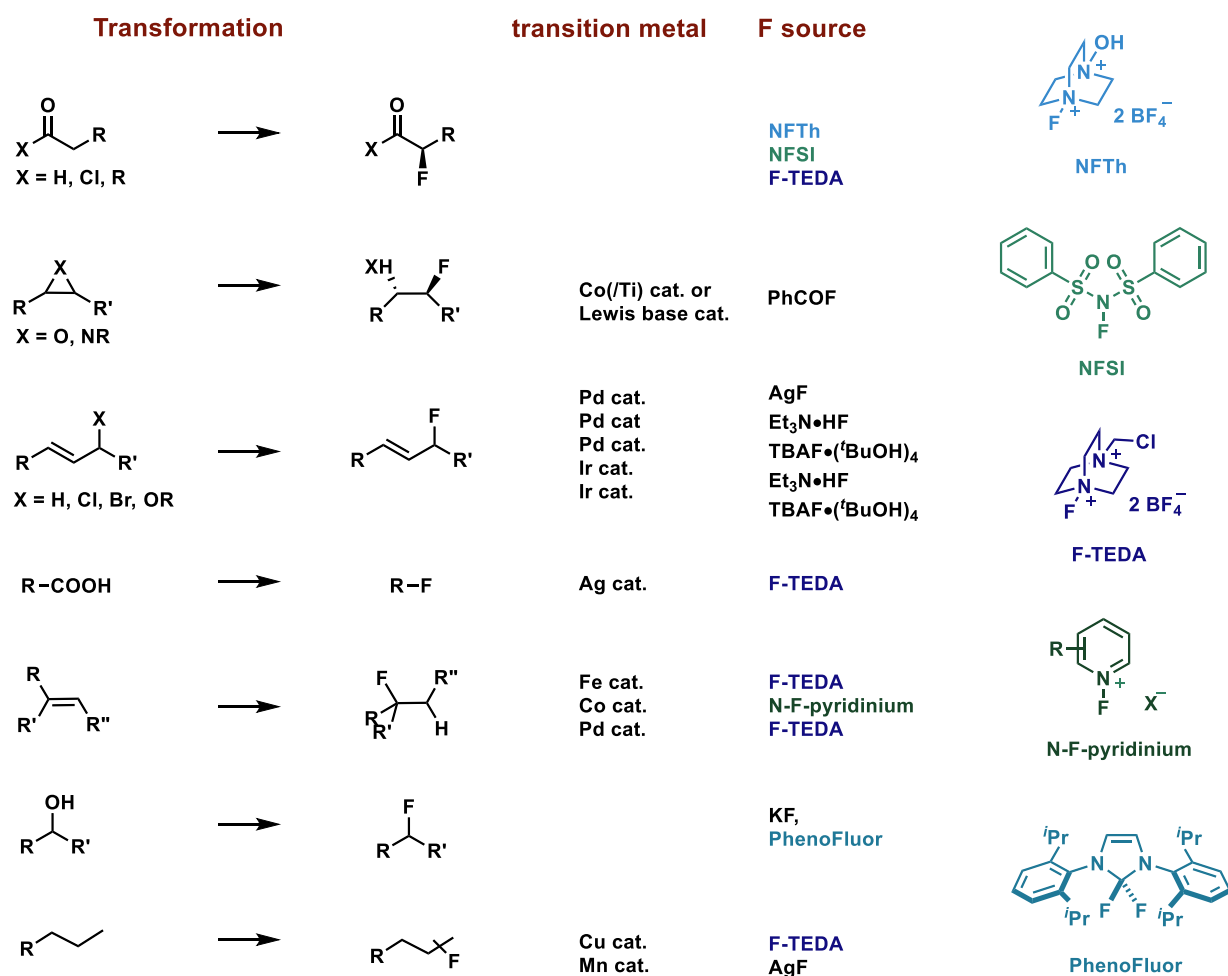
For over a century fluorine chemistry was dominated by the use of fluorine gas, HF, and alkali metal halides, and reaction conditions were typically harsh. Fluorine seemed to be forever either too reactive ( $F_2$ ) or too unreactive (KF) to be used in selective, functional-group-tolerant transformations of even moderately complex small molecules. A number of key fundamental discoveries pertaining largely to fluorination reagents and transition metal catalysis have allowed the field to break with a tradition of harsh reaction conditions. A few decades ago, the development of a small range of reagents such as Select-Fluor, N-Fluoropyridinium salts and  $Et_3N \cdot HF$  have enabled more selective fluorination chemistry.<sup>1-31</sup> Over the past decade, another wave of fluorination chemistry has mainly focused on the development of suitable methods for late-stage fluorination, that is, the chemo- and stereoselective fluorination of molecules with higher structural and functional complexity, which could not be achieved with conventional fluorination methods. To date, the relatively recent advances in late-stage fluorination have not yet had a substantial impact on the synthesis of bulk chemicals,  $^{18}F$  positron emission tomography (PET) tracers, or materials. Their synthesis procedures are still dominated by classical fluorination methods.

Several fundamental discoveries in the field that provide a better fundamental understanding were made within the last few years.<sup>32-42</sup> For example, the first well-defined reductive elimination reaction to form C–F bonds was reported only in 2008.<sup>43,44</sup> A substantial part of the recent developments is based on transition-metal chemistry, which may explain why fluorination chemistry is experiencing a rapid development right now: Making C–F bonds with metals often proceeds by reductive elimination reactions, which typically have high free enthalpies of activation. In our opinion, three independent developments substantially

contributed to the advent of late-stage fluorination: 1) the progress in effecting challenging reductive elimination reactions from mid-valent transition-metal complexes as pioneered, for example, by the Buchwald group, 2) the exploration of the more facile reductive elimination processes from high-valent transition-metal complexes as pioneered by the Sanford group, for example, and 3) the availability of new fluorination reagents, both nucleophilic and electrophilic, which enabled the development of practical, functional-group-tolerant reactions.<sup>45-50</sup> Contributions from several research groups have advanced the field of fluorination chemistry substantially over the recent past; we have chosen to summarize some of them in Figure 1 and Figure 2 rather than mentioning them separately as has already been done in recent reviews.<sup>32,42,51-67</sup>



**Figure 1:** Selected modern fluorination methods at  $sp^2$  hybridized carbon centers arranged by functional group interconversion in order of publication date.<sup>45-49,66,68-78</sup> (IMes=1,3-dimesitylimidazol-2-ylidene)



**Figure 2:** Selected modern aliphatic fluorination methods arranged by functional group interconversion in order of publication date.<sup>79-98</sup>

Fluorinated products find uses in many different areas of modern society as is highlighted at the beginning of most publications in the field. It is too early to tell which, if any, of the modern late-stage fluorination methods will have a substantial and measurable impact beyond the creation of new fundamental knowledge. It seems prudent, however, to evaluate whether the current shortcomings in the field with respect to their real-life applications are temporary or conceptual. Even thoughtful analyses as to why C–F bond formation is challenging rarely go beyond electronegativity arguments, rendering it likely that a lot of fundamental knowledge is still lacking. Carbon–fluorine reductive elimination is more challenging than any other reductive elimination between carbon and the other first-row elements with a partially filled p shell.<sup>32,34,38,43,55,99,100</sup> The high electronegativity of fluorine

results in strong metal–fluorine bonds owing to a strong polar contribution to the bond, and the associated s-bond orbital is highly contracted and largely localized on the fluorine atom.<sup>101,102</sup>

The transition state for reductive elimination requires electron reorganization, with electron density shifting away from the fluorine atom towards the forming C–F bond, which results in a high kinetic barrier even in systems where reductive elimination is thermodynamically highly favorable. The development of ligands tailored to facilitate the C–F bond-formation step as well as an improved understanding of how to access high-valent transition-metal intermediates has enabled a substantial reduction of the activation energy for C–F reductive elimination. Nonetheless, reductive elimination is still generally the rate-limiting step in metal-mediated C–F bond formation and thus dictates the selection of metals and ligands for a particular transformation. New insights into how the kinetic barrier could be further reduced, possibly through a better understanding of the bonding interactions as a function of the transition metal, its oxidation state, and the nature of the ancillary ligands, would enable to shift the focus of research towards the identification of appropriate starting materials and inexpensive reagents.

The selection of the ideal starting materials for a C–F bond-forming reaction defies a simple answer. Currently, functional-group-tolerant transformations frequently rely on starting materials disproportionately complex for the introduction of a simple monoatomic substituent: Starting from aryl metal species, such as those of tin or boron, leads to a transformation that displaces a heavy fragment, such as  $\text{SnBu}_3$  or  $\text{B(OR)}_2$ , which is commonly accessed from the corresponding halide, by a single atom. The direct fluorination of carbon–halide bonds can suffer from a complicated purification of the final fluorinated compound if the reaction does not proceed to completion, unless purification by distillation is possible. Alcohols, phenols, and carboxylic acids are convenient starting materials in many

respects, but suffer from a lack of general reactions to access them directly from C–H bonds. The direct fluorination of C–H bonds appears to be the obvious solution and would clearly be desirable for the synthesis of a number of fluorinated materials with various applications. However, compared to other C–H functionalization reactions, such as oxygenation reactions, fluorination poses a set of special challenges: The fluorinated reaction products often exhibit a similar reactivity to the starting materials, which can hamper selective monofunctionalization. Aryl fluorides, for example, are only marginally less electron-rich than the corresponding arenes, and a fluorine substituent provides almost no steric deactivation. If selective reactions can be achieved, the separation of the fluorinated products from the starting materials is often complicated by their similar physical properties. Therefore, C–H fluorination reactions that require excess starting material or do not proceed to complete conversion may not be as practical as they seem. Exceptions exist, however, such as the  $\text{AgF}_2$  mediated fluorination of pyridines, in which the physical properties of the fluorinated product differ sufficiently from those of the starting material to permit facile isolation.<sup>78,103</sup> A good indication that a reaction meets certain criteria for practicality are yields that correspond to the purified, isolated material rather than yields determined by  $^{19}\text{F}$  NMR spectroscopy. Given the current challenges for enabling direct transformations of C–H into C–F bonds, it may also be advisable to invest in research directed towards the better purification of fluorinated molecules and towards developing slightly more circuitous pathways for C–H to C–F transformations, for example, the formation of C–OH moieties (or another polar functional group) from a C–H bond, coupled with a deoxyfluorination reaction, which might yield more practical routes to pure fluorinated products.

With some of the challenges in current late-stage fluorination chemistry identified, we are curious which future directions would significantly advance the field. Beyond the fairly obvious requirements, such as high functional-group tolerance and operational simplicity, we believe that an improved fundamental understanding of the bonding interactions of fluorine,



including ionic and hydrogen bonding and covalent bonding with transition metals, may teach us how to better tackle the problem of improving its reaction chemistry. It has long been understood that fluoride forms exceptionally strong hydrogen bonds to protic solvents, particularly water, which typically reduces the nucleophilicity of the fluoride ion.<sup>104,105</sup> On the other hand, the high lattice energy of fluoride salts renders them virtually insoluble in all but the most polar solvents.<sup>106,107</sup> Both facts leave nucleophilic fluoride chemistry with the dilemma of either unfavorable desolvation or a high kinetic barrier owing to low solubility. Given its high electronegativity, fluoride is a hard nucleophile, generally preferring charge-controlled interactions over the desired orbital control leading to C–F bond formation. Rather than exacerbating fluoride's inherent tendency towards charge-controlled interactions through desolvation, new reagents with fluoride biased towards forming bonds to carbon by orbital control could prove advantageous.<sup>99,108</sup> The use of TBAF·<sup>t</sup>BuOH and of bifluoride in S<sup>VI</sup> fluoride exchange as well as the use of ionic liquids and alcohol co-solvents in <sup>18</sup>F radiolabeling are notable examples for the enhancement of the effective fluoride nucleophilicity through media that can provide hydrogen bond stabilization.<sup>109-114</sup> “Soft” fluoride nucleophiles that are suitable for C–F bond formation can also be obtained by binding to transition metals as demonstrated by the synthesis of allylic fluorides by attack of a palladium-bound fluoride on a palladium allyl complex.<sup>88</sup> Attempts to achieve attack on palladium allyl complexes by extraneous fluoride ions, on the other hand, led to elimination products rather than fluoride incorporation.<sup>115</sup> A fundamental understanding of the nature of transition-metal fluorides the ability to predict their reactivity are still lacking: For example, fluoride ligands bound to sulfonamide-supported Pd<sup>II</sup> or Pd<sup>IV</sup> complexes persist in wet organic solvents, whereas the fluoride ligand on Pd<sup>II</sup> BrettPhos complexes shows pronounced basic properties, with likely hydrolysis of the metal–fluorine bond.<sup>43-50,116,117</sup> Given our poor fundamental understanding of the properties of metal fluorides, tailoring the properties of the metal fluoride to the desired transformation is hardly possible, and further research is warranted to gain insight into the promising area of metal-bound fluoride

chemistry. Given the dramatic reactivity differences of different fluoride species, it seems advisable to suggest the development of more appropriate reagents. Conventional reagents frequently limit the achievable substrate scope: For example, nucleophilic fluorination reactions are often sensitive to moisture, and the basic nature of dry fluoride can lead to elimination reactions and is commonly incompatible with protic functional groups. The successful use of the TBAF·<sup>t</sup>BuOH reagent teaches us that nucleophilic fluorination does not categorically need to be free of a hydrogen bond donor.<sup>111</sup> Electrophilic fluorination reactions are largely executed with only three reagents, namely Selectfluor (F-TEDA), NFSI, and N-fluoropyridinium salts. These reagents are comparatively expensive and can lead to side reactions with basic heteroatoms. Generally, electrophilic and nucleophilic fluorinating reagents are largely complimentary in the restrictions that they place on the substrate scope.

The field of fluorination is unusual in that late-stage modification processes are more developed in the laboratory than in nature; only a single enzyme that introduces fluorine into organic molecules has been identified. The highly oxidizing conditions required for the formation of an electrophilic fluorination reagent combined with the limited nucleophilicity of the fluoride ion in water are likely causes for the dearth of fluorinated natural products.

Despite nature's limited reliance on organofluorine compounds, the synthesis of fluorinated derivatives of salinosporamide A, an anticancer drug candidate, has been achieved through the introduction of the fluorinase gene from *S. cattleya* into a heterologous host.<sup>118,119</sup>

Enzymatic radiolabeling procedures based on the fluorinase enzyme have also been developed; S-adenosylmethionine (SAM) was radiolabeled and subsequently subjected to oxidation to yield <sup>18</sup>F-fluoroacetate with a radiochemical conversion of 36% in two hours.<sup>120</sup>

Another avenue for the rapid construction of complex fluorinated molecules involves a biochemical pathway that consists of two polyketide synthase systems engineered to accept fluoroacetate as a substrate.<sup>121</sup> The combination of synthetic biology approaches with

fluorinated building blocks appears to be an attractive and promising strategy to quickly access complex fluorinated molecules that currently cannot be accessed by other means.

The lack of chiral-pool organofluorine compounds makes the development of asymmetric fluorination methods particularly crucial.<sup>122-124</sup> Halogen functionalization is often accomplished through alkene halogenation, but whereas chlorine, bromine, and iodine readily react with non-activated alkenes via cyclic halonium ions, the corresponding fluoronium ion is not formed.<sup>125-127</sup> Given the relatively low reactivity of unactivated alkenes towards electrophilic fluorinating reagents, a lot of work has focused on activated alkene derivatives, such as enols, enamines, and allyl silanes.<sup>128,129</sup> Several methods have been developed that allow highly enantioselective fluorination at the  $\alpha$ -position of carbonyl groups.<sup>80-83,130,131</sup> Aside from the strategies that build on chiral amine catalysis, anion exchange processes of F-TEDA, which is virtually insoluble in many organic solvents, with chiral anions that increase the solubility of the fluorinating agent have proven very fruitful in the development of synthetic routes towards enantioenriched chiral organofluorine compounds.<sup>132-137</sup> The fact that fluoride readily engages in hydrogen bonding and dipolar interactions seems to render it uniquely suitable for reactions catalyzed by chiral organocatalysts. Whereas its potential for strong interactions with a catalyst appears promising for achieving substantial levels of catalyst control, the often reduced nucleophilicity of fluoride ions involved in polar interactions limits the potential for bond formation with fluoride. Nevertheless, the use of hydrogen-bonded fluoride reagents is promising owing to the functional-group tolerance of such fluoride sources.

The fluorine substituent has a privileged nature in a diverse range of fields, and synthetic methods for fluorine introduction into complex structures are highly sought after. Modern fluorination methods cannot yet compete with the Halox process and fluorination with  $F_2$  for the synthesis of bulk chemicals owing to the expensive nature of the majority of the

reagents, starting materials, and catalysts used. For applications where the scale permits the use of reagents such as Selectfluor or AgF, however, late-stage fluorination has opened new avenues in terms of functional-group tolerance and substrate scope. In order to advance the field further, fundamental insights into the interplay between nucleophilicity, basicity, hydrogen bonding, and electrostatic interactions of fluoride species may be beneficial. A range of low-cost fluorination reagents with controlled reactivity that are capable of reacting in largely orbital-controlled carbon–fluorine bond-forming transformation while possible side reactions are prevented are needed to create a toolbox of mild and general late-stage fluorination reactions. Direct C–H fluorination reactions have to be held to particularly high standards to achieve general utility owing to potentially challenging purifications.

### **Late-stage fluorination with $^{18}\text{F}$**

In the last decade significant developments were made in the field of fluorination chemistry, mainly enabled by the application of transition-metal- and organo-catalysis to a field that used to be dominated by stoichiometric transformations. Potential application of modern late-stage fluorination to the synthesis of  $^{18}\text{F}$  PET tracers is often listed as a motivation for the development of novel fluorination reactions. Tracer development is still impeded by challenges in chemistry and the difficulties of translating  $^{19}\text{F}$  chemistry to  $^{18}\text{F}$  chemistry and the broadening of radiolabeling strategies is crucial to the development of PET imaging. Traditional labeling reactions tend to be operationally simple, but suffer from low functional group tolerance and large restrictions on the scaffolds susceptible to labeling reactions.

In addition to the commonly appreciated need for fast reaction time, late-stage  $^{18}\text{F}$  incorporation and the use of reagents derived from fluoride, potential radiolabeling reactions need to fulfill additional criteria.<sup>138,139</sup>  $^{18}\text{F}$ -Fluoride is created by proton bombardment of  $^{18}\text{O}$ - $\text{H}_2\text{O}$  and, while the bulk of water can be removed, the large hydration energy of fluoride

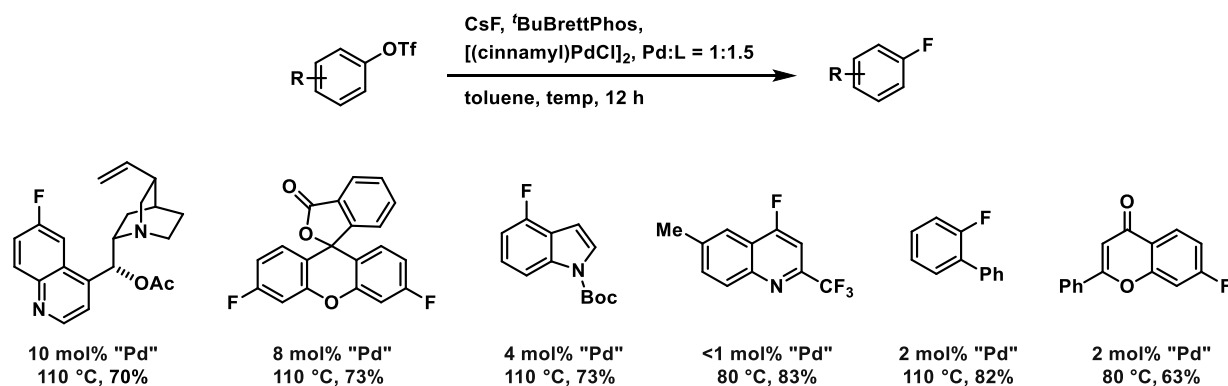
renders complete drying of the radioisotope impractical on the timescale of PET synthesis.<sup>104,140,141</sup> Therefore, reactions suitable for PET need to be able to tolerate at least trace amounts of water even when conducted in dry organic solvents. Given the very low concentration of  $^{18}\text{F}$  in solution, two or three orders of magnitude excess precursor is typically used in radiofluorinations to increase the rate of the transformation. Thus, if a significant decrease in the yield, rate or selectivity occurs when translating a fluorination method from the macroscopic (stoichiometric) to the tracer level, the fluorination method is likely not suitable for PET applications. The separation of the labeled molecules from the excess precursor needs to be rapid and complete; by-products formed from side reactions or decomposition of the precursor may also be in large excess of the desired tracer resulting in long purification times and large losses in yield if the impurities are difficult to separate.

While both  $^{18}\text{F}$ -fluoride and  $^{18}\text{F}\text{-F}_2$  can be generated, radiofluorination with electrophilic  $^{18}\text{F}$  is challenging because the reagent most often used,  $^{18}\text{F}\text{-F}_2$ , is difficult to work with, requires specialized equipment, and is made in low specific activity.<sup>138,142</sup> Gouverneur et al. developed a synthesis of  $^{18}\text{F}\text{-F-TEDA}$  starting from  $^{18}\text{F}\text{-F}_2$ , which addresses the low functional group tolerance of fluorine gas, but necessitates a two-step radiolabeling procedure and handling of  $^{18}\text{F}\text{-F}_2$ .<sup>143</sup>

### **Nucleophilic late-stage fluorination reactions**

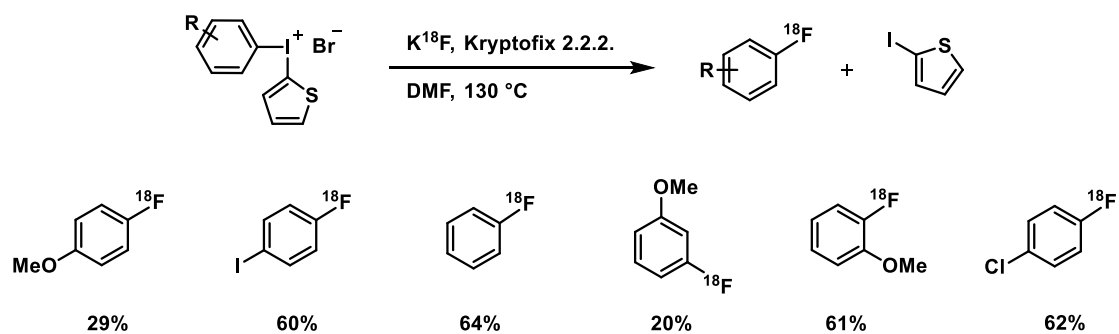
Nucleophilic  $^{18}\text{F}$ -fluoride is a more practical source of  $^{18}\text{F}$ , but it is generated in aqueous solution and the presence of water, which diminishes fluoride's nucleophilicity renders the transition from  $^{19}\text{F}$  to  $^{18}\text{F}$  chemistry challenging. Furthermore, many substrates are biased towards reactions with electrophiles and thus exclusive reliance on nucleophilic radiolabeling strategies poses severe limitations on the substrate scope of labeling methodologies.<sup>55</sup> The Buchwald group has developed a palladium-catalyzed fluorination of aryl triflates with cesium

fluoride or spray-dried potassium fluoride, which allows the synthesis of electron-neutral and electron-deficient aryl fluorides (Figure 3). While electron-rich aromatics also give rise to the desired product, formation of a constitutional isomeric side product can occur, which is hard to separate from the desired aryl fluoride<sup>46,49,116</sup>. The development of novel ligands such as ALPhos successfully curbed the formation of the undesired regioisomer for a large number of substrates as well as enabling the use of aryl bromide starting materials for the fluorination reaction<sup>117,144</sup>. A challenge in adapting Buchwald's nucleophilic fluorination of aryl triflates to radiochemistry is the reaction's sensitivity to moisture – it is typically set up in a dry box using spray-dried KF, conditions which cannot be mimicked using <sup>18</sup>F. Nonetheless, initial breakthroughs towards the application of this reaction to radiochemistry have been made through the addition of <sup>19</sup>F-KF.<sup>145</sup>



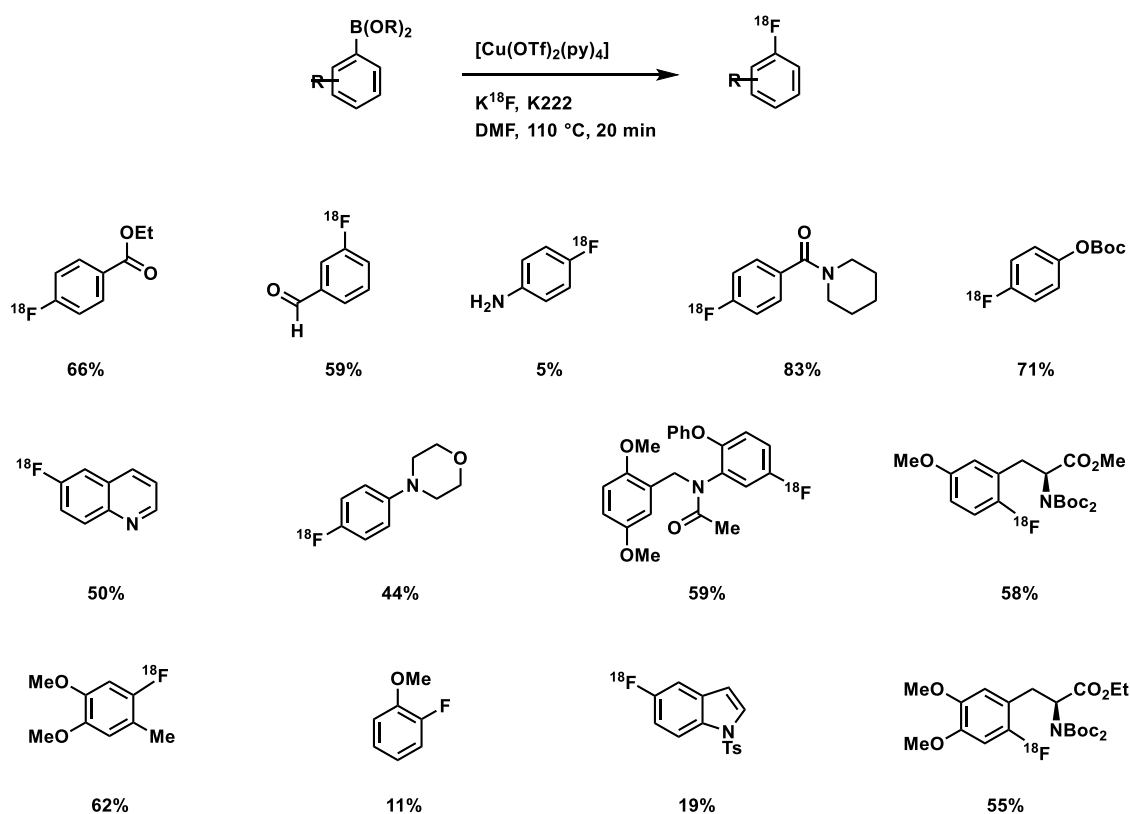
**Figure 3:** Palladium-catalyzed nucleophilic fluorination of aryl triflates.

In addition to late-stage fluorinations, which are being adapted from <sup>19</sup>F to <sup>18</sup>F chemistry, a number of new transformations have been developed especially for PET chemistry. Pike *et al.* used diaryliodonium salts for aromatic radiofluorination reactions, where the selectivity for fluorination between the two arenes attached to iodine is based on the electronic structure of the arenes (the more electron-poor arene is fluorinated) and the steric bulk near iodine (*ortho*-substituted arenes are more susceptible to fluorination due to the *ortho*-effect) (Figure 4).<sup>146,147</sup> The availability of more straightforward syntheses of complex diaryliodonium salts would increase the utility of the method and its use for PET tracer synthesis.



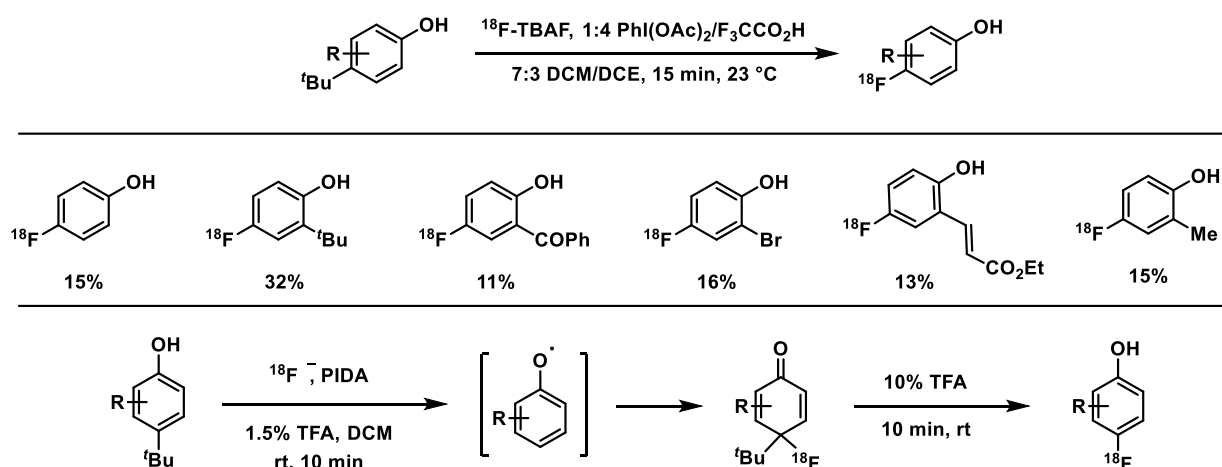
**Figure 4:** Radiofluorination of diaryliodonium salts using 2-thiophenyl as a dummy ligand to direct fluorination to the desired arene.

A radiofluorination reaction with a wide substrate scope that utilizes readily available boronic esters as labeling precursors was developed by the Gouverneur group (Figure 5).<sup>148</sup> The presence of air during the reaction was crucial; the radiochemical yield was increased and the formation of troublesome deborylated side product was minimized when the reaction vial was purged with air after drying of  $^{18}F$ -fluoride. Numerous functional groups are tolerated in the radiofluorination, but the presence of unprotected alcohol or amine functionalities led to competitive C–O or C–N bond formations.



**Figure 5:** Copper-mediated  $^{18}\text{F}$ -fluorination of boronic esters.

The Gouverneur group also developed a nucleophilic labeling strategy for phenol derivatives with a *tert*-butyl group serving as a non-traditional leaving group (Figure 6).<sup>149</sup> This reaction relies on the Umpolung of the phenol substrate through oxidation followed by nucleophilic attack of  $^{18}\text{F}$ -fluoride on the arene ring.

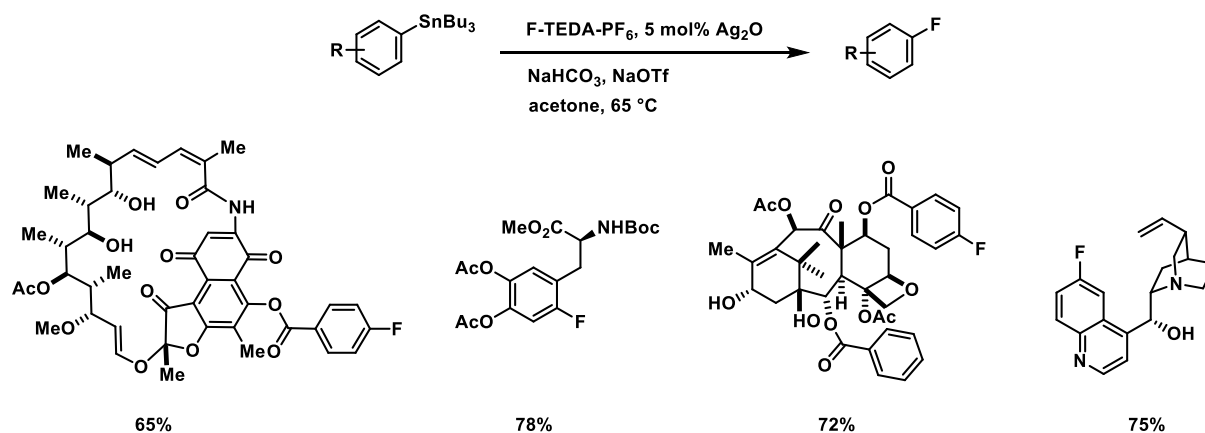


**Figure 6:** Umpolung allows radiolabeling of phenol derivatives using  $^{18}\text{F}$ -fluoride.



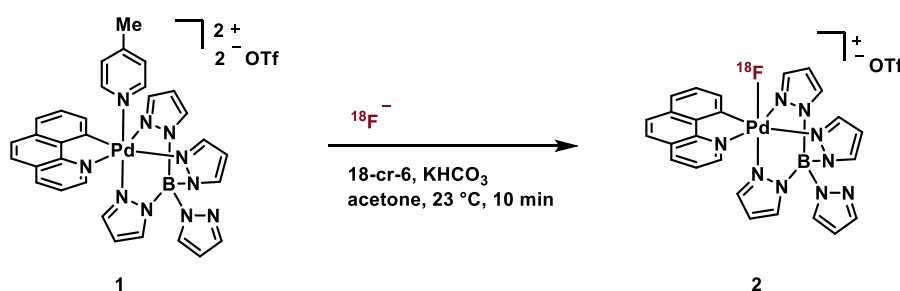
## Electrophilic aromatic fluorination reactions

The silver-catalyzed fluorination developed by the Ritter lab has arguably the largest substrate scope of any currently known aromatic fluorination reaction but necessitates the use of stoichiometric amounts of tin (Figure 7).<sup>66</sup> The reaction has been translated to <sup>18</sup>F chemistry by the Gouverneur group, however <sup>18</sup>F-F-TEDA needs to be prepared from <sup>18</sup>F-F<sub>2</sub>.<sup>143</sup>



**Figure 7:** Silver catalyzed late-stage fluorination of aryl stannanes.

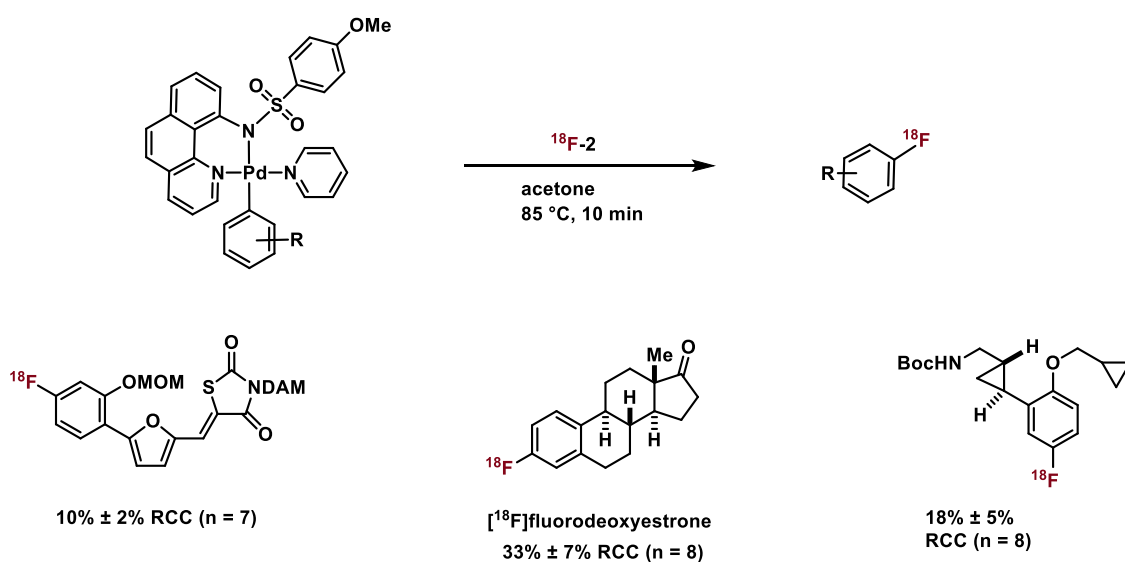
To expand the options for using electrophilic late-stage fluorination, our group has developed an electrophilic fluorinating reagent that can be prepared from <sup>18</sup>F-fluoride.<sup>150</sup> Complex **1** is capable of capturing fluoride (Figure 8) to form Pd<sup>IV</sup>-<sup>18</sup>F complex **2** that is a suitable reagent to afford aryl fluorides through our previously developed fluorination of aryl palladium complexes.<sup>151</sup>



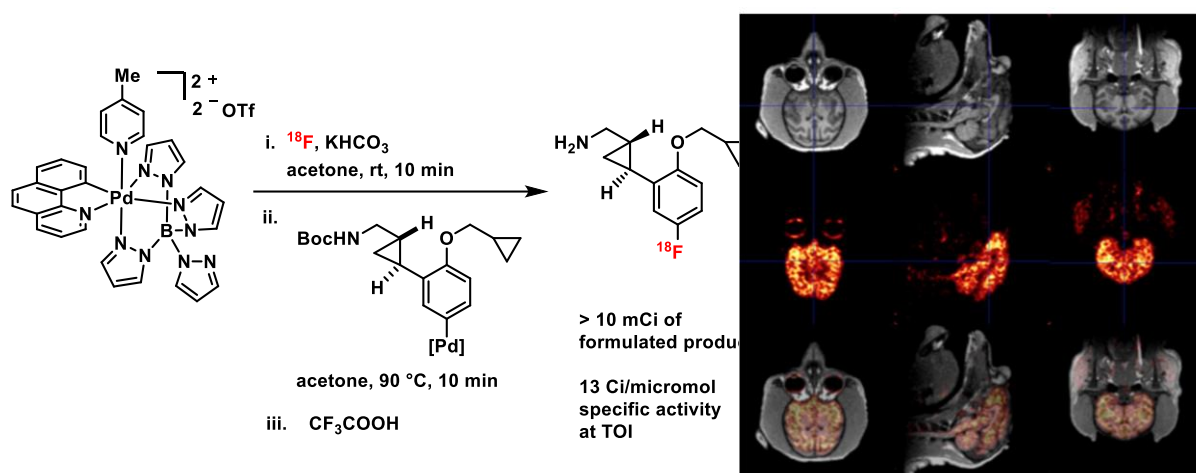
**Figure 8:** A high valent palladium complex designed to capture <sup>18</sup>F-fluoride in solution.

Through a two-step reaction sequence, a variety of aryl palladium complexes can be converted to the corresponding radiofluorinated products (Figure 9). The development of

automated synthesis procedures allowed translation of the palladium-mediated fluorination into a reliable, reproducible radiofluorination method able to afford radiolabeled molecules on a scale suitable for PET imaging in non-human primates (Figure 10).<sup>152</sup> Final samples are chemically and radiochemically pure and contain less than 5 parts per billion (ppb) palladium, well below suggested guidelines for use in humans (< 1000 ppb).<sup>153</sup> The entire sequence from <sup>18</sup>F acquisition to reformulated tracer is complete in less than 100 min, but the need for a two-step sequence with an intervening purification step renders palladium-mediated radiofluorination operationally more difficult than a typical one-step process.



**Figure 9:** Palladium-mediated radiofluorination using a fluoride derived electrophilic fluorinating reagent.



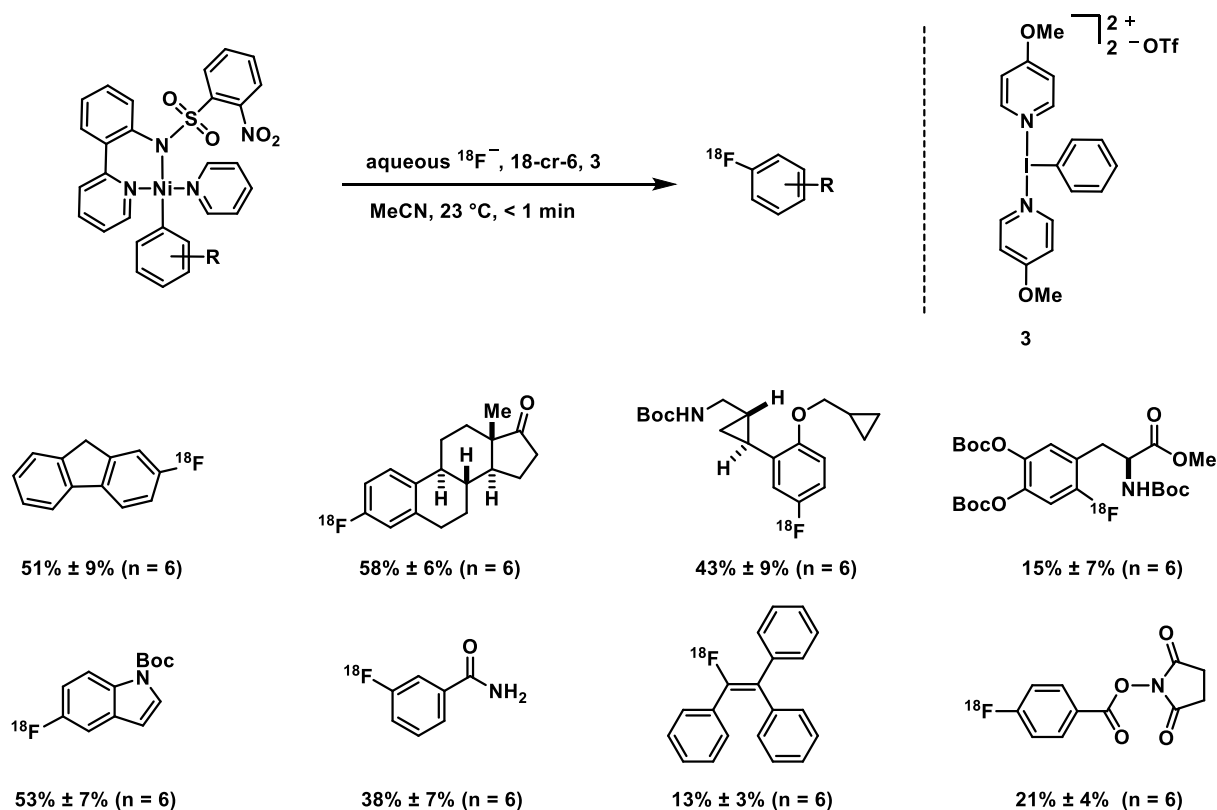
**Figure 10:** PET-MRI imaging study of a 5HT<sub>2C</sub> agonist conducted with tracer synthesized by a palladium-mediated fluorination reaction.

Palladium-mediated radiofluorination employs  $^{18}\text{F}$ -fluoride, affords only one aryl fluoride constitutional isomer, yields no inseparable byproducts and tolerated a range of functional groups including heterocycles and Boc-protected amines (Table 1). Complex **1** – from which electrophilic fluorinating reagent **2** is formed – is sensitive to air and moisture, which can be problematic operationally. Storing **1** under dry and air-free conditions prior to use, however, allows formation of  $^{18}\text{F}$ -**2**, which is itself stable to high temperature, oxygen and moisture. While performing the palladium-mediated fluorination using an automated synthesis module, care has to be taken that **1** is not exposed to air prior to reaction with  $^{18}\text{F}$ -fluoride. The need for a filtration step between the synthesis of  $^{18}\text{F}$ -**2** and its reaction with an aryl palladium complex prevents the two reaction steps from being performed in the same pot. Palladium-mediated radiofluorination is one of the most functional group tolerant  $^{18}\text{F}$  fluorinations for incorporating  $^{18}\text{F}$  into aromatic rings, but certain functional groups cannot be tolerated (see Table 1), most notably tertiary amines. Also, the steric hindrance resulting from the presence of an ortho substituent on the aromatic ring can make the synthesis of the Pd<sup>II</sup>-aryl precursor and its reaction with the Pd<sup>IV</sup>- $^{18}\text{F}$  reagent very difficult. Additionally, while the use of reagent  $^{18}\text{F}$ -**2** is fairly simple, the preparation of **1** and the Pd<sup>II</sup>-aryl starting materials require expertise in organometallic chemistry.

**Table 1:** Checklist of functional groups that are and are not tolerated in the palladium-mediated radiofluorination.

Tolerated	Not tolerated
<b>Nitrogen atoms bound to electron-withdrawing functional groups (e.g. Boc)</b>	Basic amines
<b>Furans</b>	Thiols
<b>Electron-rich aromatics</b>	Most unprotected protic functional groups
<b>Ketones</b>	Ortho substitution is problematic
<b>Amides</b>	
<b>Cyclopropanes</b>	
<b>Ethers</b>	

A significant increase in the practical application of metal-mediated radiofluorinations can be achieved through the use of nickel instead of palladium-aryl complexes (Figure 11).<sup>154</sup> Through a change of transition metal, a one-step protocol could be achieved, in which a combination of <sup>18</sup>F-fluoride and an oxidant mimics an electrophilic fluorinating agent. Direct use of aqueous <sup>18</sup>F-fluoride is also possible (up to 1% v/v water/acetonitrile in the reaction mixture) obviating the need for time-consuming azeotropic drying procedures. The presence of ortho-substitution is better tolerated than in the palladium-mediated fluorination (e.g. 6-fluoro-DOPA in Figure 11). However, as with palladium-mediated radiofluorination, the need to synthesize a nickel complex increases the difficulty of the overall procedure. Thus, while the use of transition metals is not inherently problematic in radiolabeling, having precursors that can be synthesized more conveniently by non-specialists is highly desirable.



**Figure 11:** The nickel-mediated oxidative radiofluorination does not require azeotropic drying of  $^{18}\text{F}$ -fluoride and is complete after one minute at room temperature.

A combination of reactions specifically developed for PET and late-stage fluorinations being adapted to  $^{18}\text{F}$ -chemistry have achieved a significant expansion in the pool of structures that can be radiolabeled without resorting to cumbersome multi-step syntheses. Despite the adaption of several modern fluorination methods to  $^{18}\text{F}$ -radiosynthesis, however, the projected, dramatic increase of the number of available PET tracers has not yet occurred.<sup>68,143,145,147-149,155-157</sup> More hurdles need to be crossed for a reaction to show promise in practical PET tracer synthesis than short reaction time and the use of fluoride as a limiting reagent. A particular focus needs to lie on simplifying existing and future reactions to allow facile automation and widespread use by non-specialists. Proof-of-concept manual testing of a reaction under  $^{18}\text{F}$  conditions is important, but constitutes only the first step towards developing a new radiolabeling tool. Many more challenges need to be faced in addressing automation and purification, which are often overlooked by the synthetic community.

Purification is an issue commonly addressed when a reaction has been successfully developed; in the context of  $^{18}\text{F}$  chemistry, facile product purification should enter the reaction design at the outset to ensure that pure radiofluorinated product can be obtained from a reaction mixture containing thousands of equivalents of starting material and reagents. Several modern methods applied to  $^{18}\text{F}$  radiolabeling are transition metal catalyzed or mediated, which makes hydrodefunctionalization, a common side reaction observed in many cross-coupling reactions, of particular concern.

Operational simplicity is another important criterion for PET. Our palladium-mediated late-stage fluorination is an example of a conceptually remarkable, but operationally flawed  $^{18}\text{F}$  reaction: the transformation consists of two reaction steps, separated by a filtration and necessitates the use of a moisture-sensitive precursor molecule. While neither of those two operational hurdles posed significant challenges in the original development of the reaction, nor in small-scale labeling experiments conducted manually, they rendered automation of the procedure for non-human primate imaging challenging, and clinical translation prohibitively difficult.<sup>152</sup> In addition to operational practicality being judged by different standards in a chemistry laboratory and in an imaging context, the selection of reaction substrates is no longer dictated by chemical goals but by real clinical needs. In order to develop  $^{18}\text{F}$ -fluorination reactions with promise, true late-stage fluorination with a level of convenience that can be realized in a clinical imaging setting must be accessible. PET tracer development is difficult, also beyond synthesis, but the ability to make complex and structurally diverse  $^{18}\text{F}$ -labeled molecules more efficiently than previously possible, may shift the future challenge toward PET tracer development rather than PET tracer synthesis.

### **Late-stage deoxyfluorination**

Stringent requirements need to be fulfilled for a transformation to be deemed a late-stage reaction, but to be truly useful, a late-stage reaction requires simple starting materials. The silver-catalyzed fluorination developed by the Ritter lab (Figure 7) shows exceptional

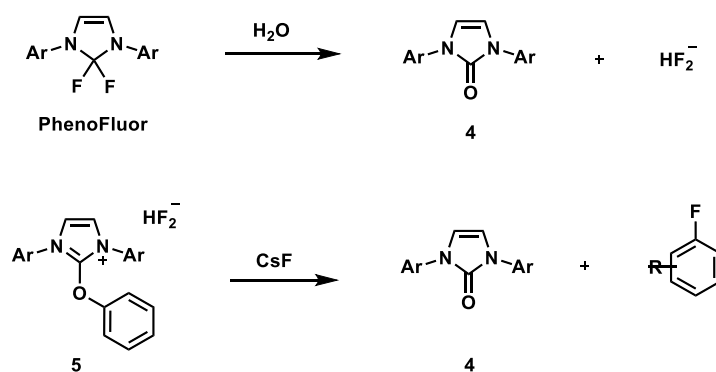
substrate scope and functional group tolerance, but its use is limited by the hazardous nature of the aryl stannane starting materials and limitations in the synthesis of those precursors.<sup>70</sup> More drastic examples are to be found in <sup>18</sup>F-fluorination chemistry. The utility of both the radiolabeling of aryl diazonium salts and isolated transition metal complexes is severely restricted by difficulties in accessing and handling those starting materials.<sup>68,150,154</sup>

Chemists have long been in the business of enabling difficult transformations by raising the energy of the starting materials used in a transformation. 'Spring-loaded' substrates ensure that the energy difference between the starting material and the transition state for the desired bond formation or cleavage is decreased and the reaction can occur. As a particular field evolves, transformations involving lower-energy (and generally more useful) starting materials are found due to the development of better reagents or catalysts. A number of late-stage fluorination methods are available, which show that high energy starting materials are not required to achieve a large fluorination substrate scope. Among those are the palladium-mediated fluorination of aryl triflates and aryl bromides reported by the Buchwald group and the fluorination of aryl boronates disclosed by the Ritter and Sanford group.<sup>45,46,48,71-73,117,144</sup>

A reagent can assume the role of the 'spring-loaded' reaction component since it can undergo a reaction that is highly exergonic. Coupling of the exergonic transformation that the reagent undergoes to the endergonic reagent of the substrate can enable a difficult bond formation. When the exergonicity of the reagent's transformation is released early in the course of the reaction, it can be employed to help the substrate overcome a high kinetic barrier as it progresses along the reaction coordinate. Electrophilic fluorinating agents typically are strong oxidants and tend to be converted to lower-energy reduced products over the course of a reaction. The energy released by the reagent is often indirectly coupled to the C–F bond formation step through the intermediacy of transition metal oxidation. The role of electrophilic fluorinating agents such as F-TEDA in aromatic fluorinating reactions

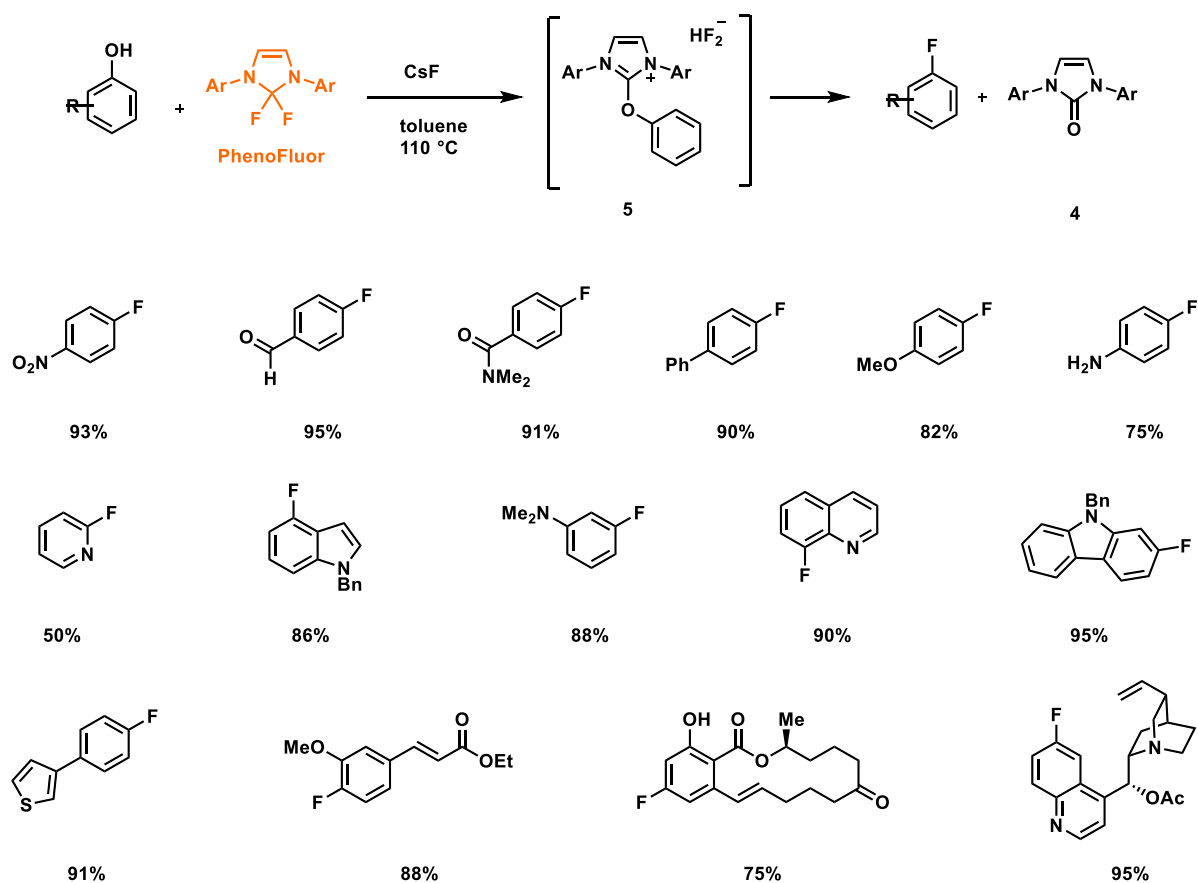
commonly consists in the oxidation of a transition metal aryl complex (e.g. Pd<sup>II</sup> to Pd<sup>IV</sup>) as well as the transfer of fluorine to the oxidized transition metal center. The barrier for C–F bond formation *via* reductive elimination is considerably lower on a Pd<sup>IV</sup> than a Pd<sup>II</sup> center with a comparable ligand set. Therefore, oxidation of the transition metal provides a bridge between the exothermic reaction of the electrophilic fluorinating reagent and the difficult C–F bond formation step. A condition for the coupling of a favorable reagent-based transformation to a difficult desired transformation of a substrate is that the energy release on the reagent takes place concurrently or prior to the rate-limiting step of the substrate transformation.

The PhenoFluor-mediated deoxyfluorination of phenols developed by Pingping Tang in the Ritter lab is based on a reagent capable of converting the hydroxyl group of phenols into a good leaving group. Nucleophilic displacement on the arene leads to the expulsion of urea **4**, which is energetically very favorable (Figure 12). Reaction between PhenoFluor and phenols is facile and occurs at room temperature with formation of uronium bifluoride **5**.



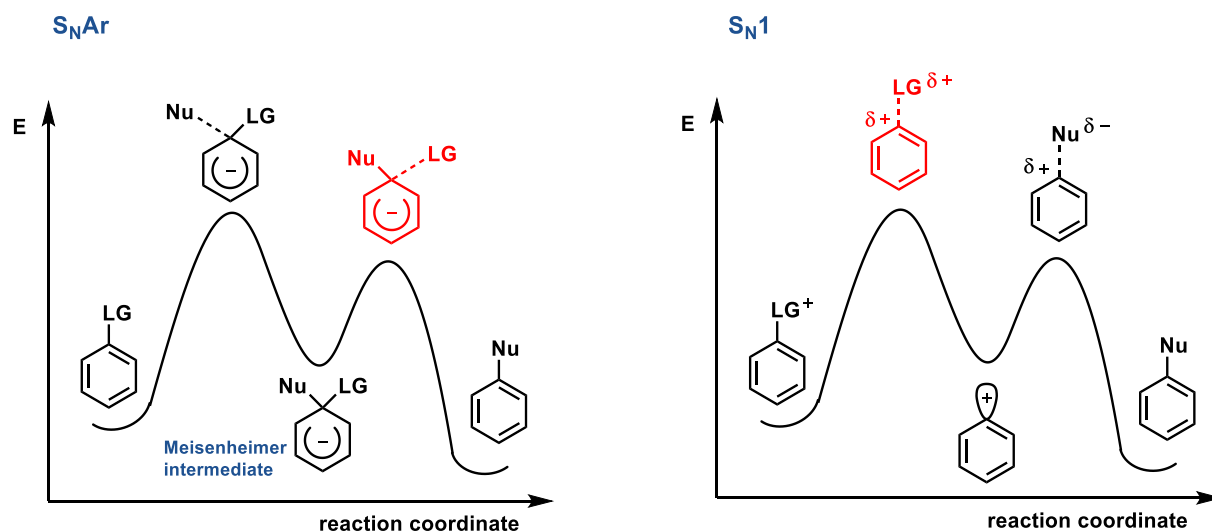
**Figure 12:** The formation or release of urea **4** is energetically very favorable.





**Figure 13:** Deoxyfluorination of both electron-rich and electron-poor phenols can be accomplished with the PhenoFluor reagent.

PhenoFluor-mediated deoxyfluorination tolerates a large number of functional groups and proceeds efficiently on both electron-poor and electron-rich arenes (Figure 13). The extensive substrate scope of the deoxyfluorination incited interest in the reaction mechanism of PhenoFluor-mediated deoxyfluorination early on during reaction development.



**Figure 14:** Steps associated with exergonic leaving group loss for a  $S_NAr$  and an  $S_N1$  mechanism are highlighted in red on the respective energy diagrams.

The highly favorable hydrolysis of PhenoFluor to the corresponding urea makes this reagent a good candidate for the coupling of a favorable leaving group release to an unfavorable or slow C–F bond formation step. A necessary condition for such a coupling is, however, that the exergonic urea formation step (leaving group loss) occurs concurrently to the potentially challenging C–F bond formation step. Alternatively, exergonic leaving group loss could occur prior to C–F bond formation *via* the creation of a high energy intermediate capable of facile C–F bond formation. A  $S_NAr$  mechanism (Figure 14) would not account for an unusually large substrate scope through energetic coupling since exergonic leaving group loss occurs in a separate step that is decoupled from rate-limiting fluoride attack. An  $S_N1$  mechanism would allow for energetic coupling via the formation of a reactive intermediate; it was found early on in the development of PhenoFluor deoxyfluorination, however, that electron-poor phenols, which are less activated towards leaving group loss via an  $S_N1$  mechanism react faster than electron-rich phenols.

A detailed investigation into the mechanism of PhenoFluor deoxyfluorination seemed necessary to explain how electron-rich phenols are rendered viable substrates for

nucleophilic displacement.  $S_NAr$  reactions proceed efficiently with a wide range of nucleophiles but the need for the presence of strongly electron-withdrawing substituents on the arene severely restricts the scope of nucleophilic displacement reactions. Understanding the origin of the PhenoFluor reagent's ability to push the substrate pool for nucleophilic displacement far beyond the usual bounds might allow the development of analogous transformations with other nucleophiles.

Initial reaction between phenol substrates and PhenoFluor leads to uronium **5**, in which the bifluoride anion forms a hydrogen-bond to a C–H bond on the imidazolium backbone. The large uronium cation ensures that **5** is soluble in the apolar reaction solvent toluene. The limited solubility of fluoride salts in organic solvents is a major challenge in the development of nucleophilic aromatic fluorination reactions. In  $S_NAr$  reactions as well as reactions proceeding via a number of other mechanisms, the reaction rate is directly proportional to the concentration of fluoride in solution. Polar solvents such as DMSO, DMF or alcoholic solvents increase the solubility of most fluoride salts, but the strong interactions between fluoride anions and solvent molecules also contribute to the reaction barrier. Since partial desolvation of the nucleophile has to occur upon or prior to C–F bond formation the use of non-polar solvents that interact only weakly with fluoride nucleophiles would likely lead to lower reaction barriers but is commonly prevented by low fluoride solubility. The PhenoFluor reagent is not only able to convert simple starting materials such as phenols into viable substrates for nucleophilic displacement with fluoride, but the formation of reaction intermediates where a bulky, non-polar cation derived from the substrate stabilizes the (bifluoride) nucleophile in solution in a non-polar solvent minimizes the contribution of fluoride desolvation to the reaction barrier.

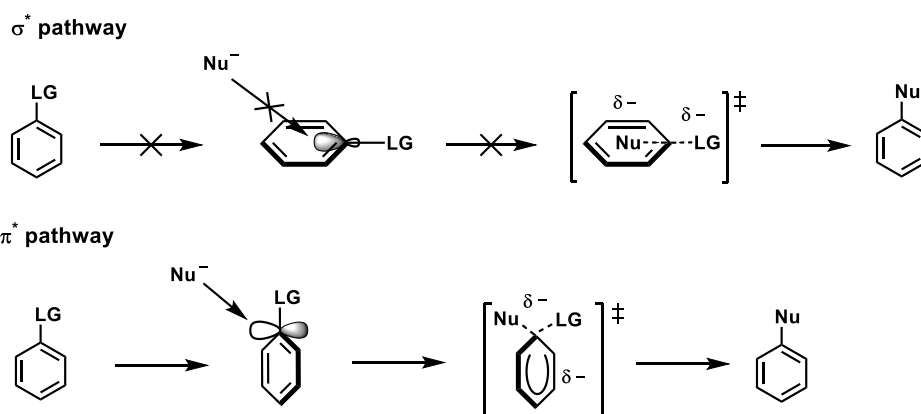
## CHAPTER 1: CONCERTED NUCLEOPHILIC AROMATIC SUBSTITUTION (CS<sub>N</sub>AR) WITH <sup>19</sup>F<sup>-</sup> AND <sup>18</sup>F<sup>-</sup>

Nucleophilic aromatic substitution (S<sub>N</sub>Ar) is widely used for the construction of functionalized aromatic molecules, and it is by far the most common method for the functionalization of arenes with <sup>18</sup>F for use in PET imaging.<sup>158</sup> A wide range of nucleophiles exhibit S<sub>N</sub>Ar reactivity, and the operational simplicity of the reaction allows the transformation to be conducted reliably and on large scales.<sup>159</sup> During S<sub>N</sub>Ar, attack of a nucleophile at a carbon atom bearing a leaving group leads to a negatively charged intermediate called a Meisenheimer complex. But only arenes with electron-withdrawing substituents can sufficiently stabilize the build-up of negative charge during Meisenheimer complex formation, which limits the scope of S<sub>N</sub>Ar reactions - most common S<sub>N</sub>Ar substrates contain strong π-acceptors in the ortho and/or para position.<sup>160</sup> Here we present an unusual *concerted* nucleophilic aromatic substitution reaction (CS<sub>N</sub>Ar) that is not limited to electron-poor arenes because it does not proceed through Meisenheimer intermediates. We show a phenol deoxyfluorination reaction for which *concerted* nucleophilic aromatic substitution (CS<sub>N</sub>Ar) is favored over a stepwise displacement. Mechanistic insights enabled us to develop a functional-group-tolerant <sup>18</sup>F-deoxyfluorination of phenols in high specific activity for the practical synthesis of <sup>18</sup>F-PET probes. Selective <sup>18</sup>F introduction, without the need for common but cumbersome azeotropic drying of <sup>18</sup>F, can now be accomplished from phenols as starting materials, and provides access to <sup>18</sup>F-labeled compounds not accessible through conventional chemistry.

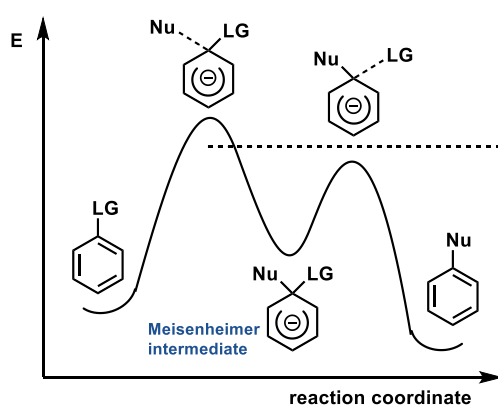
Nucleophilic aromatic substitution reactions generally take place *via* either an addition-elimination or elimination-addition mechanism. Both two-step mechanisms display a high-energy intermediate, either an aryne species (elimination-addition) or a Meisenheimer complex (addition-elimination).<sup>159,161</sup> A *concerted displacement* of the leaving group by an

incoming nucleophile could avoid the formation of high-energy intermediates and thus broaden the scope of suitable electrophiles. Displacements at primary aliphatic centers, where charge build-up in a hypothetical S<sub>N</sub>1 mechanism is unfavorable, commonly take place *via* a concerted mechanism involving the  $\sigma^*$  (C<sub>alkyl</sub>-LG) orbital (S<sub>N</sub>2 mechanism). For aromatic substrates a direct substitution pathway involving the  $\sigma^*$  orbital of the arene-leaving group bond ( $\sigma^*$  (C<sub>aryl</sub>-LG)) is deemed to be impossible: the  $\sigma^*$  orbital is shielded because its large lobe points inwards into the arene ring (Figure 15A).<sup>162</sup> Concerted S<sub>N</sub>Ar substitutions *via* the  $\pi$  orbital framework are considered “*possible but restricted to aromatic structures devoid of the ring activation to generate an intermediate sigma complex of some stability*”.<sup>2</sup> The intramolecular Newman-Kwart rearrangement has been reported to occur *via* concerted displacement for a wide range of arene substrates, albeit mostly with high activation barriers (35-43 kcal/mol) that reduce synthetic utility.<sup>163</sup> We show here that the deoxyfluorination reaction of phenols with the reagent PhenoFluor (Figure 16B) reported by our group<sup>76,77</sup> proceeds *via* a concerted pathway with electron-rich as well as electron-poor substrates, and how a detailed mechanistic analysis enabled us to design a deoxyfluorination reaction of phenols with <sup>18</sup>F. A concerted reaction with activation energies between 20 and 25 kcal/mol is observed because the concerted pathway is favored rather than because the classic two-step mechanism is disfavored, which sets our reaction apart from previous transformations that proceed with substantially higher activation barriers.<sup>158,160,163,164</sup> Gas phase nucleophilic aromatic substitutions can take place by concerted nucleophile attack and loss of the leaving group but only isolated cases of intermolecular C<sub>S</sub>NAr reactions in solution or ionic melt have been reported.<sup>165-172</sup>

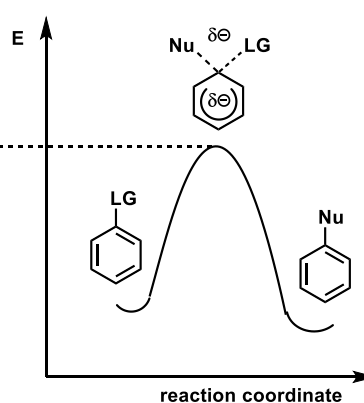
### A Potential Concerted Nucleophilic Aromatic Substitution Pathways



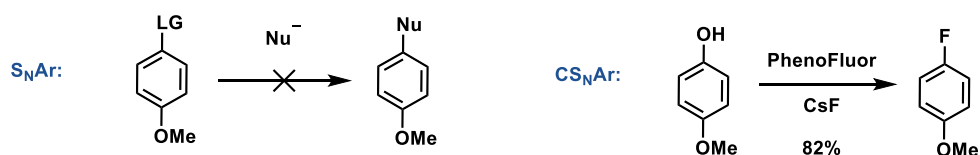
### B $S_NAr$



### $CS_NAr$



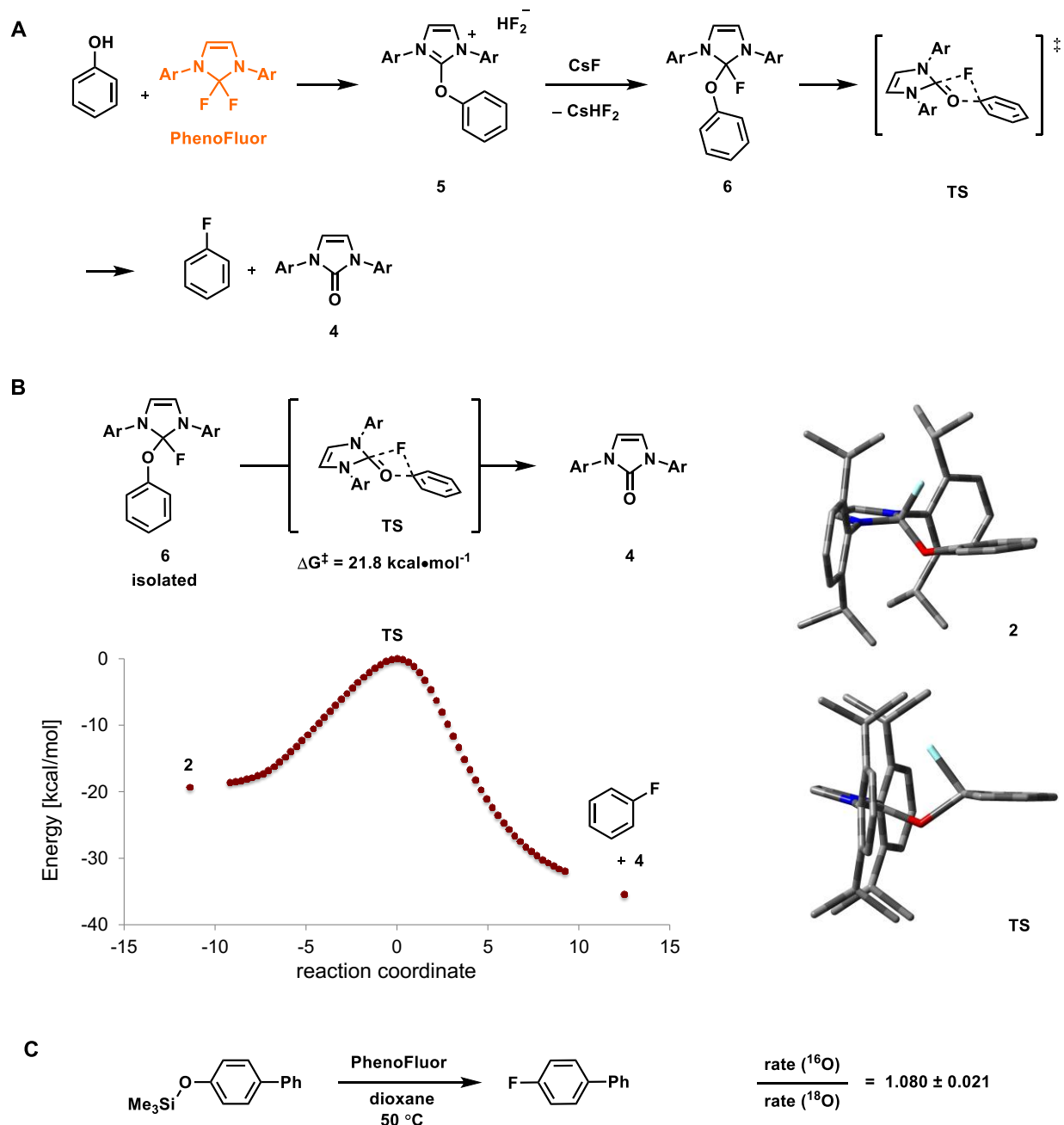
### C



**Figure 15:** Comparison of orbital interactions and energy profiles in  $S_NAr$  and  $CS_NAr$ . A: The aromatic ring blocks the approach of the nucleophile to the  $\sigma^*_{C-LG}$  orbital; attack on the  $\pi$ -framework is feasible. B: The energy profiles of  $S_NAr$  and  $CS_NAr$  differ in the number of transition states and in the magnitude of the activation energies. C: Minimization of charge build-up in the transition state renders nucleophilic displacement feasible even on electron-rich arenes in  $CS_NAr$  reactions.

The orbital interactions involved in a concerted mechanism are similar to those of classical addition-elimination pathways, but the extent of bond-formation and -cleavage in the transition

state is crucially different: In the transition state of concerted nucleophilic aromatic substitution ( $CS_{\text{N}}\text{Ar}$ ) both the nucleophile and leaving group are attached to the arene by partial rather than full bonds. Loss of the leaving group in the rate-determining step allows the negative charge associated with nucleophilic attack to be located on the incoming nucleophile and the departing leaving group, as opposed to the arene in conventional  $S_{\text{N}}\text{Ar}$ . We propose that selection of leaving groups and reaction conditions tailored to a concerted displacement make it possible to utilize the minimization of charge build-up on the arene to lower the activation barrier (Figure 15B), which expands the scope of electrophiles to include deactivated substrates that feature strong  $\pi$ -donors in the para-position (Figure 15C). The PhenoFluor-mediated deoxyfluorination reaction allows the interconversion of 4-hydroxyanisole to 4-fluoroanisole at only 110 °C<sup>76,77</sup> – far below the temperature commonly observed for aromatic substitutions on unactivated arenes.<sup>160,163,164</sup>



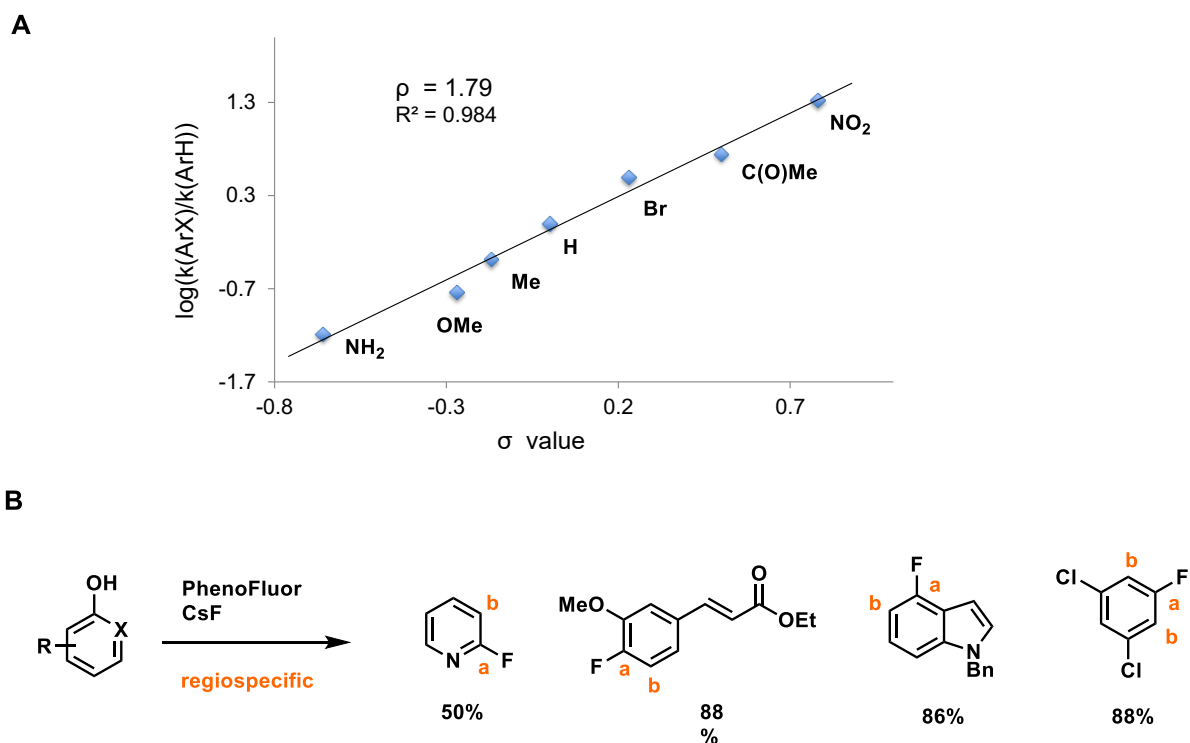
**Figure 16:** Proposed mechanism of PhenoFluor-mediated deoxyfluorination. A Following formation of uronium intermediate **5**, external CsF abstracts HF to form tetrahedral adduct **6**, which undergoes concerted nucleophilic substitution via fluoride shift (Ar = 2,6-diisopropylphenyl). B The intrinsic reaction coordinate obtained from DFT calculations (B3LYP/6-31G(d), toluene solvent model) shows a single barrier between tetrahedral adduct **6** and reaction products (Ar = 2,6-diisopropylphenyl). Structures obtained from DFT calculations are shown for **6** and **TS**.  $\Delta G^\ddagger = 21.8 \pm 0.2 \text{ kcal}\cdot\text{mol}^{-1}$  was measured for the transformation of **6** to aryl fluoride and urea **4**. C The primary  $^{16}\text{O}/^{18}\text{O}$  kinetic isotope effect is



consistent with cleavage of the C–O bond during the rate-limiting step. Silylated phenols react with PhenoFluor to form tetrahedral intermediate **6** without added CsF.

We propose a reaction sequence for the deoxyfluorination reaction in which fluoride attacks the imidazolium core of the reagent to yield tetrahedral intermediate **6** prior to participating in concerted displacement on the arene (Figure 16A); independently synthesized and characterized tetrahedral intermediate **6** is converted to aryl fluoride and urea **4** under the reaction condition (Figure 16B). A single transition state (**TS**) was localized in a DFT study (B3LYP/6-311++G(d,p), toluene solvent model) with partial bonds between the nucleophile and arene as well as the leaving group and the arene, the characteristic feature of a concerted transformation.<sup>173</sup> An internal reaction coordinate analysis revealed that the transition state connects tetrahedral intermediate **6** to urea **4** and aryl fluoride, which excludes the existence of additional maxima along the reaction path (Figure 16B).

Crucial to the proposal of a concerted substitution mechanism is that loss of the leaving group occurs concurrently with attack of the incoming nucleophile. The rate observed for the fluorination of <sup>16</sup>O-4-phenyl-phenol is  $1.08 \pm 0.02$  times as fast as the rate of fluorination of <sup>18</sup>O-4-phenyl-phenol, corresponding to a large primary kinetic isotope effect (Figure 16C).<sup>174</sup> A primary <sup>16</sup>O/<sup>18</sup>O kinetic isotope effect shows that cleavage of the C–O bond (and therefore loss of the leaving group) occurs during the rate-determining step.<sup>173,175,176</sup>



**Figure 17:** **A** Hammett plot for the deoxyfluorination of para-substituted phenols at 110 °C. **B** Regioselective product formation occurs for substrates prone to nucleophilic attack at position b if arynes were formed.<sup>161,177</sup>

The rate of deoxyfluorination with PhenoFluor is greater for electron-deficient than for electron-rich substrates, and the continuity in the Hammett plot reveals that no change in mechanism or rate-determining step occurs when the electron density on the phenol is varied (Figure 17A). An SET mechanism, in which an electron is transferred from the phenol arene to the positively charged imidazolium core, is inconsistent with the observed Hammett plot: For rate-determining electron transfer, reaction rates should be fastest for electron-rich substrates, which is not the case. SET occurring under pre-equilibrium conditions followed by rate-determining fluoride attack, in which case a positive  $\rho$ -value would be expected, is unlikely due to the primary <sup>16</sup>O/<sup>18</sup>O isotope effect. Fast and reversible fluoride attack followed by rate-limiting expulsion of the leaving group would give rise to a negative  $\rho$ -value in the Hammett plot. The regiospecificity of the deoxyfluorination reaction discounts an aryne mechanism (Figure 17B).

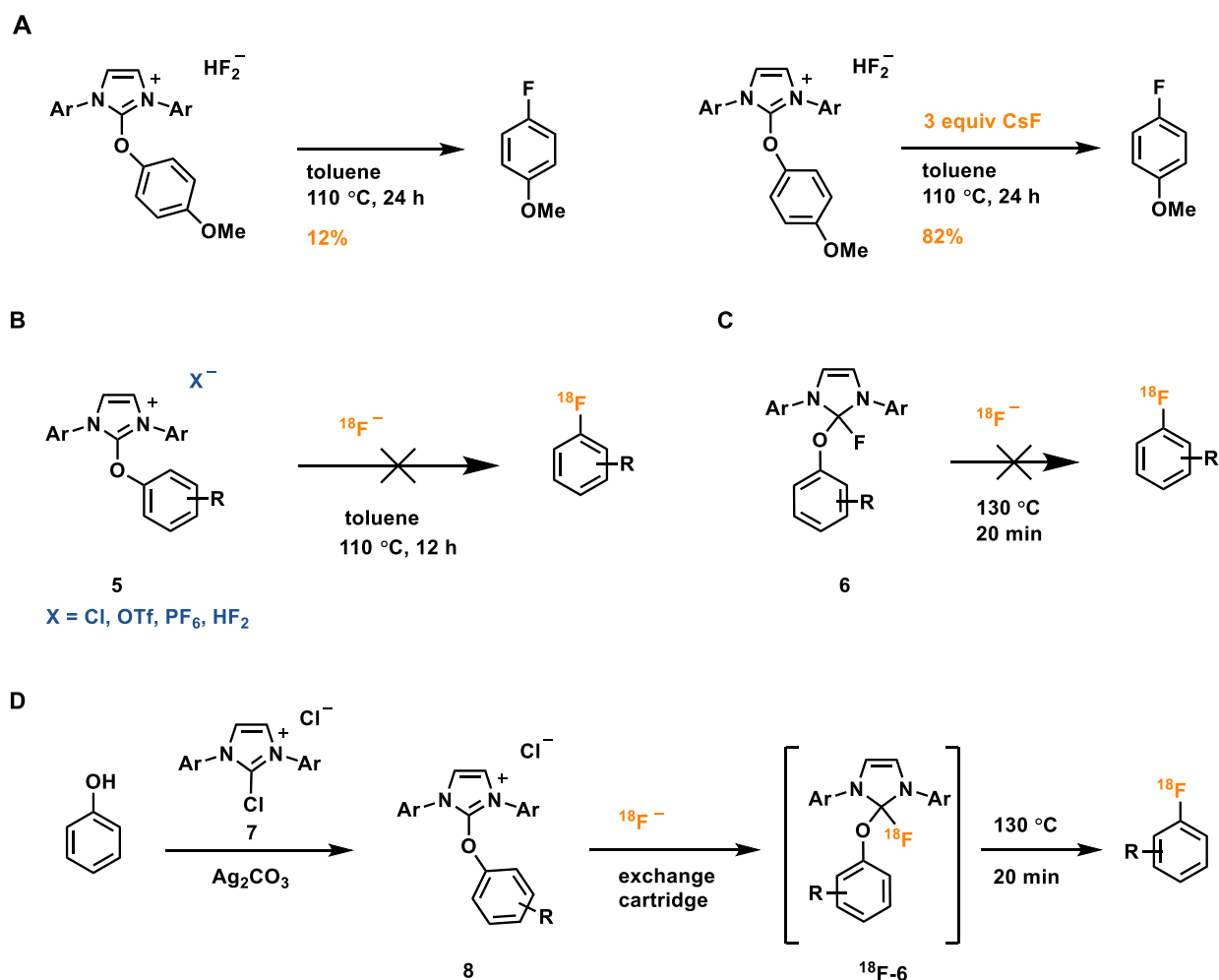
Eyring plots were constructed for a selection of substrates, which revealed  $\Delta G^\ddagger = 20.3 \pm 0.1$  kcal·mol<sup>-1</sup> for 4-nitrophenol,  $\Delta G^\ddagger = 21.0 \pm 0.2$  kcal·mol<sup>-1</sup> for 4-cyanophenol,  $\Delta G^\ddagger = 21.2 \pm 0.5$  kcal·mol<sup>-1</sup> for 4-trifluoromethylphenol and,  $\Delta G^\ddagger = 23.4 \pm 0.2$  kcal·mol<sup>-1</sup> for phenol, respectively. Computational activation barriers  $\Delta G^\ddagger = 20.8$  kcal·mol<sup>-1</sup> for 4-nitrophenol and  $\Delta G^\ddagger = 25.0$  kcal·mol<sup>-1</sup> for phenol are in good agreement with the experimental values. Compared to classical S<sub>N</sub>Ar reactions, the increase in activation energies as the aromatic system becomes more electron-rich is far less pronounced for concerted S<sub>N</sub>Ar reactions, which is also apparent from the smaller Hammett  $\rho$ -values; conventional S<sub>N</sub>Ar reactions have  $\rho$ -values ranging from 3 to 8, compared to 1.8 for the CS<sub>N</sub>Ar reaction reported here (Figure 17B).<sup>165</sup> Limited delocalization of negative charge onto the aromatic substrate in the transition state can thus extend the scope of nucleophilic aromatic substitution to electron-rich substrates.

Why is the barrier for CS<sub>N</sub>Ar in the presented deoxyfluorination low relative to hypothetical S<sub>N</sub>Ar reactions on electron-rich arenes? Firstly, facile loss of the leaving group is crucial for a concerted nucleophilic aromatic substitution reaction.<sup>178</sup> Unlike in a two-step sequence, where a second smaller activation barrier is associated with loss of the leaving group, a concerted transformation has a single barrier to which both nucleophilic attack, disruption of aromaticity, and loss of the leaving group contribute. A neutral leaving group (urea **4**) will aid in stabilizing the partial negative charge which resides on both the nucleophile and the leaving group in the transition state.<sup>178</sup> An earlier transition state with a lower reaction barrier will occur for CS<sub>N</sub>Ar reactions if loss of the leaving group is energetically favorable.<sup>158</sup> Formation of urea **4** is highly exergonic, and because partial C–O cleavage occurs in the transition state, the exergonicity of the overall transformation is expected to lower the activation barrier for deoxyfluorination, an effect also apparent in the <sup>18</sup>F displacement of arenes from triarylsulfonium salts.<sup>178</sup> Compared to the Newman-Kwart rearrangement, which can take place on substrates

deactivated by electron-donating substituents, the PhenoFluor mediated deoxyfluorination proceeds with considerably lower reaction barriers, likely due to the higher enthalpic gain associated with leaving group loss. Secondly, rearrangement of solvent molecules is commonly a large contributor to the activation barriers of nucleophilic aromatic substitutions, particularly when anionic nucleophiles are employed.<sup>179</sup> Association of the (bi)fluoride nucleophile with the cationic uronium **5** solubilizes the nucleophile in the non-polar solvent toluene, and can subsequently form neutral tetrahedral adduct **6**. We propose that the contribution of solvation to the activation barrier is small because neither the associated reaction partners nor the transition state carry an overall charge and little nuclear motion is required to proceed from **6** to **TS**. Computational data suggests that the use of a non-polar solvent favors the occurrence of a concerted deoxyfluorination reaction (Figure 61 and Figure 62).

<sup>18</sup>F-Fluoride is a desirable nucleophile for the development of  $CS_NAr$  reactions, particularly concerted deoxyfluorination: Phenols are easily accessible and their high polarity facilitates purification of aryl fluoride product from phenol starting material.<sup>148</sup> However, in addition to the two equivalents of fluorine inherent to PhenoFluor itself, additional fluoride must be added for efficient deoxyfluorination (Figure 18A), which, a priori, renders PhenoFluor-mediated deoxyfluorination effectively useless for <sup>18</sup>F chemistry. Even attempts towards a low-specific activity radiodeoxyfluorination initially proved fruitless: Both isolated reaction intermediate **5** (and derivatives featuring different counteranions) and tetrahedral intermediate **6** did not react with external <sup>18</sup>F-fluoride to yield <sup>18</sup>F-aryl fluoride products (Figure 18B, C). Mechanistic work (Figure 55) revealed that fluoride was not incorporated into tetrahedral intermediate **6** via attack by external fluoride on uronium **5** or anion metathesis; instead the fluoride on the aryl fluoride originated from PhenoFluor. We thus devised a strategy to alter the mechanism of fluoride incorporation into **6** to access <sup>18</sup>F-**6** in high specific activity: While anion exchange of **8** with <sup>18</sup>F does not occur in solution, productive anion exchange occurs on an anion exchange

cartridge (Figure 18D).

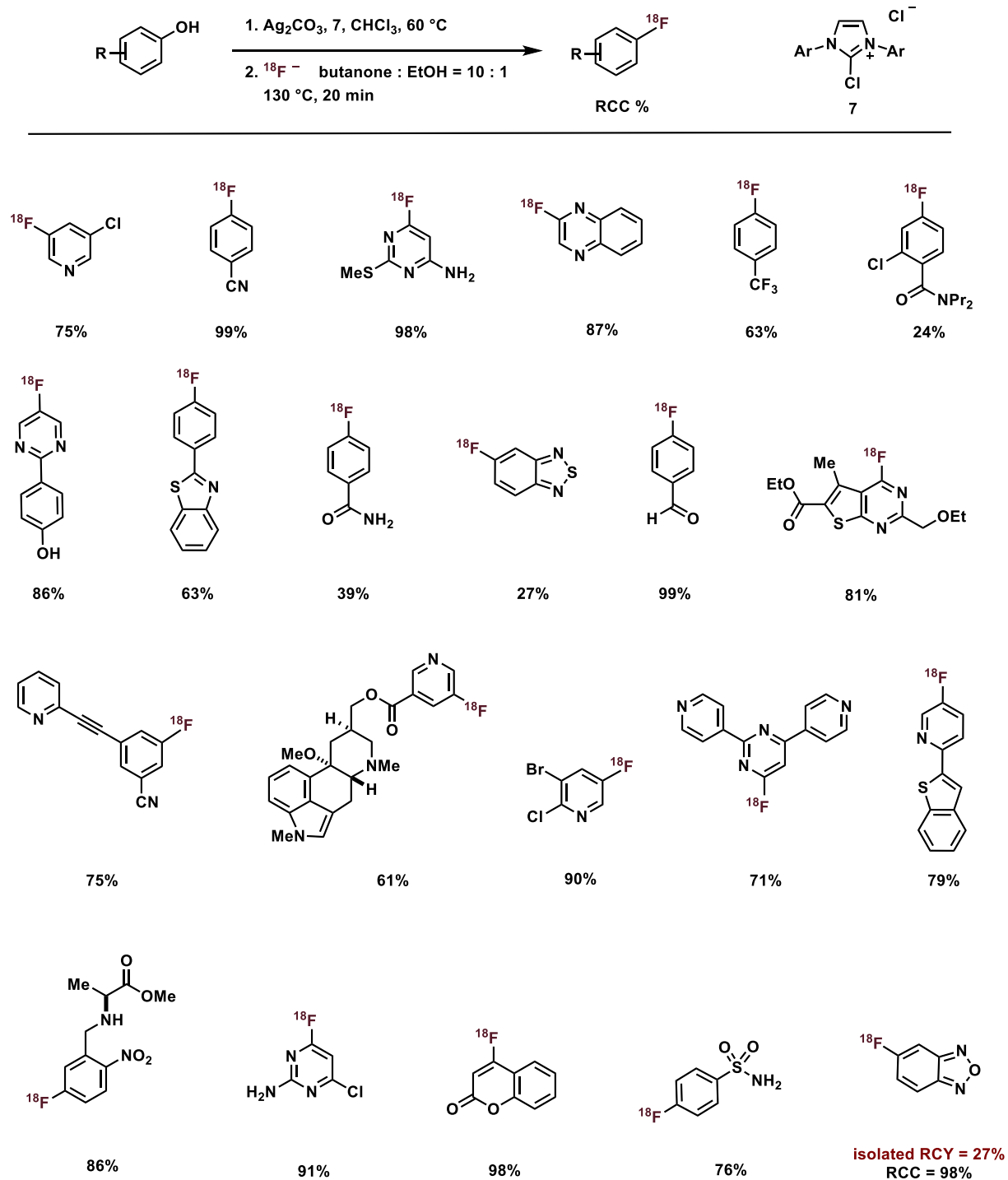


**Figure 18:** **A** CsF abstracts HF from the  $\text{HF}_2^-$  counteranion: without CsF, deoxyfluorination occurs *via* a different mechanism in which  $\text{HF}_2^-$  attacks the arene. DFT studies reveal that the barrier for C–F bond formation is 6.0 kcal/mol lower with a fluoride instead of a bifluoride nucleophile (see Figure 49). **B** Treatment of uronium **5** with  $^{18}\text{F}^-$  does not give aryl fluoride due to the lack of anion exchange between X and  $^{18}\text{F}^-$  in solution. **C** No  $^{18}\text{F}$  incorporation is observed. **D** Anion exchange with extraneous fluoride takes place on an anion exchange cartridge (Ar = 2,6-diisopropylphenyl).

$^{18}\text{F}$ -Fluoride is typically prepared by proton bombardment of  $^{18}\text{O}\text{-H}_2\text{O}$ , and  $^{18}\text{F}$ -fluoride is subsequently trapped on an ion exchange cartridge. Elution of the radioisotope is commonly achieved with an aqueous solution of a base.<sup>175</sup> Here we can use uronium **8** directly for elution of  $^{18}\text{F}$ -fluoride from the anion exchange cartridge. Uroneum **8** can readily be prepared from

chloroimidazolium chloride **7** and a suitable phenol and used after simple filtration. The elution procedure obviates the need for azeotropic drying of  $^{18}\text{F}$ -fluoride, and subsequent heating of the resulting solution of  $^{18}\text{F}$ -**6** directly provides aryl fluoride.

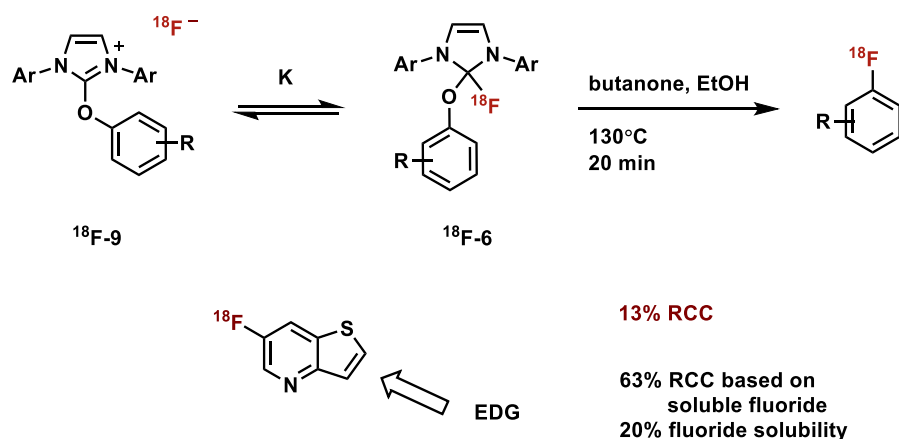
No special care is required to exclude air or moisture from the  $^{18}\text{F}$ -deoxyfluorination reaction, and the radiolabeled product can be conveniently separated from the reaction precursor. A wide variety of functional groups including amines and phenols as well as thioethers and amides are tolerated, and arenes as well as heteroarenes undergo radio-deoxyfluorination with high radiochemical conversion (Figure 19). Substrates containing carboxylic acids did not undergo  $^{18}\text{F}$ -deoxyfluorination because carboxylic acids inhibit the formation of uronium **5**. Competing nucleophilic aromatic substitution of activated chloride does not occur under the reaction conditions. Classical  $\text{S}_{\text{N}}\text{Ar}$  chemistry is the most widely applied method for the synthesis of PET probes but suffers from a very limited reaction scope, and protic functional groups are commonly not tolerated. Modern methods,<sup>68,148-150,154</sup> while capable of introducing  $^{18}\text{F}$ -fluoride into a more diverse range of structures, often suffer from the need for complex starting materials, operating- or purification procedures. Heterocycles are present in many bioactive compounds but are often problematic substrates for metal-mediated fluorination protocols with  $^{18}\text{F}$ ; several heterocycles undergo PhenoFluor deoxyfluorination with high radiochemical conversion. To highlight the operational simplicity of  $^{18}\text{F}$ -deoxyfluorination,  $^{18}\text{F}$ -5-fluorobenzofurazan was synthesized from 34 mCi aqueous  $^{18}\text{F}$ -fluoride and subjected to HPLC purification. Within 34 minutes from the end of bombardment, 9.3 mCi of isolated and purified  $^{18}\text{F}$ -5-fluorobenzofurazan could be obtained in 27% non-decay-corrected radiochemical yield (RCY) with a specific activity of  $3.03 \text{ Ci} \times \mu\text{mol}^{-1}$ .



**Figure 19:** Deoxyfluorination of phenols and heterophenols with  $^{18}\text{F}$ . A Decay-corrected radiochemical conversions were determined by comparing the amount of  $^{18}\text{F}$  incorporated into the product to the amount of  $^{18}\text{F}$  not incorporated.

We have established that tetrahedral intermediate **6** is in equilibrium with uronium fluoride **9** (Figure 20, Figure 43). Clean first order decay of **6** was observed in the presence of added

fluoride, but a marked deviation from first order kinetics was observed for the deoxyfluorination of silylated phenols in the absence of added fluoride. Hence, the fluoride anion in **6** likely engages in unproductive processes, such as precipitation or other fluoride sequestrations. In  $^{19}\text{F}$  deoxyfluorination, excess CsF negates such potential side reactions, but for radiofluorination, fluoride is present in small quantities (nmol).



**Figure 20:** Electron-rich phenols will result in a smaller equilibrium constant  $K$ , resulting in fluoride expulsion and decomposition before productive deoxyfluorination from tetrahedral intermediate  $^{18}\text{F}$ -**6** can occur. (Ar = 2,6- diisopropylphenyl).

For most compounds shown in Figure 19, potential decomposition of **6** does not disrupt productive fluorination, but when more electron-rich phenols are employed, the equilibrium constant  $K$  between **9** and tetrahedral intermediate **6** decreases. We have already shown that more electron-rich substrates can afford acceptable radiochemical conversions, when the conversion is based on soluble fluoride (Figure 20). While fluoride sequestration from **6** currently precludes the isolation of electron-rich  $^{18}\text{F}$  aryl fluorides in high radiochemical yields, efficient C- $^{18}\text{F}$  bond formation bodes well for mechanism-based strategies to increase  $K$ , that would render electron-rich arenes accessible.



## Mechanism Experiments

### Hammett Plot

A Hammett correlation was obtained using A)  $\sigma$  and B)  $\sigma^-$  values for the ArX substituents in the deoxyfluorination of para-X-phenols.<sup>180</sup> Reaction rates were determined by following the formation of aryl fluoride products by  $^{19}\text{F}$ -NMR. Aliquots were removed from the reaction mixture at regular intervals and stopped by addition of acetone. 1,4-Difluorobenzene was added to serve as an internal standard for analysis by  $^{19}\text{F}$ -NMR ( $^{19}\text{F}$ -NMR shift  $\delta = -139.0$  ppm in toluene). PhenoFluor and phenol substrates react rapidly at room temperature to form uronium intermediates **5**, which then undergoes a first order transformation to aryl fluoride and urea **4**. A better Hammett correlation was obtained when  $\sigma$  (Figure 21) rather than  $\sigma^-$  values (Figure 22) for the X substituents were used, which is in line with the proposal that minimal delocalization of negative charge on to the arene occurs in the transition state. Hammett  $\sigma$  values are based upon the effect of substituents on the  $\text{pK}_a$  of benzoic acids and therefore only include the electronic effect of the substituent that is transmitted *via* the  $\sigma$ -framework of the arene. The  $\sigma^-$  scale, on the other hand, is based on the ionization of para-substituted phenols and includes resonance (de)stabilization effects of the substituent transmitted *via* the  $\pi$ -framework of the arene.<sup>181,182</sup>

$$\log(k_{\text{ArX}}) - \log(k_{\text{ArH}}) = \sigma * \rho$$

para-	$\sigma$	$\sigma^-$
$\text{NO}_2$	0.78	1.27
$\text{C(O)Me}$	0.5	0.874
Br	0.23	0.23
H	0	0
Me	-0.17	-0.17
OMe	-0.27	-0.27
$\text{NH}_2$	-0.66	-0.66

A)

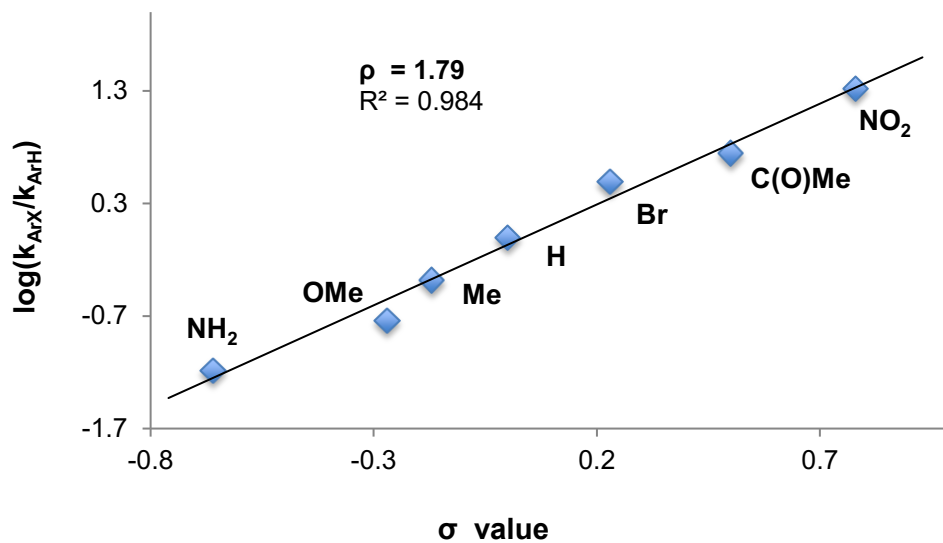


Figure 21: Hammett correlation using the  $\sigma$ -value of the para-substituent of the phenol.

B)

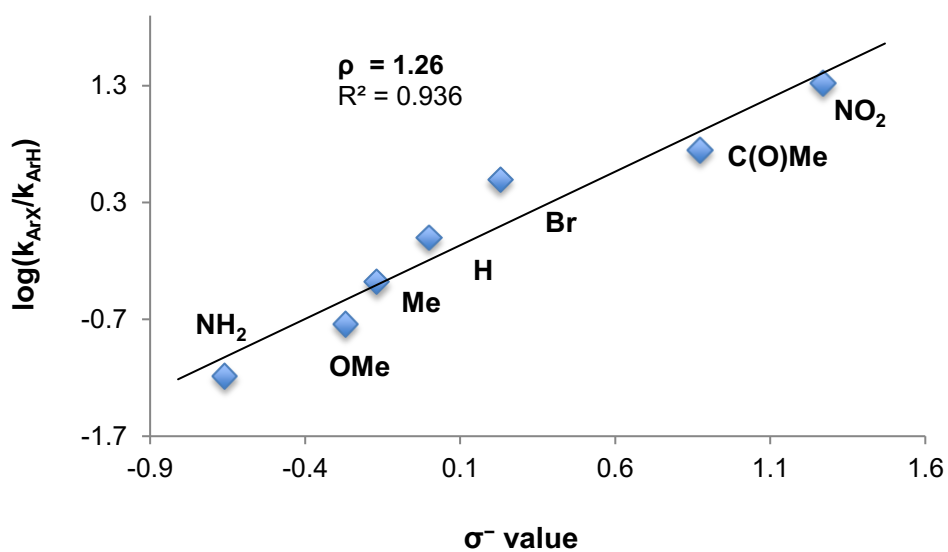


Figure 22: Hammett correlation using the  $\sigma^-$ -value of the para-substituent of the phenol.

### Eyring Plots

Rate constants for the deoxyfluorination of phenol, 4-cyanophenol, 4-trifluoromethylphenol, 4-nitrophenol and trimethylsiloxybenzene were measured at a variety

of temperatures by following aryl fluoride formation by  $^{19}\text{F}$ -NMR. 1,4-Difluorobenzene ( $\delta = -139.0$  ppm in toluene) was used as an internal standard and yields were determined by comparing the integration of the aryl fluoride signal to the integration of the internal standard. Chemical shifts of aryl fluoride products: fluorobenzene ( $\delta = -113.1$  ppm in toluene), 4-fluorobenzonitrile ( $\delta = -103.4$  ppm in toluene), 4-trifluoromethylfluorobenzene ( $\delta = -107.2$  ppm in toluene), 4-nitrofluorobenzene ( $\delta = -103.2$  ppm in toluene).

$$\ln(k/T) = -\Delta H^\ddagger/R \times 1/T + \ln(k_B/h) + \Delta S^\ddagger/R$$

$k_B$  ..... Planck's constant

$R$  ..... gas constant

$\Delta H^\ddagger$  was determined from the slope and  $\Delta S^\ddagger$  was determined from the intercept of a plot of  $\ln(k/T)$  versus  $1/T$ .  $\Delta G^\ddagger$  was determined from the reaction rate at 383 K, which was derived from the trendline of the Eyring plot. An error analysis was performed for  $\Delta H^\ddagger$ ,  $\Delta S^\ddagger$  and  $\Delta G^\ddagger$  using a 95% confidence interval.

Phenol:

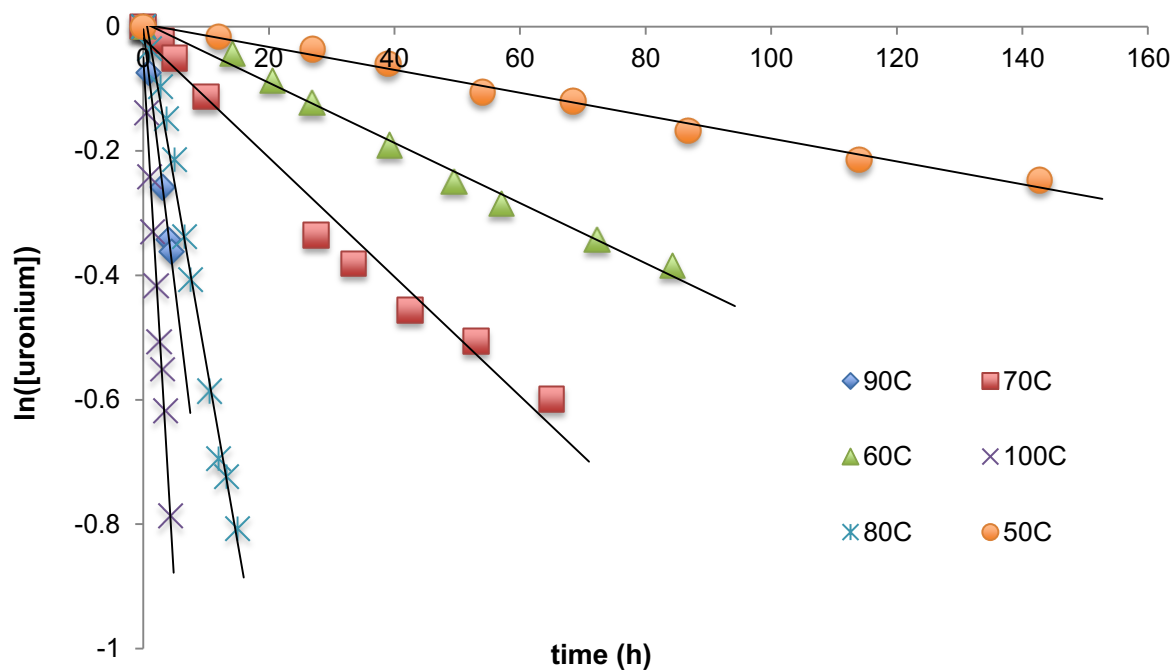


Figure 23: Rates for the deoxyfluorination of phenol at a range of temperatures.

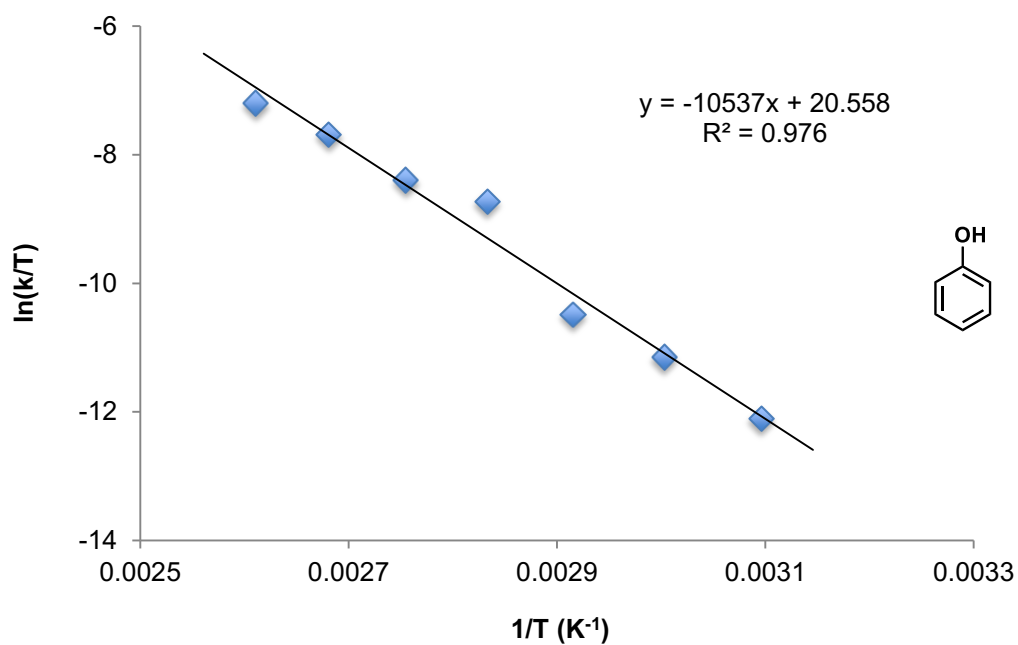


Figure 24: Eyring plot for phenol.

$$\Delta H^\ddagger = 20.9 \pm 3.8 \text{ kcal}\cdot\text{mol}^{-1}$$

$$\Delta S^\ddagger = -6.4 \pm 11 \text{ cal}\cdot\text{K}^{-1}\cdot\text{mol}^{-1}$$

$$\Delta G^\ddagger (110 \text{ }^\circ\text{C}) = 23.4 \pm 0.19 \text{ kcal}\cdot\text{mol}^{-1}$$

#### 4-cyanophenol:

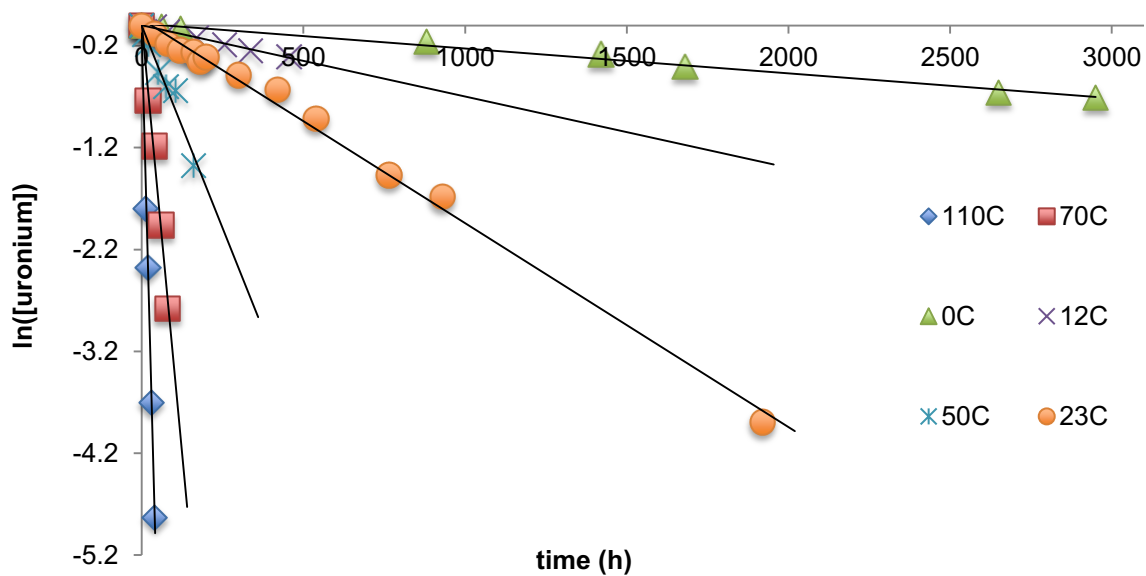
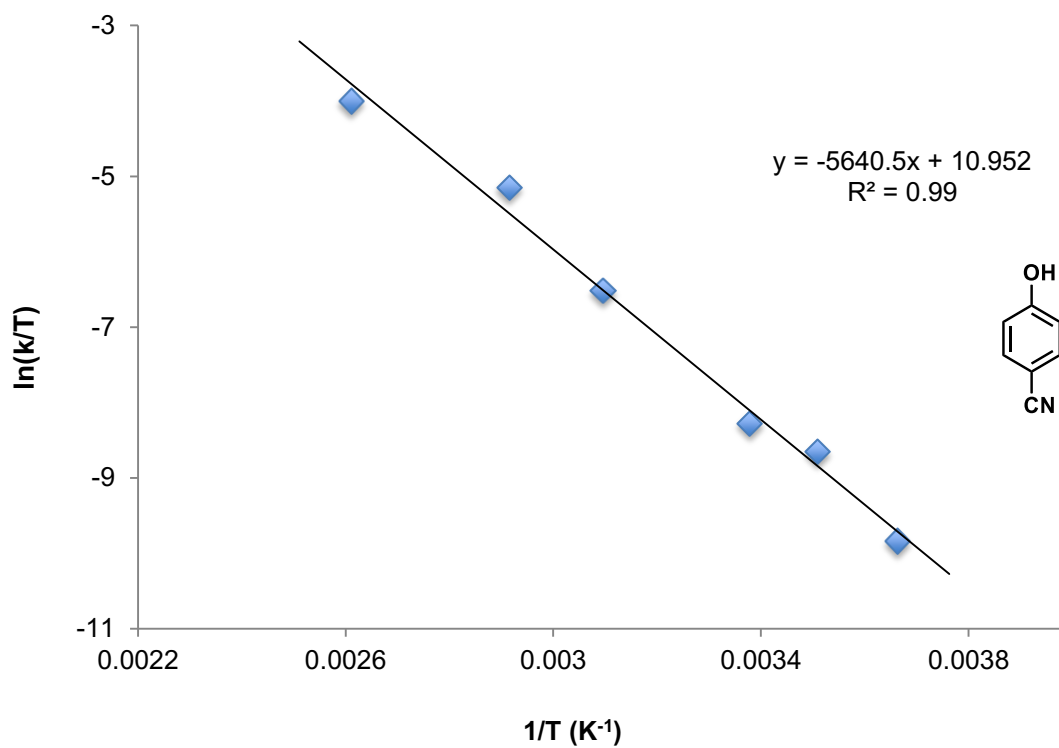


Figure 25: Rates for the deoxyfluorination of 4-cyanophenol at a range of temperatures.



**Figure 26:** Eyring plot for 4-cyanophenol.

$$\Delta H^\ddagger = 11.2 \pm 1.6 \text{ kcal}\cdot\text{mol}^{-1}$$

$$\Delta S^\ddagger = -25.5 \pm 5.0 \text{ cal}\cdot\text{K}^{-1}\cdot\text{mol}^{-1}$$

$$\Delta G^\ddagger (110 \text{ }^\circ\text{C}) = 21.0 \pm 0.16 \text{ kcal}\cdot\text{mol}^{-1}$$

4-nitrophenol:

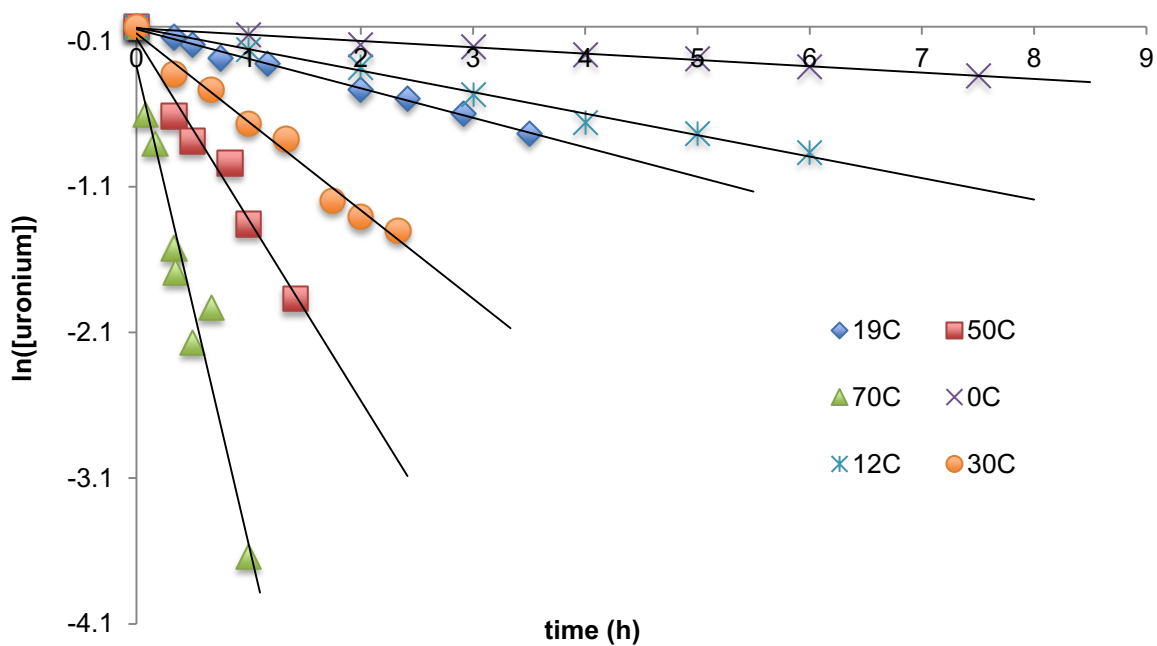


Figure 27: Rates for the deoxyfluorination of 4-nitrophenol at a range of temperatures.

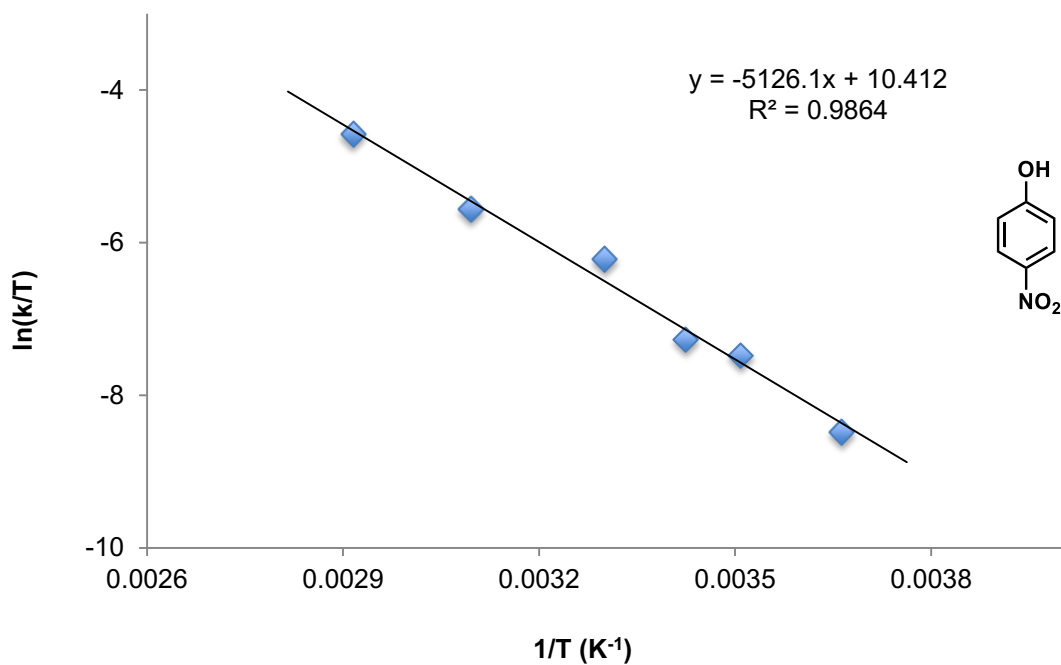


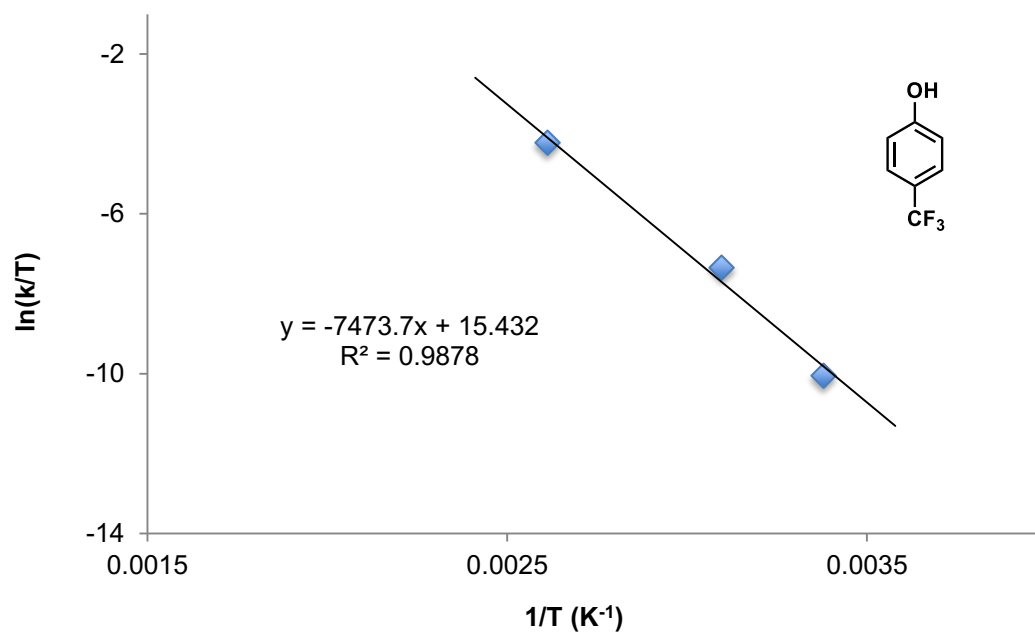
Figure 28: Eyring plot for 4-nitrophenol.

$$\Delta H^\ddagger = 10.2 \pm 1.6 \text{ kcal}\cdot\text{mol}^{-1}$$

$$\Delta S^\ddagger = -26.5 \pm 5.5 \text{ cal}\cdot\text{K}^{-1}\cdot\text{mol}^{-1}$$

$$\Delta G^\ddagger (110 \text{ }^\circ\text{C}) = 20.3 \pm 0.10 \text{ kcal}\cdot\text{mol}^{-1}$$

#### 4-Trifluoromethylphenol



**Figure 29:** Eyring plot for 4-trifluoromethylphenol.

$$\Delta G^\ddagger (110 \text{ }^\circ\text{C}) = 21.2 \pm 0.51 \text{ kcal}\cdot\text{mol}^{-1}$$



### Trimethylsilylphenoxide

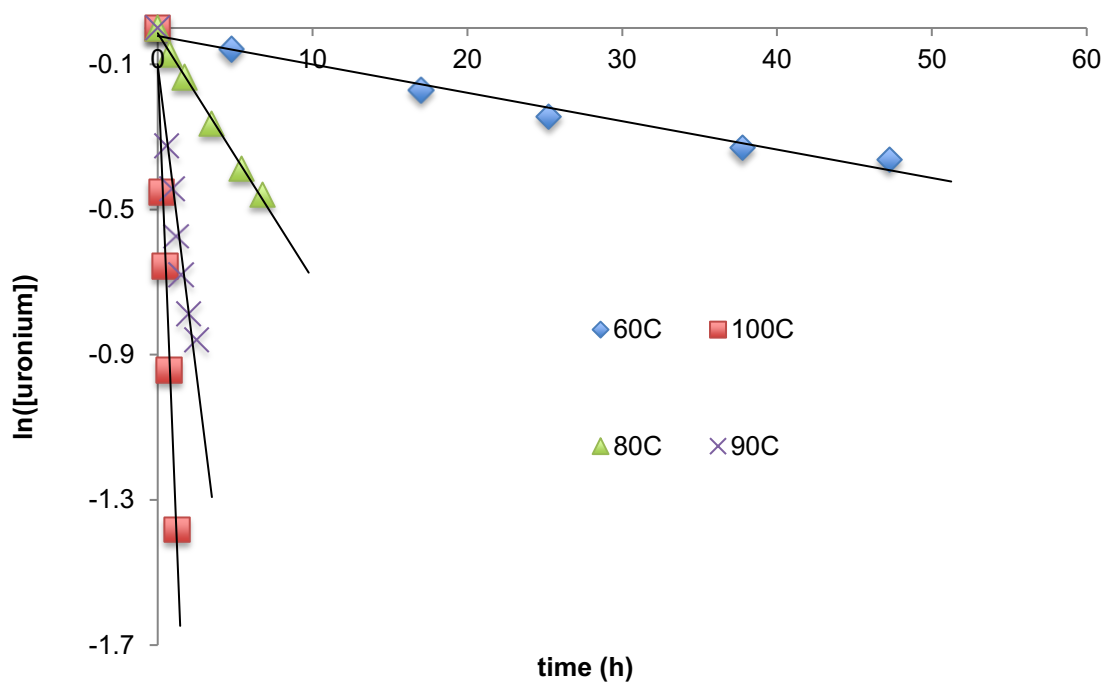


Figure 30: Rates for the deoxyfluorination of trimethylsilylphenoxide at a range of temperatures.

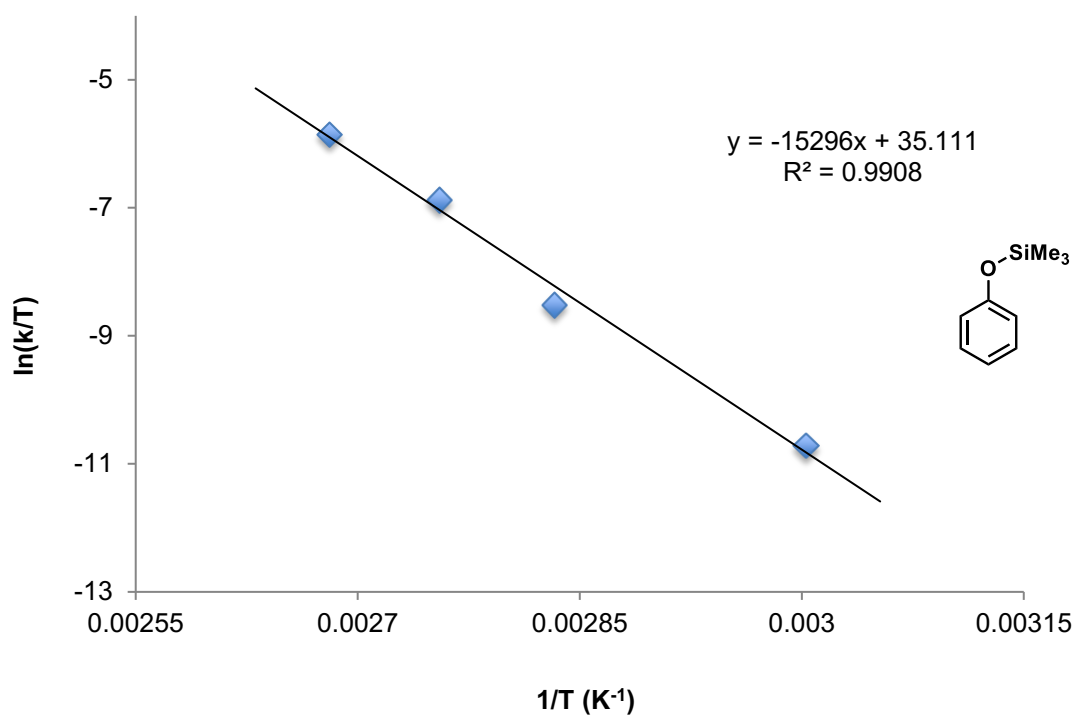


Figure 31: Eyring plot for trimethylsilylphenoxide.

$$\Delta H^\ddagger = 30.4 \pm 8.9 \text{ kcal}\cdot\text{mol}^{-1}$$

$$\Delta S^\ddagger = 22.6 \pm 25 \text{ cal}\cdot\text{K}^{-1}\cdot\text{mol}^{-1}$$

$$\Delta G^\ddagger (110 \text{ }^\circ\text{C}) = 21.8 \pm 0.23 \text{ kcal}\cdot\text{mol}^{-1}$$

**Table 2:** Experimental thermodynamic data for a range of phenol derivatives.



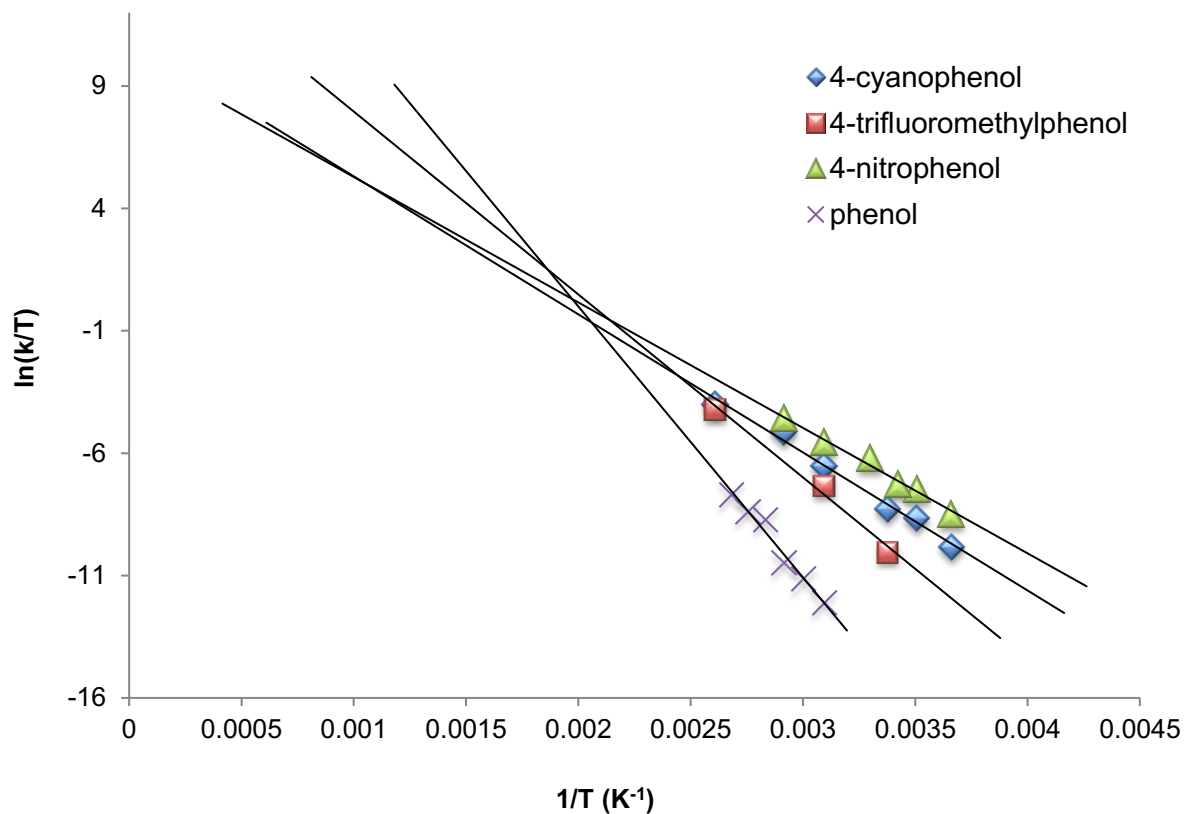
$\Delta G^\ddagger$ (kcal·mol <sup>-1</sup> )	23.4 ± 0.19	21.0 ± 0.16	20.3 ± 0.10	21.8 ± 0.23
$\Delta H^\ddagger$ (kcal·mol <sup>-1</sup> )	20.9 ± 3.8	11.2 ± 1.6	10.2 ± 1.6	30.4 ± 8.9
$\Delta S^\ddagger$	- 6.36 ± 11	- 25.9 ± 5.0	- 26.5 ± 5.0	22.6 ± 25

### Isokinetic Relationship

When a series of structurally related substrates undergo the same reaction and the enthalpies and entropies of activation satisfy the relation

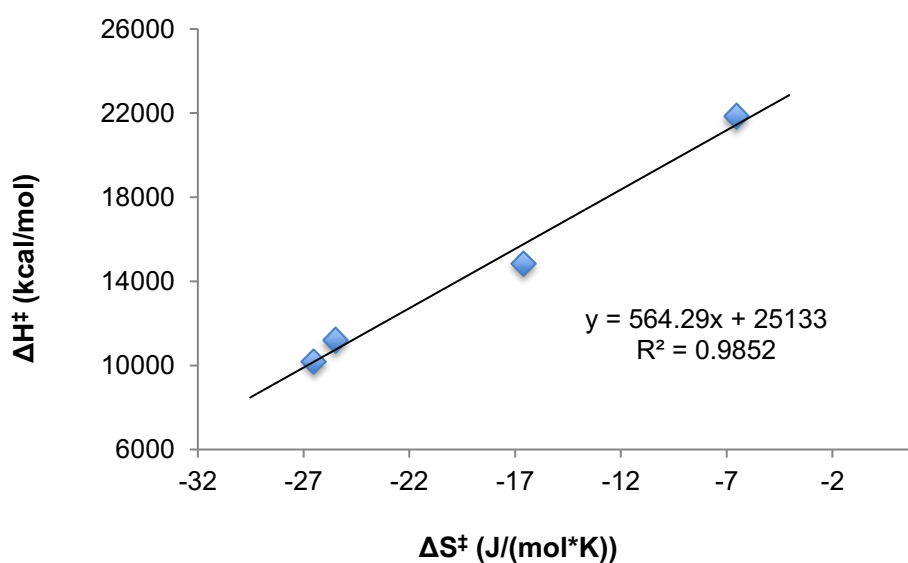
$$\Delta H^\ddagger = \beta \times \Delta S^\ddagger + \text{constant}$$

where  $\beta$  is a temperature-independent proportionality constant, the reaction is said to obey an isokinetic relationship. Direct correlation of  $\ln(k/T)$  versus  $T^{-1}$  is a more reliable indicator for the presence of an isokinetic relationship than a correlation between the enthalpies and entropies of activation. Values for  $\Delta H^\ddagger$  and  $\Delta S^\ddagger$  are interdependent because they are derived from the same set of reaction rate data, which means that when entropies and enthalpies of activation are plotted against one another, a spurious correlation may be observed between  $\Delta H^\ddagger$  and  $\Delta S^\ddagger$  that has no chemical significance. Because reaction rates were observed over a considerable temperature range, the intersection of the Eyring plots (Figure 32) and the linear enthalpy/entropy relationship (Figure 33) is likely to be meaningful and indicates presence of an isokinetic relationship.<sup>183</sup>



**Figure 32:** Isokinetic relationship for the deoxyfluorination of phenol.

The isokinetic temperature is 500 K from the intersection of the Eyring plots of the individual substrates.



**Figure 33:** Isokinetic relationship for the deoxyfluorination of phenols established *via* an enthalpy/entropy correlation.

Isokinetic temperature determined from the slope of an enthalpy/entropy correlation of phenol, 4-cyanophenol, 4-nitrophenol and 4-trifluoromethylphenol:  $\beta = 564$  K (Figure 33).

At  $T = \beta$ , the rates of all substrates comprised in the isokinetic relationship are the same, which can be verified by computing  $\Delta G^\ddagger$  for different members of the series at the isokinetic temperature (Table 3).

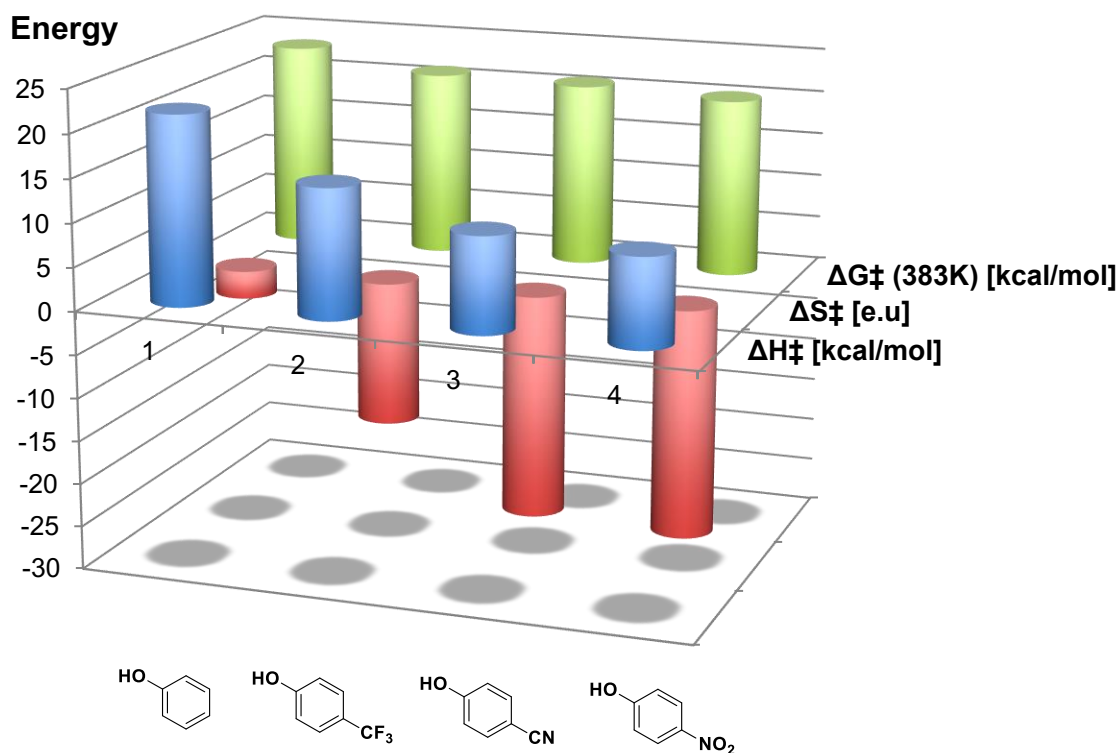
**Table 3:**  $\Delta G^\ddagger$  calculated from the trendline of the respective Eyring plots at the value for the isokinetic temperatures obtained from the intersection of Eyring plots, the value determined from the entropy/enthalpy correlation as well as at the average of the two values.

	$\Delta H^\ddagger$	$\Delta S^\ddagger$ (cal·K <sup>-1</sup> ·mol <sup>-1</sup> )	$\Delta G^\ddagger$ (564K)	$\Delta G^\ddagger$ (500K)	$\Delta G^\ddagger$ (533K)
Phenol	20.9	- 6.36	24.6	24.2	24.4
4-cyanophenol	11.2	- 25.4	25.6	23.9	24.8
4-nitrophenol	10.2	- 26.5	25.2	23.5	24.3
4-CF <sub>3</sub> -phenol	14.9	- 16.6	24.2	23.1	23.7

Above the isokinetic temperature the relative rates in a sequence of substrates are reversed, i.e. at  $T > \beta$  the deoxyfluorination of phenol proceeds at a faster rate than the deoxyfluorination of 4-nitrophenol. Given the reversal in relative rates of a sequence of substrates at the isokinetic temperature, Hammett  $\rho$ -values are dependent on the experimental temperature and decrease in value as the temperature approaches  $\beta$ .<sup>184,185</sup>

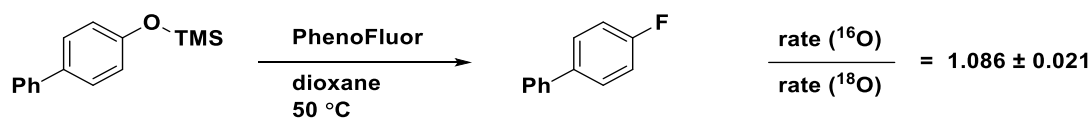
Since the isokinetic temperature is not far removed from the optimized reaction temperature for the PhenoFluor-mediated deoxyfluorination, the observed  $\rho$ -value is small. The small  $\beta$  and  $\rho$ -values are accountable for the wide substrate scope of the nucleophilic displacement in the sense that substantial enthalpy/entropy compensation decreases the effect on  $\Delta G^\ddagger$  originating from an increase in  $\Delta H^\ddagger$  as the phenol substrates become more electron-rich.

Despite the minimization of charge build-up on the arene during concerted nucleophilic substitution,  $\Delta H^\ddagger$  for the deoxyfluorination of phenols increases substantially in going from 4-nitrophenol to phenol (blue columns, Figure 34). For the same series, however,  $\Delta S^\ddagger$  becomes less negative (more favorable) as the arene becomes more electron-rich (red columns, Figure 34). The combination of those two trends leads to an only modest increase in  $\Delta G^\ddagger$  in going from 4-nitrophenol to phenol (green columns, Figure 34). Conventional  $S_NAr$  reactions, on the other hand, commonly have  $\rho$ -values between 3 and 8 and  $\Delta G^\ddagger$  increases rapidly as the arene substrates become more electron-rich.



**Figure 34:** Considerable enthalpy-entropy compensation leads to an only modest increase in  $\Delta G^\ddagger$  as the phenol substrates become more electron-rich.

## <sup>16</sup>O/<sup>18</sup>O Kinetic Isotope Effect

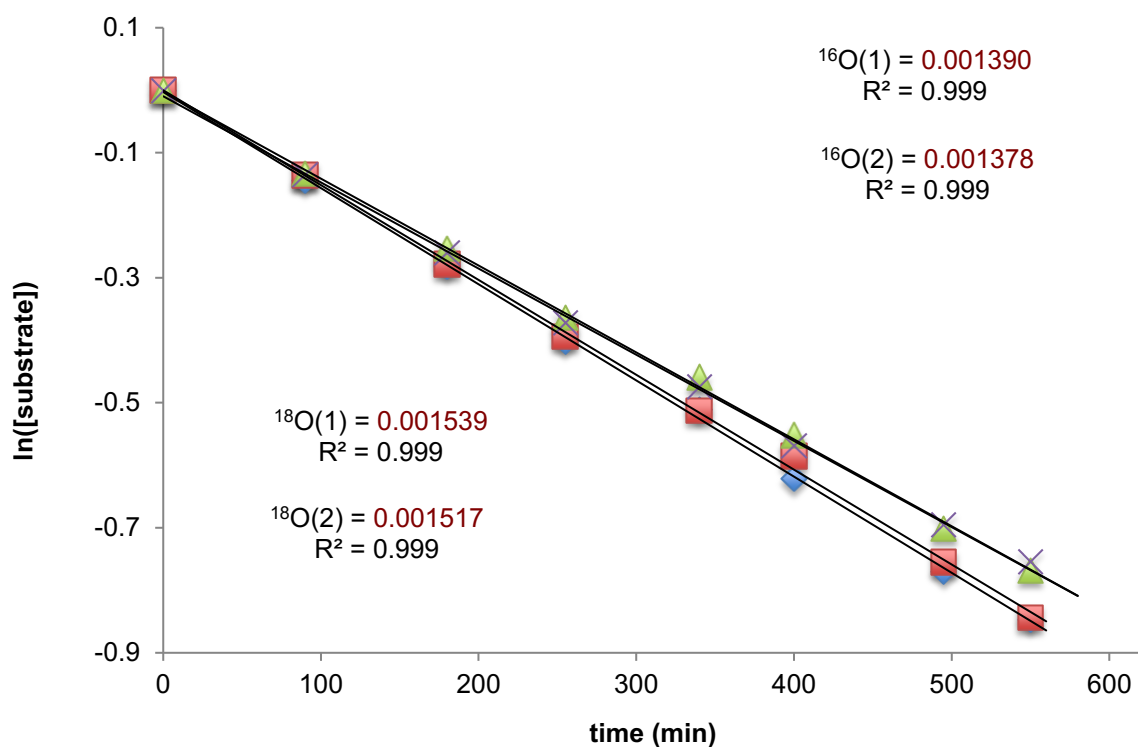


**Figure 35:** The primary kinetic isotope effect indicates that C–O bond cleavage occurs in the rate-determining step of the deoxyfluorination.

Deoxyfluorination of <sup>16</sup>O-([1,1'-biphenyl]-4-yloxy)trimethylsilane (100% isotopic purity) and <sup>18</sup>O-([1,1'-biphenyl]-4-yloxy)trimethylsilane (94% isotopic purity) with PhenoFluor was conducted and the reaction rates were determined by monitoring product formation by <sup>19</sup>F-NMR. The reaction conditions were modified compared to the standard reaction conditions in order to conduct the kinetic analysis of a homogenous solution. Through the use of the silylated phenol substrate, addition of CsF was not necessary for the achievement of acceptable reaction rates and high conversion. Tetrahedral intermediate **2** is formed directly when a silylated phenol is mixed with PhenoFluor, rather than being slowly released through the action of CsF, as is the case when phenols are utilized. 1,4-Difluorobenzene was used as an internal standard to determine the reaction conversion. As the reaction progresses, 1,4-difluorobenzene (internal standard, <sup>19</sup>F-NMR  $\delta = -139.0$  ppm in dioxane), 4-phenylfluorobenzene ( $\delta = -116.3$  ppm), PhenoFluor ( $\delta = -33.9$  ppm) as well as tetrahedral intermediate **6** ( $\delta = -12.9$  ppm) were observed by <sup>19</sup>F-NMR.

In a dry box, <sup>16</sup>O-([1,1'-biphenyl]-4-yloxy)trimethylsilane (31.0 mg, 0.128 mmol, 1.00 equiv) or <sup>18</sup>O-([1,1'-biphenyl]-4-yloxy)trimethylsilane (31.2 mg, 0.128 mmol, 1.00 equiv), PhenoFluor (60.0 mg, 0.141 mmol, 1.10 equiv) and 1,4-difluorobenzene (12.6  $\mu$ l, 0.128 mmol, 1.00 equiv) were dissolved in dioxane (9.0 ml). After vigorous shaking of the reaction vial, 2 ml of the reaction mixture were transferred into a dried NMR tube. A further 2 ml of the reaction mixture was added to another NMR tube and the NMR tubes were fitted with a screw cap. Four NMR tubes, two of which containing the reaction mixture for the deoxyfluorination of <sup>16</sup>O-([1,1'-biphenyl]-4-yloxy)trimethylsilane and two containing the reaction mixture for the

deoxyfluorination of  $^{18}\text{O}$ -([1,1'-biphenyl]-4-yloxy)trimethylsilane were removed from the dry box and heated at 50 °C in an oil bath. At regular intervals, the NMR tubes were removed from heat and  $^{19}\text{F}$ -NMR spectra were acquired to analyze the reaction progress. Yields of the deoxyfluorination reaction at each given time point was determined by comparing the peak area of the  $^{19}\text{F}$ -NMR signal corresponding to the fluorinated reaction product (4-phenyl-fluorobenzene,  $^{19}\text{F}$ -NMR signal at  $-116.3$  ppm in dioxane) to that of the internal standard (1,4-difluorobenzene,  $^{19}\text{F}$ -NMR signal at  $-139.0$  ppm in dioxane). The isotopic purity of the  $^{18}\text{O}$ -labeled starting material was established by comparing the GCMS trace of  $^{18}\text{O}$ -([1,1'-biphenyl]-4-yloxy)trimethylsilane to that of  $^{16}\text{O}$ -([1,1'-biphenyl]-4-yloxy)trimethylsilane.



**Figure 36:** Deoxyfluorination rates for  $^{16}\text{O}$  and  $^{18}\text{O}$  substrate (see Figure 35), experiment 1.

$^{16}\text{O}$ -phenol substrate

$$k_1 = 0.001539 \text{ min}^{-1} \text{ (sample 1)}$$

$$k_2 = 0.001517 \text{ min}^{-1} \text{ (sample 2)}$$

$$\text{average: } 0.001528 \text{ min}^{-1}$$

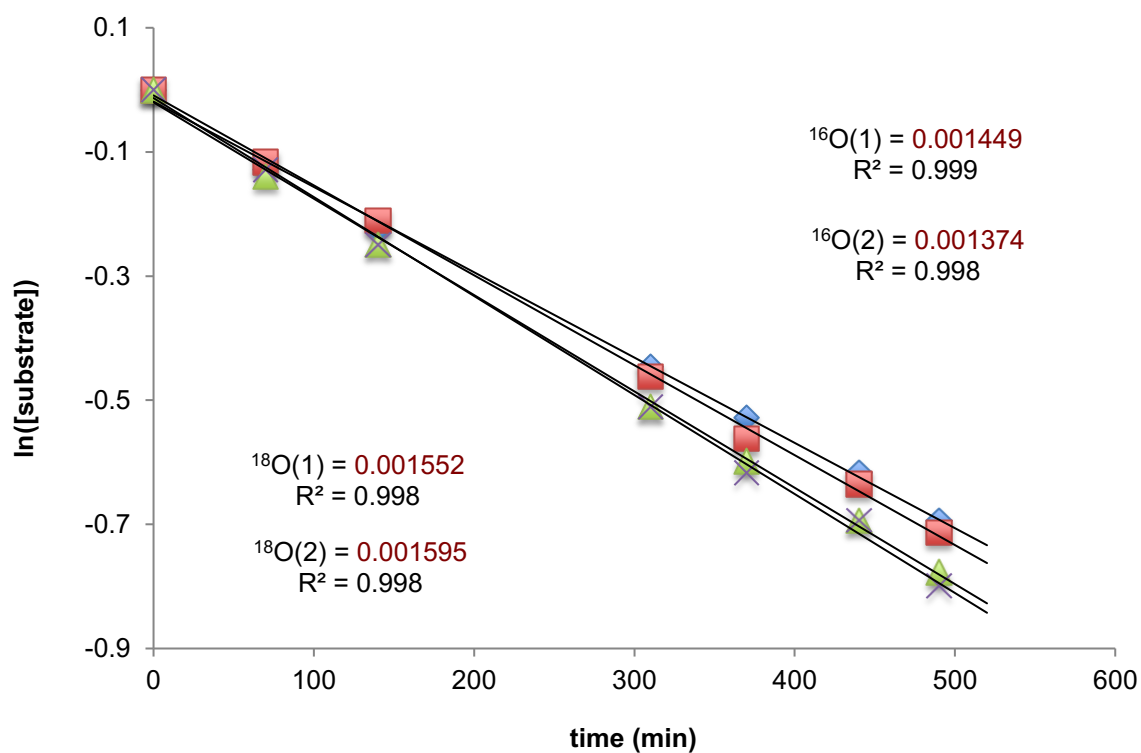
<sup>18</sup>O-phenol substrate

$$k_1 = 0.001390 \text{ min}^{-1} \text{ (sample 1)}$$

$$k_2 = 0.001378 \text{ min}^{-1} \text{ (sample 2)}$$

$$\text{average: } 0.001384 \text{ min}^{-1}$$

⇒ rate ratio: 1.104



**Figure 37:** Deoxyfluorination rates for <sup>16</sup>O and <sup>18</sup>O substrate (see Figure 35), experiment 2.

<sup>16</sup>O-phenol substrate

$$k_1 = 0.001552 \text{ min}^{-1} \text{ (sample 1)}$$

$$k_2 = 0.001595 \text{ min}^{-1} \text{ (sample 2)}$$

$$\text{average: } 0.0015735 \text{ min}^{-1}$$

<sup>18</sup>O-phenol substrate

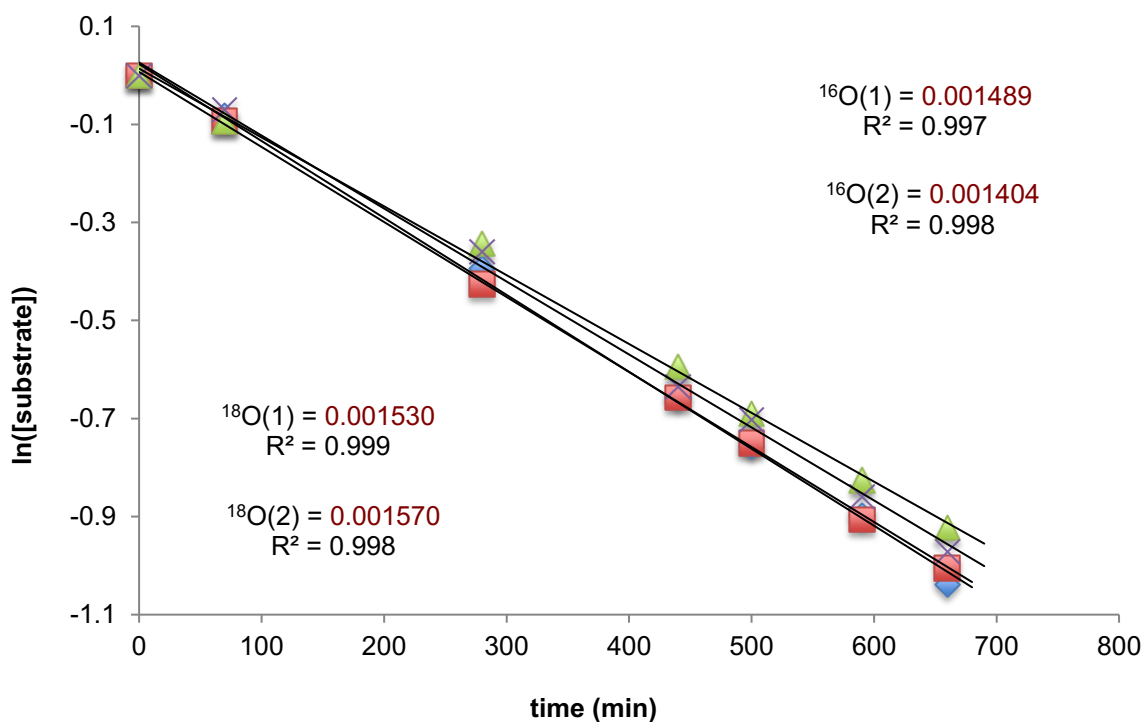
$$k_1 = 0.001449 \text{ min}^{-1} \text{ (sample 1)}$$



$$k_2 = 0.001374 \text{ min}^{-1} \text{ (sample 2)}$$

$$\text{average: } 0.0014115 \text{ min}^{-1}$$

⇒ rate ratio: 1.115



**Figure 38:** Deoxyfluorination rates for  $^{16}\text{O}$  and  $^{18}\text{O}$  substrate (see Figure 35), experiment 3.

$^{16}\text{O}$ -phenol substrate

$$k_1 = 0.001530 \text{ min}^{-1} \text{ (sample 1)}$$

$$k_2 = 0.001570 \text{ min}^{-1} \text{ (sample 2)}$$

$$\text{average: } 0.001550 \text{ min}^{-1}$$

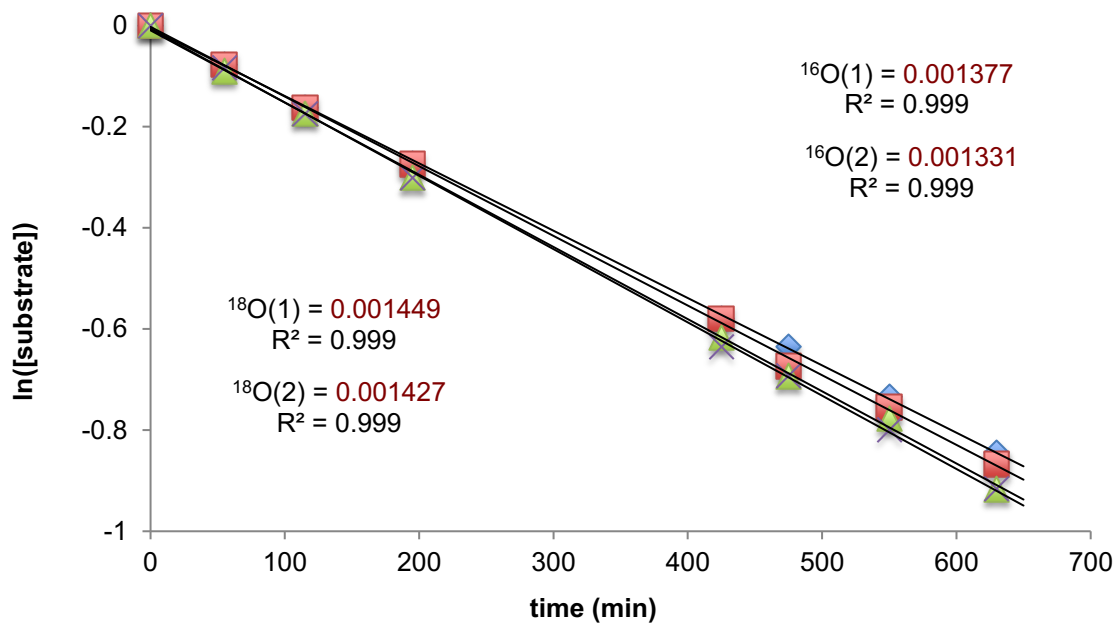
$^{18}\text{O}$ -phenol substrate

$$k_1 = 0.001480 \text{ min}^{-1} \text{ (sample 1)}$$

$$k_2 = 0.001404 \text{ min}^{-1} \text{ (sample 2)}$$

$$\text{average: } 0.001442 \text{ min}^{-1}$$

⇒ rate ratio: 1.075



**Figure 39:** Deoxyfluorination rates for <sup>16</sup>O and <sup>18</sup>O substrate (see Figure 35), experiment 4.

<sup>16</sup>O-phenol substrate

$$k_1 = 0.001449 \text{ min}^{-1} \text{ (sample 1)}$$

$$k_2 = 0.001427 \text{ min}^{-1} \text{ (sample 2)}$$

$$\text{average: } 0.001438 \text{ min}^{-1}$$

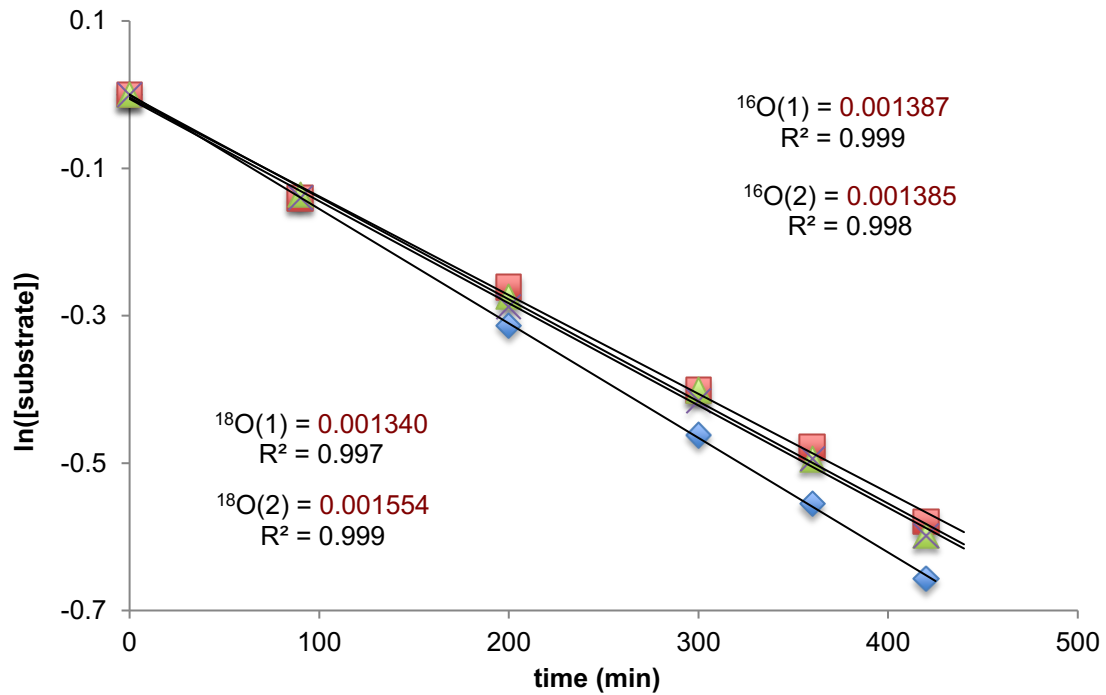
<sup>18</sup>O-phenol substrate

$$k_1 = 0.001377 \text{ min}^{-1} \text{ (sample 1)}$$

$$k_2 = 0.001331 \text{ min}^{-1} \text{ (sample 2)}$$

$$\text{average: } 0.001354 \text{ min}^{-1}$$

⇒ rate ratio: 1.062



**Figure 40:** Deoxyfluorination rates for  $^{16}\text{O}$  and  $^{18}\text{O}$  substrate (see Figure 35), experiment 5.

$^{16}\text{O}$ -phenol substrate

$$k_1 = 0.001554 \text{ min}^{-1} \text{ (sample 1)}$$

$$k_2 = 0.001340 \text{ min}^{-1} \text{ (sample 2)}$$

$$\text{average: } 0.001447 \text{ min}^{-1}$$

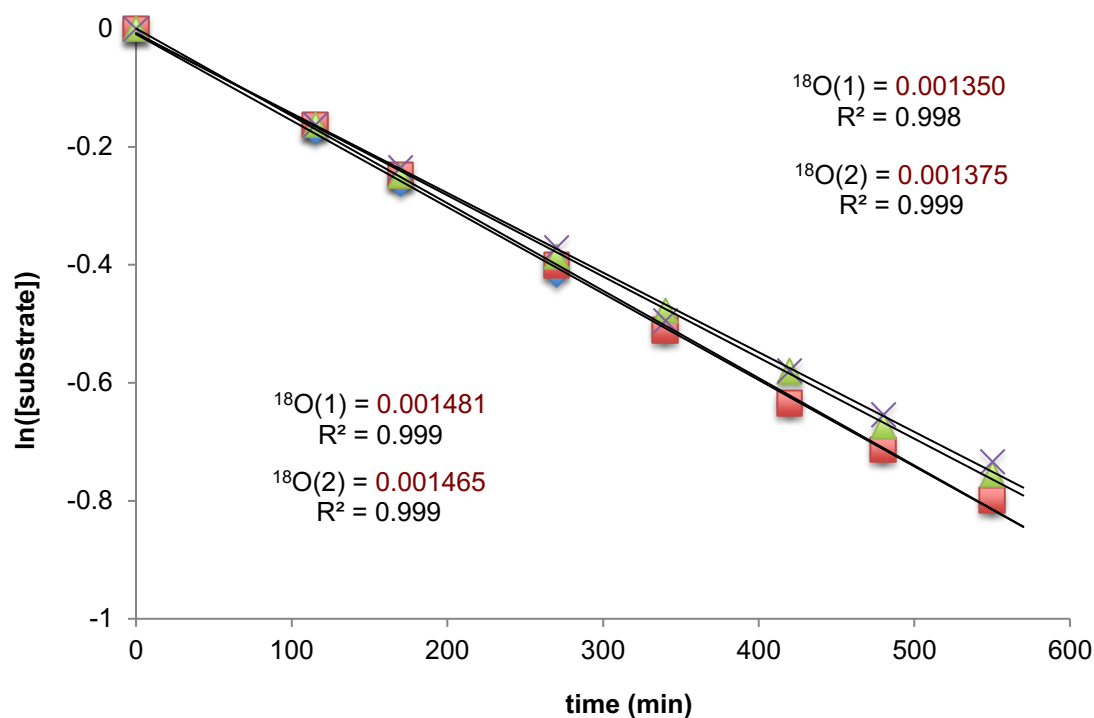
$^{18}\text{O}$ -phenol substrate

$$k_1 = 0.001387 \text{ min}^{-1} \text{ (sample 1)}$$

$$k_2 = 0.001385 \text{ min}^{-1} \text{ (sample 2)}$$

$$\text{average: } 0.001386 \text{ min}^{-1}$$

⇒ rate ratio: 1.044



**Figure 41:** Deoxyfluorination rates for  $^{16}\text{O}$  and  $^{18}\text{O}$  substrate (see Figure 35), experiment 6.

$^{16}\text{O}$ -phenol substrate

$$k_1 = 0.001481 \text{ min}^{-1} \text{ (sample 1)}$$

$$k_2 = 0.001465 \text{ min}^{-1} \text{ (sample 2)}$$

$$\text{average: } 0.001473 \text{ min}^{-1}$$

$^{18}\text{O}$ -phenol substrate

$$k_1 = 0.001350 \text{ min}^{-1} \text{ (sample 1)}$$

$$k_2 = 0.001375 \text{ min}^{-1} \text{ (sample 2)}$$

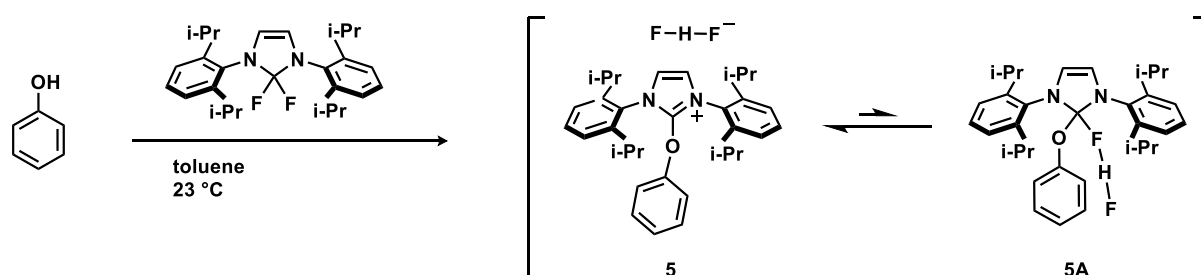
$$\text{average: } 0.0013625 \text{ min}^{-1}$$

⇒ rate ratio: 1.081

The ratio of rates of deoxyfluorination rates for  $^{16}\text{O}$ -([1,1'-biphenyl]-4-yloxy)trimethylsilane and  $^{18}\text{O}$ -([1,1'-biphenyl]-4-yloxy)trimethylsilane is  $1.080 \pm 0.021$ . Reactions of  $^{16}\text{O}$ -([1,1'-biphenyl]-4-yloxy)trimethylsilane and  $^{18}\text{O}$ -([1,1'-biphenyl]-4-yloxy)trimethylsilane were run side-by-side, in duplicate, and the ratio of rates was averaged over six experiments.

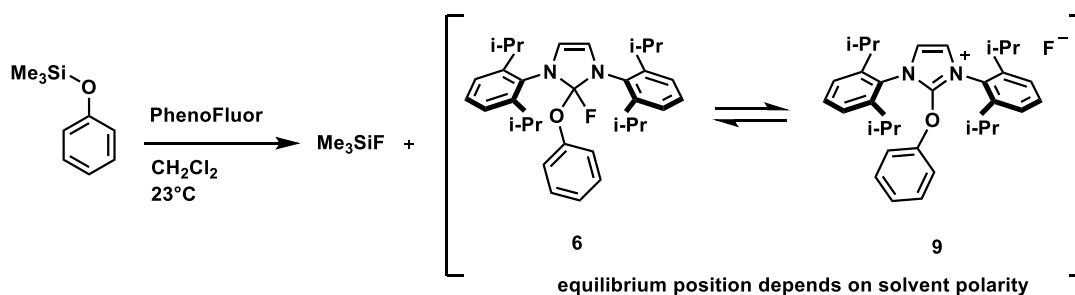
## Tetrahedral adduct 6

By DFT, minima for 4 tetrahedral adducts and uronium species were found; the HF<sub>2</sub> tetrahedral adduct **5A** could not be observed experimentally because the equilibrium is heavily biased towards uronium **5** (Figure 42). By DFT (B3LYP/6-311++G(d,p), uronium **5** was found to be 4.0 kcal/mol lower in energy than HF<sub>2</sub> tetrahedral adduct **5A**.



**Figure 42:** Synthesis of uronium **5**.

With a fluoride counteranion, the equilibrium position favors either tetrahedral adduct **6** or uronium fluoride **9**, depending on the polarity of the solvent. Tetrahedral adduct **6** could be formed essentially quantitatively in benzene; <sup>1</sup>H-NMR analysis shows small amounts of urea **4** as the only side product (PhenoFluor is hydrolyzed to urea **4** in the presence of water). When the sample is evaporated under reduced pressure and a second <sup>1</sup>H-NMR spectrum is recorded in CD<sub>2</sub>Cl<sub>2</sub>, only uronium **9** was observed. Uronium **9** was also observed by NMR when PhenoFluor and trimethylsilylphenoxide were mixed in CD<sub>2</sub>Cl<sub>2</sub> (Figure 43). When CD<sub>2</sub>Cl<sub>2</sub> is removed, however, and the sample is dissolved in benzene-*d*<sub>6</sub> or toluene-*d*<sub>8</sub>, tetrahedral adduct **6** is observed by <sup>1</sup>H-NMR. If the sample is dissolved in acetone-*d*<sub>6</sub>, MeCN-*d*<sub>3</sub> or DMSO-*d*<sub>6</sub>, on the other hand, only uronium **9** could be detected by <sup>1</sup>H-NMR. Tetrahedral adduct **6** was also found to be stable in Et<sub>2</sub>O-*d*<sub>10</sub>, but the poor solubility of **6** rendered this solvent less practical for NMR experiments than benzene-*d*<sub>6</sub> or toluene-*d*<sub>8</sub>. The equilibrium position is also shifted from **6** to **9** when more electron-rich phenols are used.



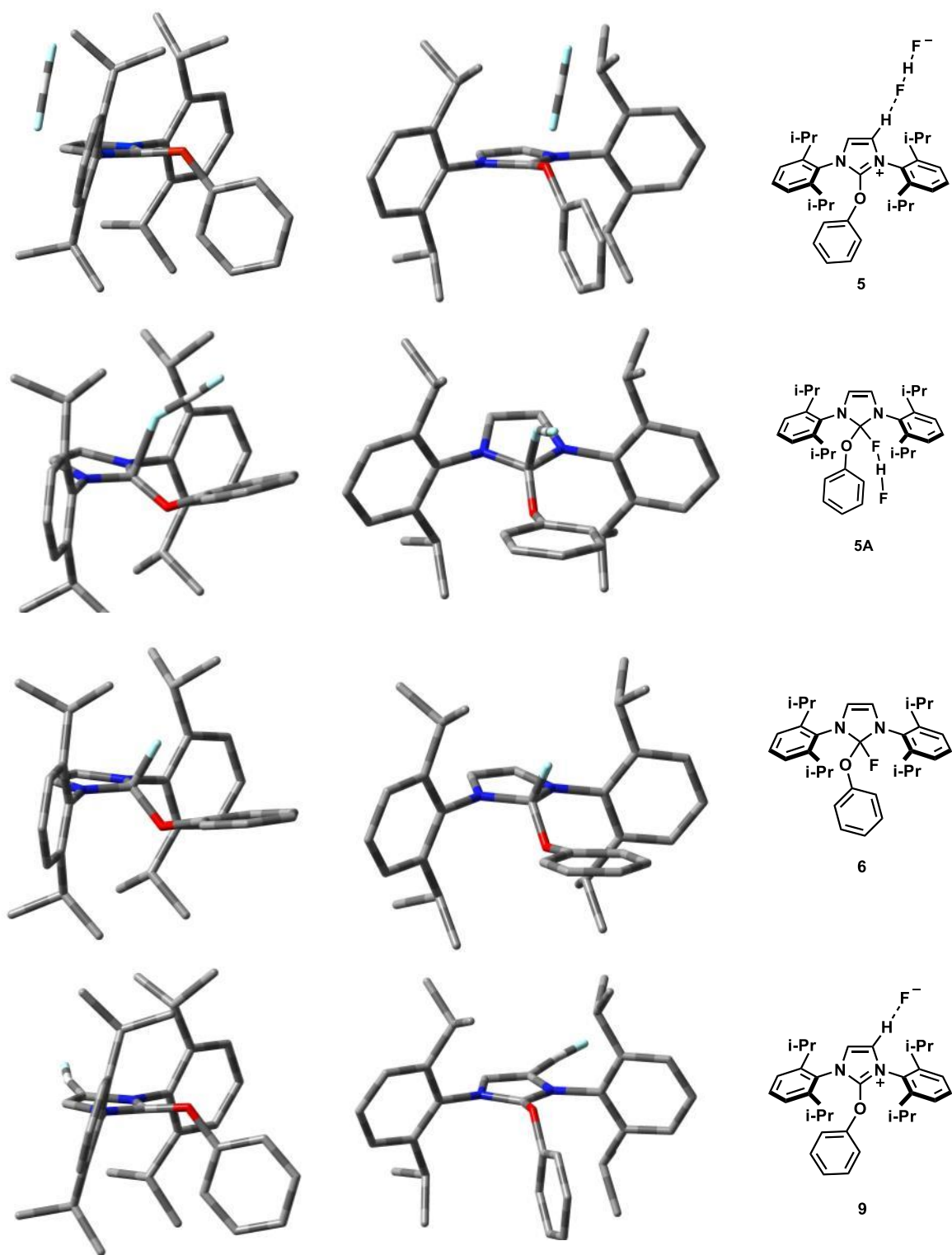
**Figure 43:** Synthesis of tetrahedral adduct **6**.

We have observed the presence of a combination of tetrahedral adduct **6** and uronium fluoride **9** in a 3:1 ratio at room temperature in dioxane. Both signals appear at chemical shifts comparable to the pure uronium fluoride and tetrahedral adducts observed in other solvents and upon raising the temperature of the solution to 50°C, no appreciable broadening or coalescence of the signals was observed. The lack of signal broadening or coalescence suggest that, at least in dioxane, spectra were acquired in the slow exchange regime. To exclude that differing rates of exchange in other solvents under discussion would mask a spectrum averaged through chemical exchange, we acquired NMR data in a 10:1 mixture of benzene-*d*<sub>6</sub> and CD<sub>2</sub>Cl<sub>2</sub>: a 1:10 mixture of tetrahedral adduct and uronium fluoride was observed. We have found that there exists a good correlation between the dielectric constant of the solvent and the concentration of tetrahedral adduct **6** and uronium fluoride **9** present in solution (Table 4).

**Table 4:** Correlation between the dielectric constant of the solvent and the predominant species observed in solution. The very limited solubility of the uronium species in diethylether may explain this apparent divergence from the expected trend. Precipitate was detected at the bottom of the NMR tube during the experiment.

Solvent	$\epsilon$ (for the non-deuterated solvent)	Species observed
DMSO-d <sub>6</sub>	47.2	<b>9</b>
MeCN-d <sub>3</sub>	37.5	<b>9</b>
Acetone-d <sub>6</sub>	20.7	<b>9</b>
CD <sub>2</sub> Cl <sub>2</sub>	8.93	<b>9</b>
Et <sub>2</sub> O-d <sub>10</sub>	4.33	<b>6</b>
Toluene-d <sub>8</sub>	2.38	<b>6</b>
Benzene-d <sub>6</sub>	2.27	<b>6</b>
Dioxane	2.25	<b>9 : 6 = 1 : 3</b>
CD <sub>2</sub> Cl <sub>2</sub> : Benzene-d <sub>6</sub> = 1 : 10		<b>9 : 6 = 10 : 1</b>

Under the standard conditions for PhenoFluor-mediated deoxyfluorination, uronium **5** is the observed species and conversion of the bifluoride to the fluoride counteranion occurs slowly under the influence of the poorly added CsF base. Tetrahedral adduct **6** or uronium **9** were only observed when a fluoride scavenger is added to the reaction. Given the instability of tetrahedral adduct **6** and the slow anion exchange of PhenoFluor derived uronium ions (see section 'The Role of CsF'), we believe the slow formation of **6** from **5** is crucial for the extension of the substrate scope to electron-rich substrates. Under the reaction conditions used for the <sup>18</sup>F-deoxyfluorination, tetrahedral adduct **6** is formed directly rather than through slow release from uronium **5** under the influence of a base. The limited stability of tetrahedral adduct **6** in the case of electron-rich phenols is therefore the likely cause why such substrates fail to incorporate <sup>18</sup>F.



**Figure 44:** Structures for tetrahedral intermediates and uronium species (B3LYP/6-311++G(d,p), toluene continuous solvent model). Hydrogens not involved in hydrogen bonds to fluoride were omitted for clarity.

The stability of tetrahedral adduct **6** was studied in various solvents and rapid decay to urea



**4** was observed in many cases. The activation barrier for the transformation of tetrahedral adduct **6** to aryl fluoride and urea **4** in toluene was obtained by studying the rate of fluorobenzene formation from trimethylsilylphenoxide at a range of temperatures (see Section on Eyring plots, page 49):

$$\Delta G^\ddagger (110\text{ }^\circ\text{C}) = 21.8 \pm 0.23 \text{ kcal}\times\text{mol}^{-1}$$

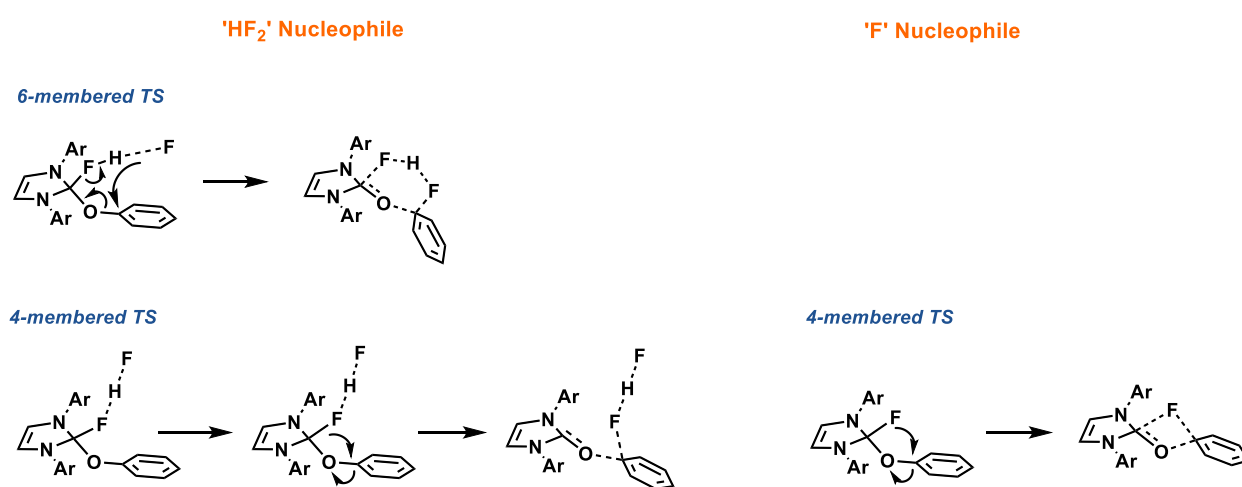
The corresponding activation barrier for PhenoFluor mediated deoxyfluorination of phenol at 110 °C:

$$\Delta G^\ddagger (110\text{ }^\circ\text{C}) = 23.4 \pm 0.19 \text{ kcal}\times\text{mol}^{-1}.$$

## Role of added CsF

### Fluoride versus bifluoride pathway

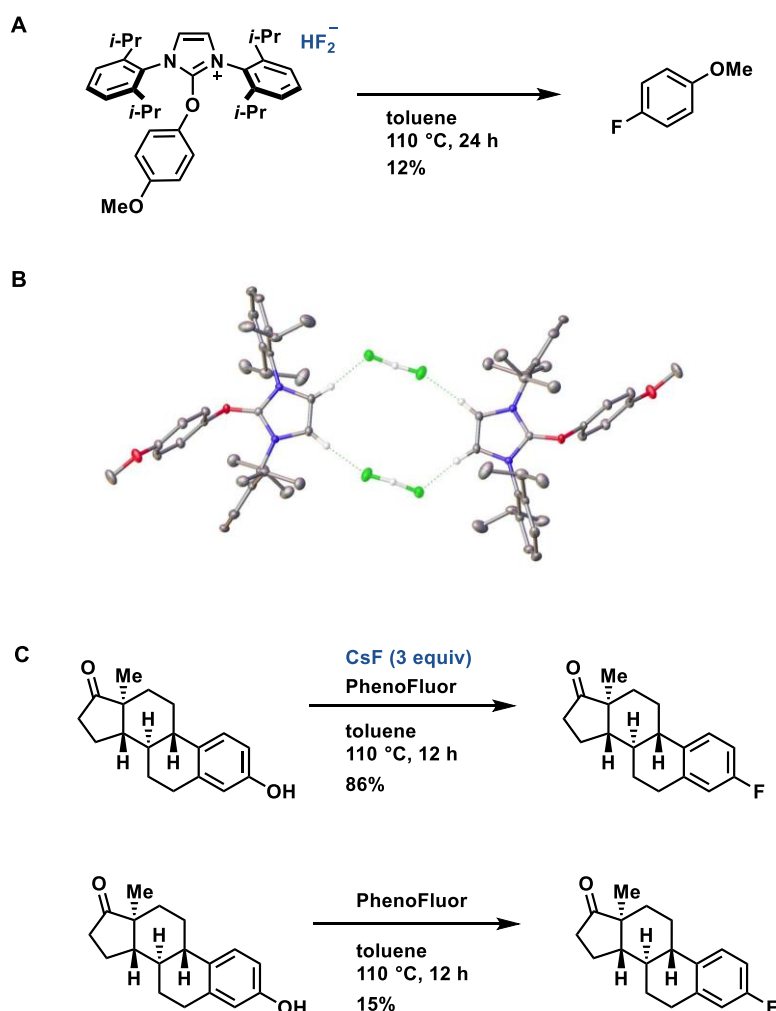
The optimized conditions for PhenoFluor mediated deoxyfluorination of phenols include 2 equivalents of fluoride contained in the reagent as well as 3 equivalents of additional CsF. The origin of the fluoride atom incorporated into the aryl fluoride product was therefore unclear at the outset of the mechanistic investigation and three generalized mechanistic schemes were considered. Upon formation of uronium intermediate **5** the two fluoride atoms originally bound to PhenoFluor reagent are part of the bifluoride counteranion of the uronium intermediate. Fluorination could thus proceed with either the bifluoride counteranion or the added cesium fluoride acting as the nucleophile. By DFT, energy minima for tetrahedral intermediates containing either bifluoride or fluoride could be localized and the fluoride containing tetrahedral intermediate **6** could also be observed experimentally.



**Figure 45:** Generalized mechanism for deoxyfluorination.

If bifluoride acted as the nucleophile in the deoxyfluorination reaction, conversion of the tetrahedral adduct to aryl fluoride and urea **4** could conceivably occur *via* either a four- or a six-membered transition state. For a fluoride nucleophile, only a four-membered transition state is possible for a concerted pathway. DFT reaction coordinates could be obtained both for a fluoride-mediated reaction and a bifluoride mediated reaction proceeding via a 4-

membered transition state. All attempts to localize a transition state structure for a six-membered transition state with a bifluoride nucleophile failed. We attempted to localize such a transition state using a scan of the potential energy surface, QST2 and QST3 calculations as well as optimizations of several reasonable guesses for the transition state, but in all cases the calculations either failed or rearranged to a 4-membered transition state.<sup>186,187</sup> Guesses for a six-membered transition state were manually generated from optimized structures of transition state **TS** (through addition of HF), tetrahedral intermediate **5A** or the four-membered transition state found for the bifluoride nucleophile.



**Figure 46:** Fluoride versus bifluoride pathway.

Experimentally it was observed that simple heating of isolated uronium salts in the absence of added CsF led to sluggish formation of aryl fluoride products and low conversions (Figure

46A, B).<sup>76</sup> Yields of PhenoFluor mediated deoxyfluorination reactions were significantly lower in the absence of added CsF (Figure 46C). Given that uronium formation proceeds rapidly at ambient temperature in the absence of added fluoride, the role of CsF cannot be to act as a base, which facilitates deprotonation of the phenol to form the uronium intermediate.

### **DFT energy profiles for fluoride and bifluoride mediated pathways**

Energy profiles of PhenoFluor mediated deoxygenation were created using structures optimized at B3LYP 6-31G(d) level using a toluene continuous solvent model with single point energies obtained using a 6-311++G(d,p) basis set.<sup>188</sup> All structures relevant to the proposed reaction mechanism for the deoxyfluorination of phenol were subsequently re-optimized using a 6-311++G(d,p) basis set with a toluene continuous solvent model.

Reaction profiles were constructed for three potential mechanisms and internal reaction coordinates were obtained to verify that no significant intermediates or transition states were neglected. To simplify comparison, the energy of the lowest energy reaction intermediate prior to the transition state was set to zero for all three energy profiles.

Fluoride pathway:

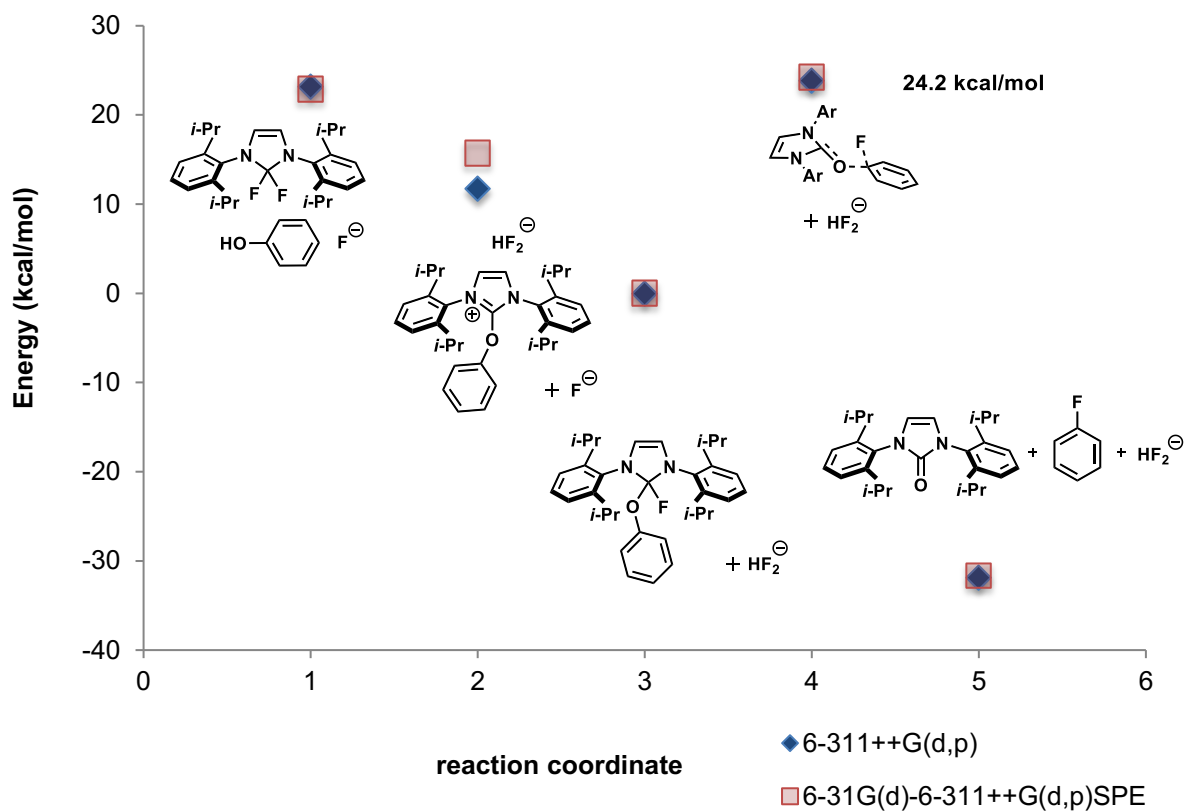


Figure 47: DFT energy profile for the fluoride pathway in the presence of added CsF.

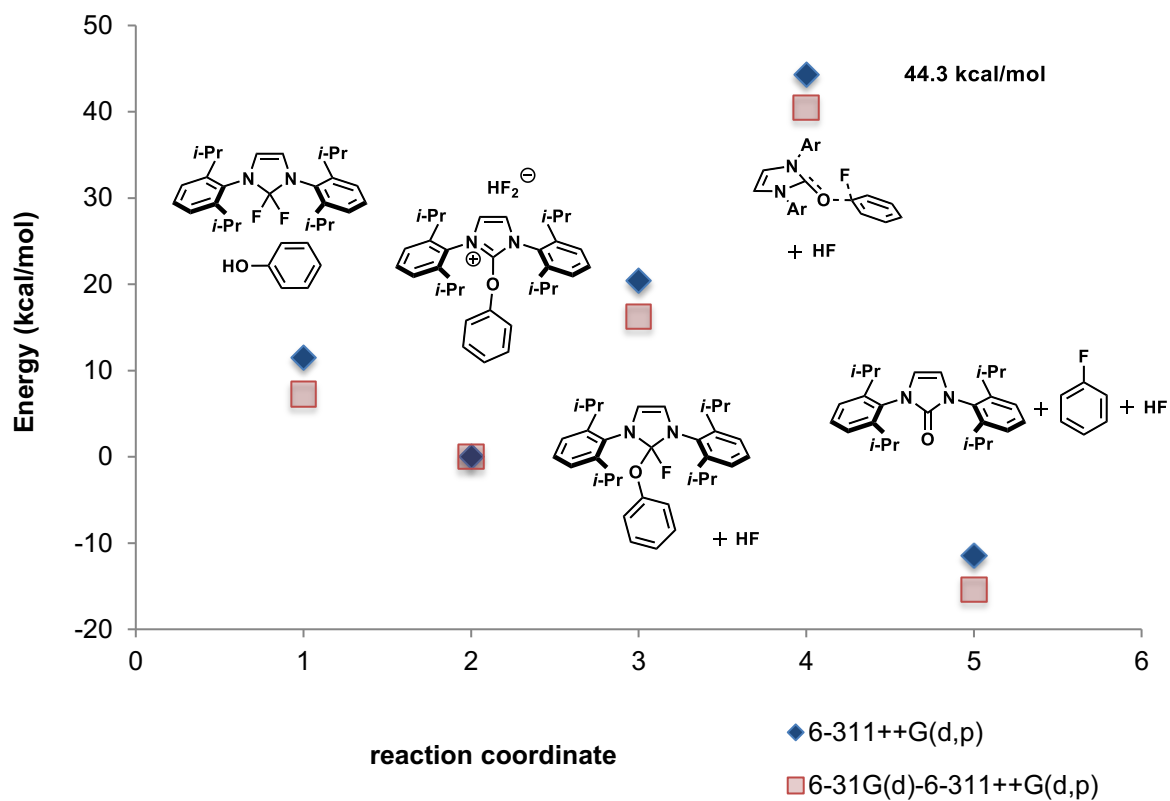
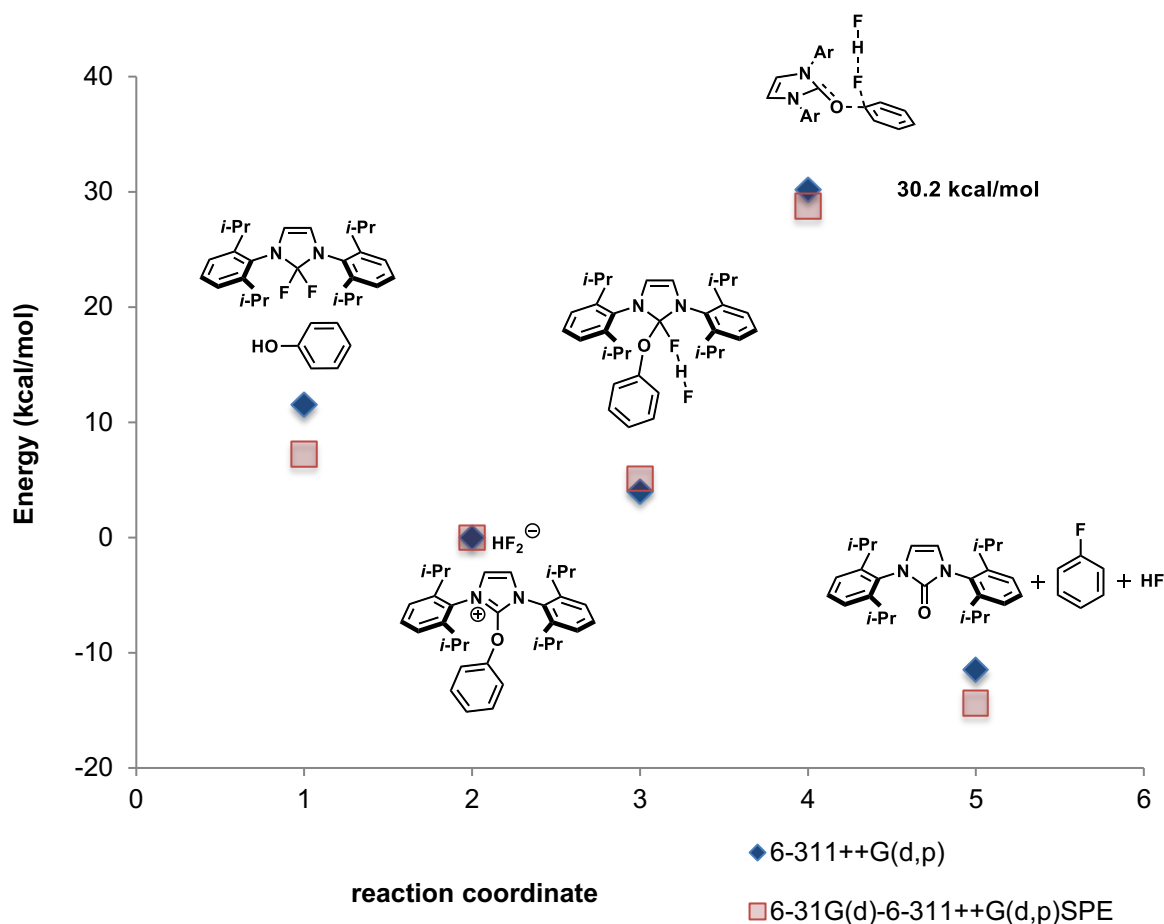


Figure 48: DFT energy profile for the fluoride pathway in the absence of added CsF.

### Bifluoride pathway (4-membered transition state):



**Figure 49:** DFT energy profiles for the bifluoride pathway proceeding via a 4-membered TS.

Two variants are presented for a pathway with a fluoride nucleophile: the first energy profile shows deoxyfluorination in the presence of fluoride and the second energy profile corresponds to fluorination in the absence of CsF. The fluoride pathway has an activation energy of 24 kcal/mol in the presence and 44 kcal/mol in the absence of fluoride. The third energy profile corresponds to deoxyfluorination with a bifluoride nucleophile. The activation energy calculated for this pathway is 30 kcal/mol. Energies obtained from structures optimized using a 6-311++G(d,p) basis set (blue) and structures optimized using a 6-31G(d) basis set and single point energies calculated using a 6-311++G(d,p) basis set (red) are both displayed for all structures.

Comparison of the activation energies of the different pathways shows that two different pathways are operative depending on whether or not CsF is added to the reaction mixture. Fluoride serves the nucleophile, which attacks the arene as long as CsF is present to convert uronium **5** to tetrahedral adduct **6**. The activation energy for the transformation is 24 kcal/mol in the presence of CsF. In the absence of CsF, the pathway involving a fluoride nucleophile is 44 kcal/mol and fluorination *via* a fluoride nucleophile cannot occur. Instead, deoxyfluorination in the absence of added CsF occurs *via* attack of bifluoride on the arene (with an activation energy of 30 kcal/mol). The calculated values for the activation energy are consistent with the difference in reaction efficiency in the presence and absence of CsF additive (Figure 46). Furthermore, the activation energy for the fluoride pathway is in accord with the experimental value obtained from the Eyring plot for the deoxyfluorination of phenol:  $\Delta G^\ddagger (110\text{ }^\circ\text{C}) = 23.4 \pm 0.19\text{ kcal}\times\text{mol}^{-1}$ .

Intrinsic reaction coordinates (IRC) were calculated to ensure that nucleophilic displacement on the arene is indeed a concerted transformation without a local minimum corresponding to a Meisenheimer intermediate (Figure 50 and 51). An IRC is generated by following the gradient downhill from the transition state to ensure that it interconnects reactants and products. Since the gradient is zero in the transition state (it is a stationary point), the IRC calculation is initiated by displacing the geometry along the normal mode associated with an imaginary frequency. IRCs interconnecting tetrahedral adducts, transition states and reaction products were obtained for both fluoride and bifluoride nucleophiles using a 6-31G(d) basis set (see Figure 60 for an intrinsic reaction coordinate using a toluene continuous solvent model):



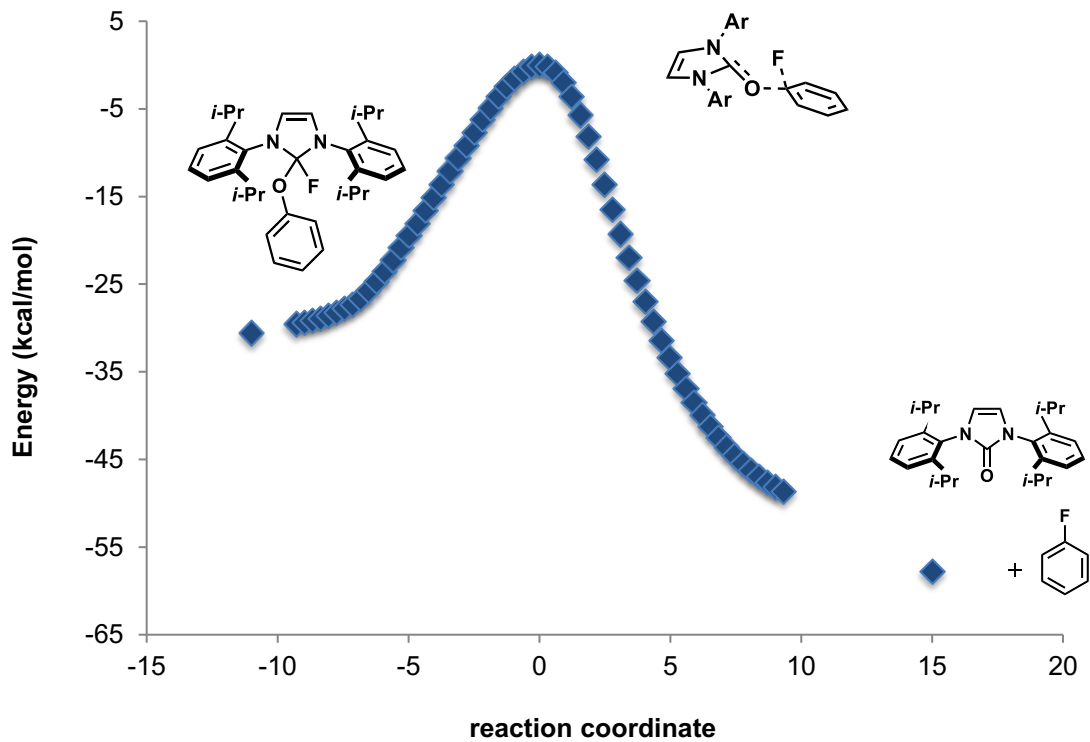


Figure 50: IRC with a fluoride nucleophile (B3LYP/6-31G(d)).

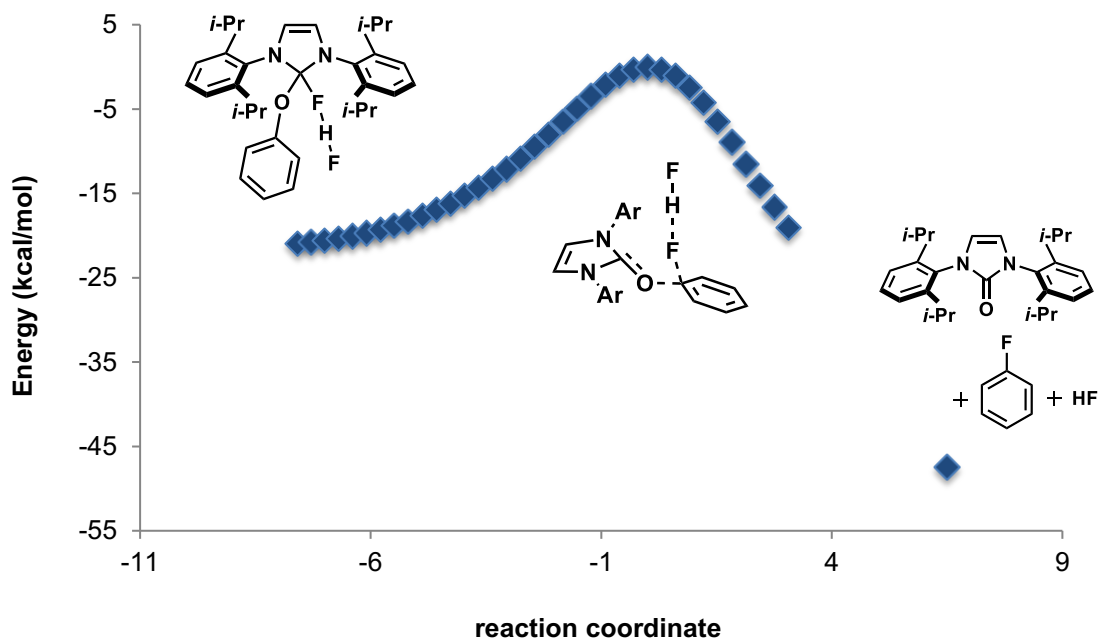
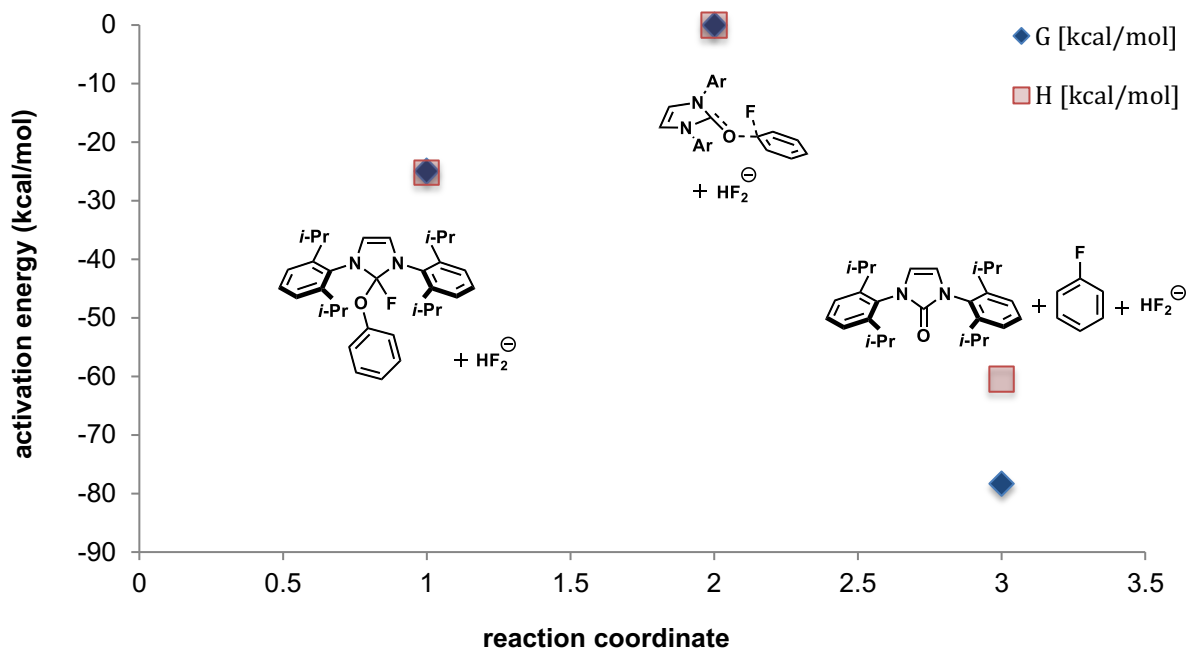


Figure 51: IRC with a bifluoride nucleophile (B3LYP/6-31G(d)).



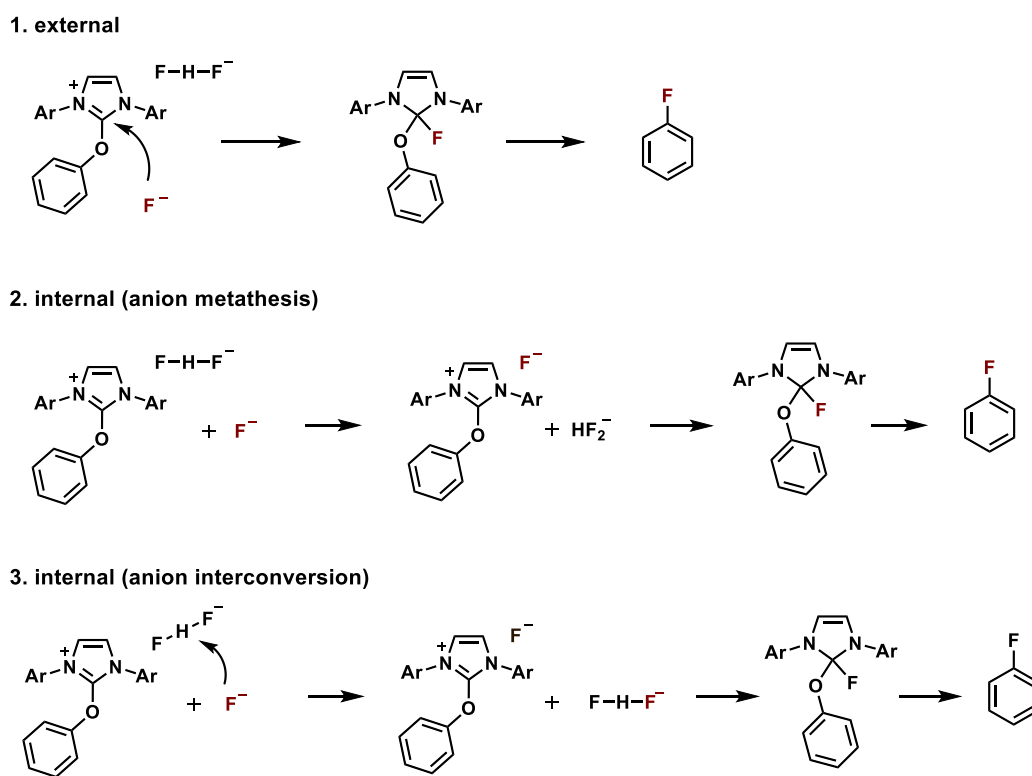
**Figure 52:** Enthalpy (H) and free energy (G) profile for the deoxyfluorination of phenol (B3LYP/6-311++G(d,p), toluene continuous solvent model).

A deoxyfluorination mechanism that proceeds via a 4-membered transition state with fluoride acting as the nucleophile is consistent with both experimental and DFT data. Frequency calculations using a 6-311++G(d,p) basis set were used to calculate the thermal corrections at 383 K and obtain  $\Delta G^\ddagger$ ,  $\Delta S^\ddagger$  and  $\Delta G^\ddagger$  (Figure 52). The free energy of activation derived from DFT experiments for a CsF-mediated pathway with a fluoride nucleophile is 25 kcal/mol. The experimental value derived from the Eyring plot for the deoxyfluorination of phenol is:  $\Delta G^\ddagger$  (110 °C) =  $23.4 \pm 0.19$  kcal $\times$ mol $^{-1}$  (Figure 24). The free energy of activation calculated for the deoxyfluorination of 4-nitrophenol (B3LYP/6-31G) of  $\Delta G^\ddagger = 20.8$  kcal $\times$ mol $^{-1}$  is in good agreement with the experimentally derived value of  $\Delta G^\ddagger$  (110 °C) =  $20.3 \pm 0.10$  kcal $\times$ mol $^{-1}$  (Figure 28).

### Entry points to a fluoride pathway

With fluoride being established as the active nucleophile for the deoxyfluorination in the presence of CsF, three mechanisms were considered, which differ in the origin of the

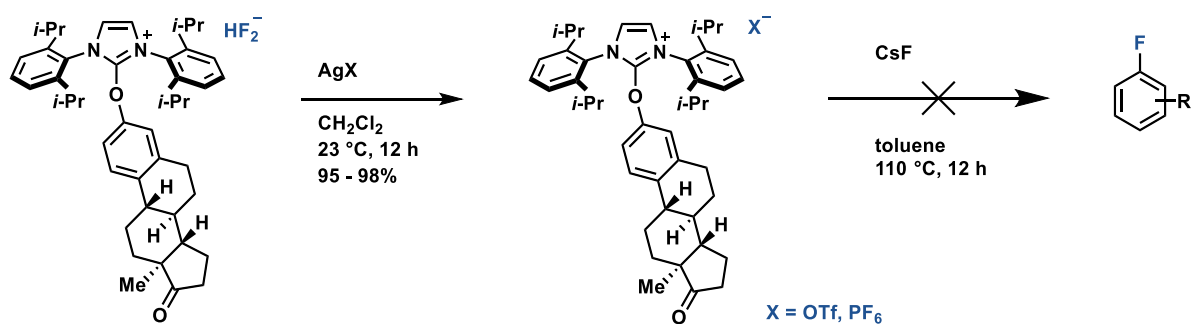
fluoride being incorporated into the product. We differentiated between ‘external’ mechanisms in which uronium **5** reacts with free fluoride in solution to form tetrahedral adduct **6** and ‘internal’ mechanisms, where an uronium fluoride reacts with its own counteranion to form neutral tetrahedral adduct **6**. The latter mechanistic proposal is further subdivided by how the uronium intermediate obtains a fluoride counteranion. External fluoride is drawn in red throughout Figure 53 to highlight that in cases 1 and 2 the fluoride incorporated into the aryl fluoride product originates with CsF, while in case 3, it originates with the PhenoFluor reagent.



**Figure 53:** Three potential mechanisms for the conversion of **5** to **6** under the influence of CsF additive.

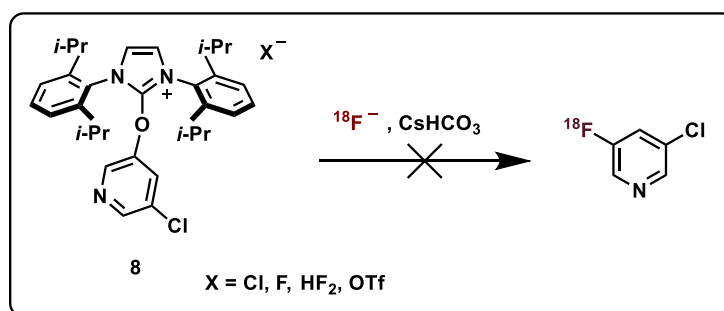
Without added CsF the rate of the deoxyfluorination reaction is considerably lower, but when the bifluoride counteranion of uronium **5** (the fluoride equivalents originating with the reagent) is exchanged for a counteranion other than fluoride or bifluoride, no reaction is observed (Figure 54). While added CsF is helpful to the progress of the reaction, the fluoride contained in the bifluoride counteranion was found to be crucial – all effort to replace it (with

any anion except fluoride) have always led to uronium salts that could not be converted to aryl fluoride products. Pathway 1 (external attack) can be excluded because neither CsF nor other fluoride sources (including soluble fluoride sources) can convert uronium salts with anions other than fluoride or bifluoride to aryl fluorides (Figure 53). External fluoride does not seem to be capable of attacking uronium salts to form tetrahedral adducts (which lead to the formation of aryl fluoride products).

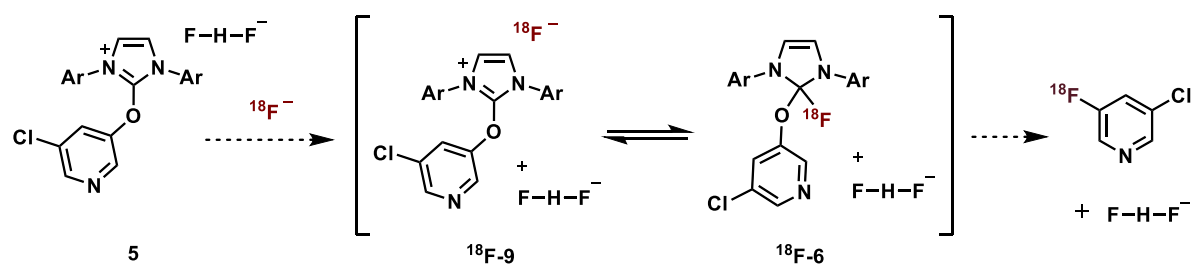


**Figure 54:** Uronium anions with non-coordinating counteranions do not undergo fluorination in the presence of external fluoride sources.

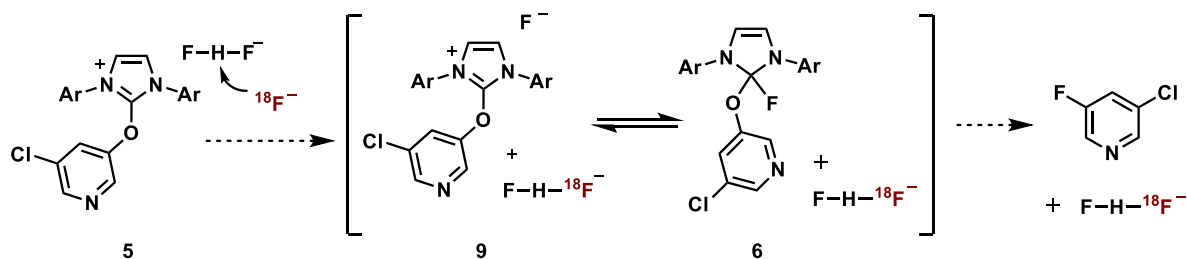
Experiments with  $^{18}\text{F}$ -labeled fluoride were used to differentiate between pathways 2 (internal, anion metathesis) and 3 (internal, anion interconversion) (Figure 55).



Pathway 2 (anion metathesis):



Pathway 3 (anion interconversion):

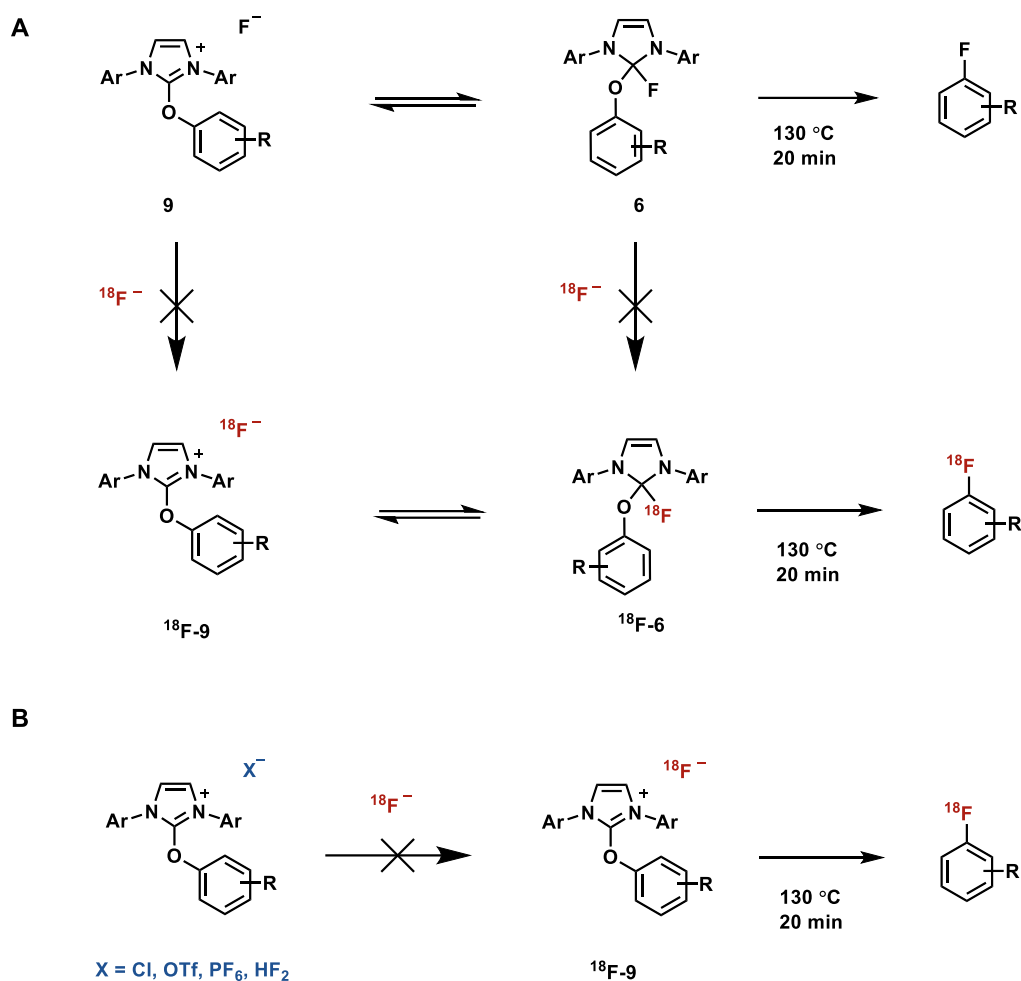


**Figure 55:** Using  $^{18}\text{F}$  as a mechanistic probe to differentiate between different mechanisms for the interconversion of uronium **5** and tetrahedral adduct **6**.

No incorporation of the radioactive isotope into the aryl fluoride product could be observed when uronium bifluoride **5** was treated with  $^{18}\text{F}$  (Figure 55). Consequently, the reaction is likely to proceed via pathway 3 and the fluoride found in the aryl fluoride product originates with the PhenoFluor reagent. The role of added CsF likely consists in abstracting HF from the bifluoride counteranion of the uronium intermediate to facilitate the formation of the tetrahedral adduct, which in turn is transformed into aryl fluoride via a 4-membered cyclic transition state.

## Introduction of $^{18}\text{F}$ fluoride

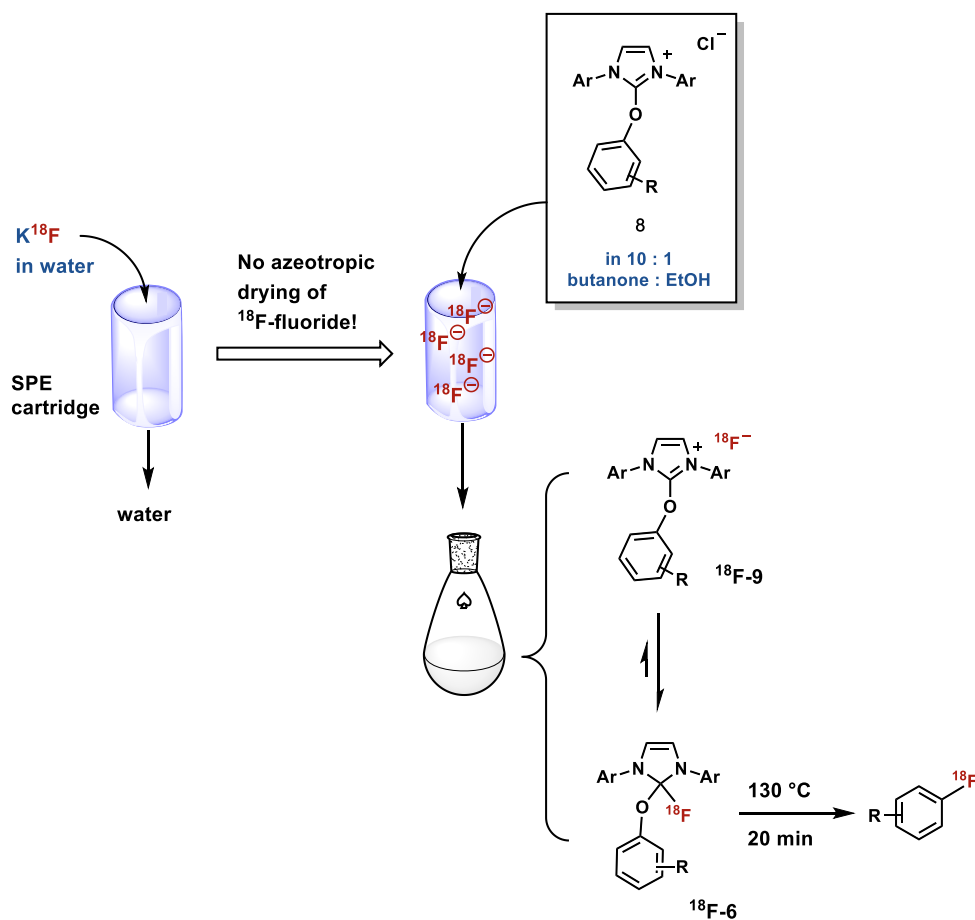
Given the postulated mechanism of PhenoFluor mediated deoxyfluorination,  $^{18}\text{F}$  fluoride would need to be introduced into tetrahedral adduct **6** in order to be incorporated into the aryl fluoride product. Tetrahedral adduct **6** is the ultimate stable intermediate prior to the transition state (DFT intrinsic reaction coordinate confirms that there are no energy minima between **6** and the transition state) and thus the fluoride atom found in **6** will be incorporated into the aryl fluoride product. Tetrahedral intermediate **6** is in equilibrium with uronium fluoride **9**. If either the fluorine atom in **9** or the counteranion of **5** can be exchanged for free fluoride in solution under suitable reaction conditions, addition of  $^{18}\text{F}$  fluoride would lead to a (low-specific-activity) deoxyfluorination reaction. No trace of anion metathesis was ever observed with either **9** or **5** under a variety of reaction conditions (Figure 56A). Next we examined whether uronium adducts featuring other counteranions such as Cl, OTf,  $\text{PF}_6$  or  $\text{HF}_2$  (Figure 56B) could undergo exchange with free fluoride in solution (either  $^{18}\text{F}$  or  $^{19}\text{F}$ ), but no evidence for such an exchange process was ever found. If such a process did occur, an equilibrium would be established and  $^{18}\text{F}$ -deoxyfluorination could proceed. We have repeatedly found that fluoride is only incorporated into the aryl fluoride product (the deoxyfluorination only proceeds) if fluoride is the counteranion of the uronium cation (with the exception of a higher energy pathway proceeding *via* a bifluoride nucleophile which occurs from uronium bifluoride intermediates).



**Figure 56:** **A** Neither uronium fluoride **9** nor tetrahedral **6** incorporate free fluoride from solution. **B** Uronium salts with a variety of anions did not undergo anion exchange with  $^{18}\text{F}$ -fluoride.

Initial experiments with uronium **5** as well as isolated tetrahedral intermediates and  $^{18}\text{F}$  have shown that no anion metathesis occurs in solution under the reaction conditions. Introduction of  $^{18}\text{F}$  into the PhenoFluor reagent would lead to a multistep low specific activity radiolabeling protocol. In order to develop a facile high-specific activity radiolabeling protocol based on PhenoFluor chemistry, we developed a protocol in the labeling precursors are used directly for the elution of  $^{18}\text{F}$  fluoride trapped on an anion exchange cartridge (Figure 57). While anion metathesis between free fluoride and the counteranion of the uronium does not proceed in solution, exchange and subsequent elution of  $^{18}\text{F}$  from an exchange cartridge could be achieved with 70% efficiency. The mechanism of the formation of the tetrahedral adduct was changed from pathway 3 (internal, anion interconversion) to pathway 2 (internal,

anion metathesis) when the labeling precursor and  $^{18}\text{F}$  were brought in contact on the exchange cartridge rather than in solution. *Via* pathway 2, introduction of  $^{18}\text{F}$  into the tetrahedral intermediate (and thus the aryl fluoride product) in high specific activity could be achieved. Finding a way to alter the origin of the fluoride anion ultimately incorporated into the product was integral to the development of a radiolabeling protocol based on PhenoFluor mediated fluorination.



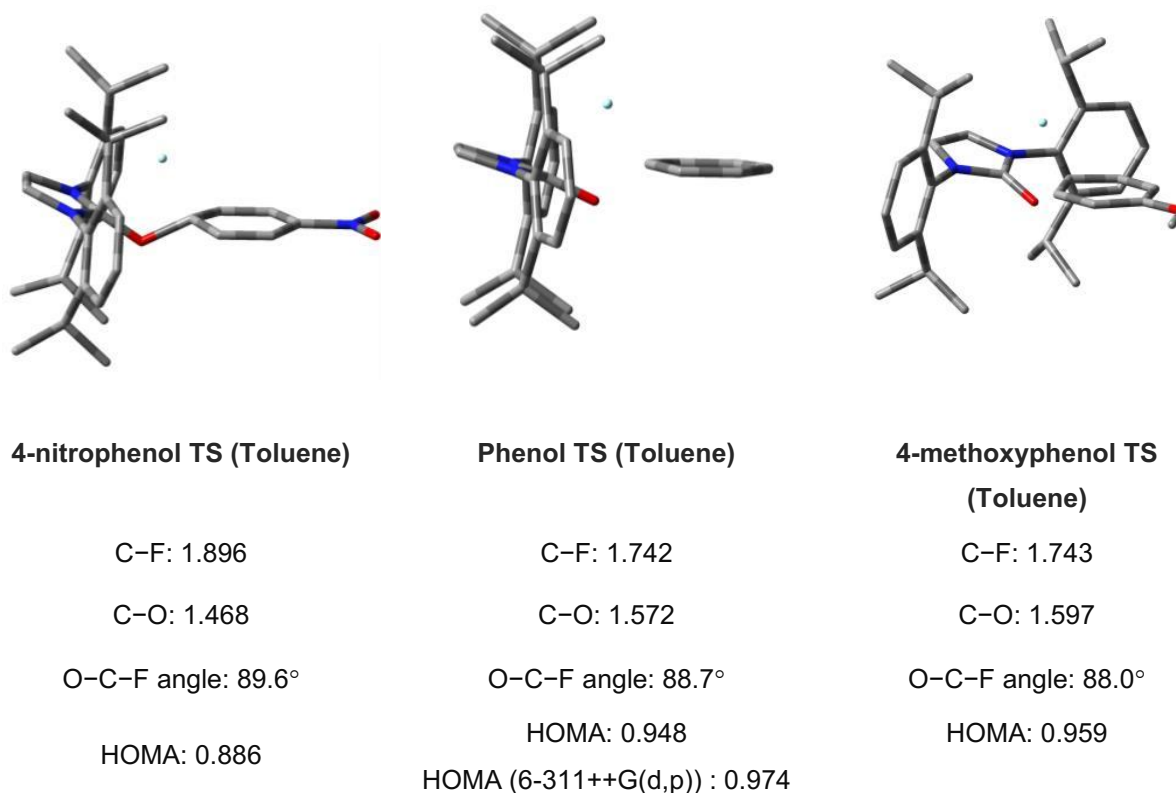
**Figure 57:** Set-up of  $^{18}\text{F}$ -deoxyfluorination reactions: Elution of  $^{18}\text{F}$ -fluoride with labeling precursor **8** leads to the formation of  $^{18}\text{F}$ -**6** and obviates the need for azeotropic drying of  $^{18}\text{F}$ -fluoride.



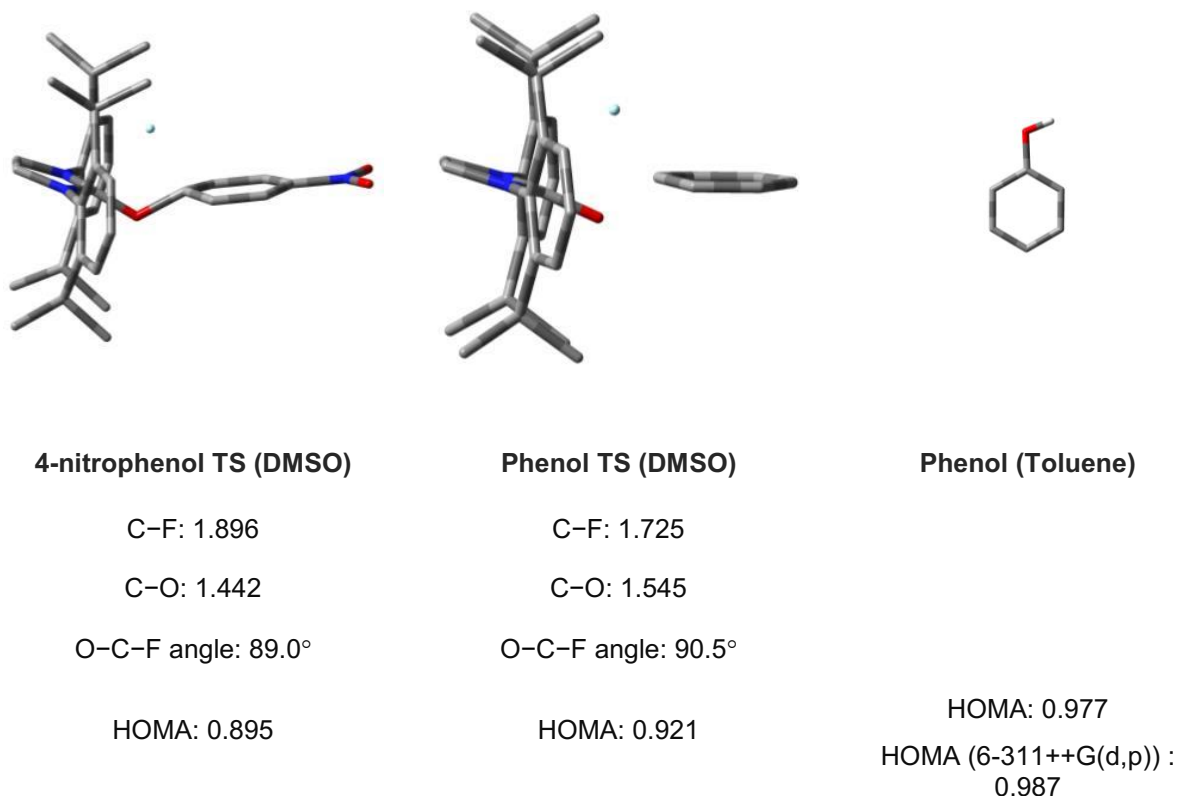
## Boundaries of a concerted mechanism

### Transition state structures

In order to gain insight into how the selection of substrates or solvent affects the propensity of PhenoFluor-mediated reaction to proceed via a concerted mechanism we conducted a series of computational experiments. Deoxyfluorination was studied with electron-rich as well as electron-poor phenols as well as in a non-polar as well as a polar solvent environment. Using DFT, we investigated how the location and structure of the transition state is affected by the substrate and solvent selection (Figure 58 and Figure 59).



**Figure 58:** C-F and C-O bond lengths, O-C-F bond angles and HOMA aromaticity indices for transition state structures calculated using B3LYP/6-31G(d) and a toluene solvent model. Frequency analysis revealed one imaginary frequency corresponding to the reaction coordinate.



**Figure 59:** C-F and C-O bond lengths, O-C-F bond angles and HOMA aromaticity indices for transition state structures using B3LYP/6-31G(d) and a toluene solvent model. Frequency analysis revealed one imaginary frequency corresponding to the reaction coordinate.

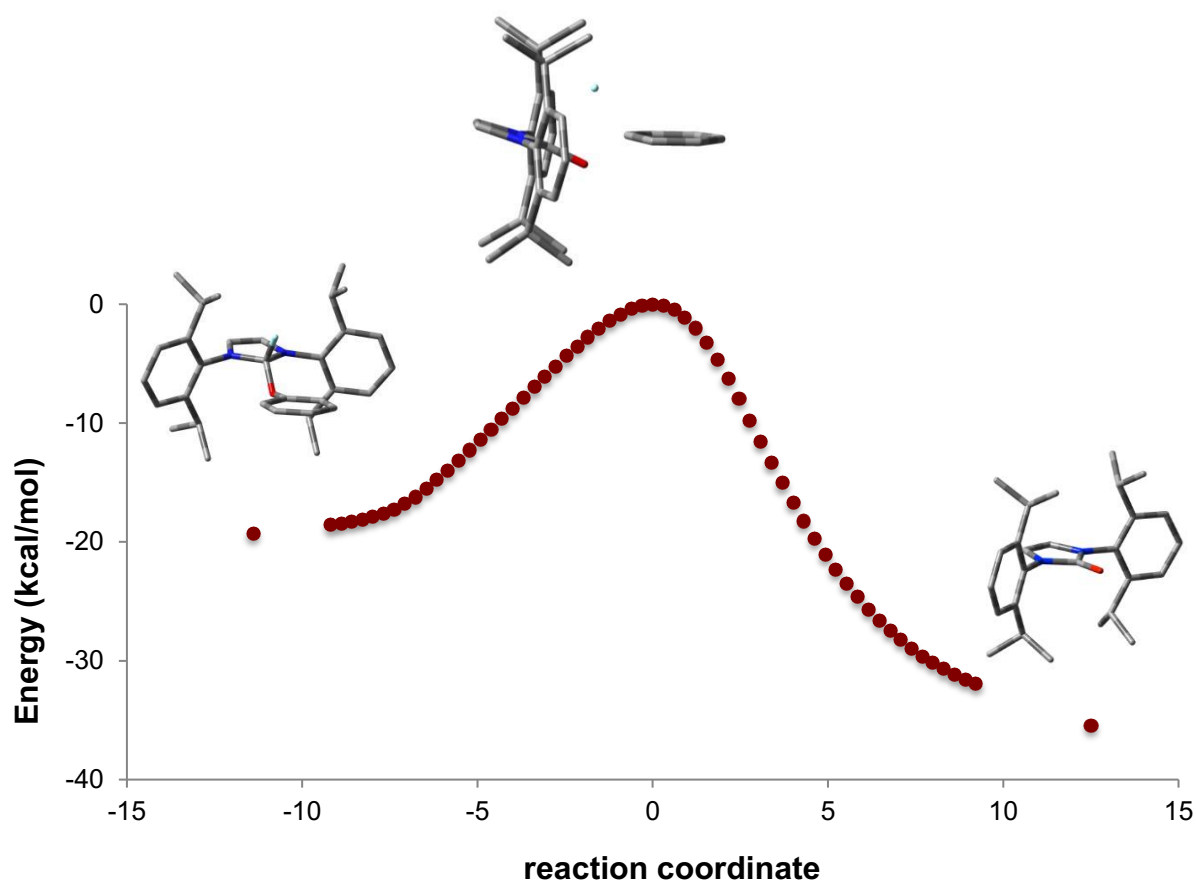
The transition state C-F and C-O bond lengths show that 4-nitrophenol undergoes deoxyfluorination *via* an earlier transition state than phenol and phenol reacts *via* an earlier transition state than 4-methoxyphenol (Figure 58 and Figure 59). This is in accordance with Marcus theory as well as the Hammond postulate, which predict that for reactions proceeding *via* the same path, the more exergonic reaction is associated with an earlier transition state. Cleavage of the C-O bond is less advanced in DMSO than it is in toluene. The calculated O-C-F bond angles for the transition states decrease with increasing activation barriers for the phenol derivative under investigation. All calculated angles for the transition states are noticeably smaller than reported values for Meisenheimer intermediates. Increasing bond angle for Meisenheimer complexes has been correlated with increased stability of the intermediate.<sup>158</sup>

HOMA indices were calculated for all transition state structures to estimate the degree of aromaticity of the phenols in the transition state.<sup>189</sup> All structures display high degrees of aromaticity, only slightly below the value obtained for free phenol at the same level of theory. For a concerted reaction with little charge delocalization onto the arene we would expect the aromatic character of the phenol to be largely intact in the transition state.

## Internal Reaction Coordinates

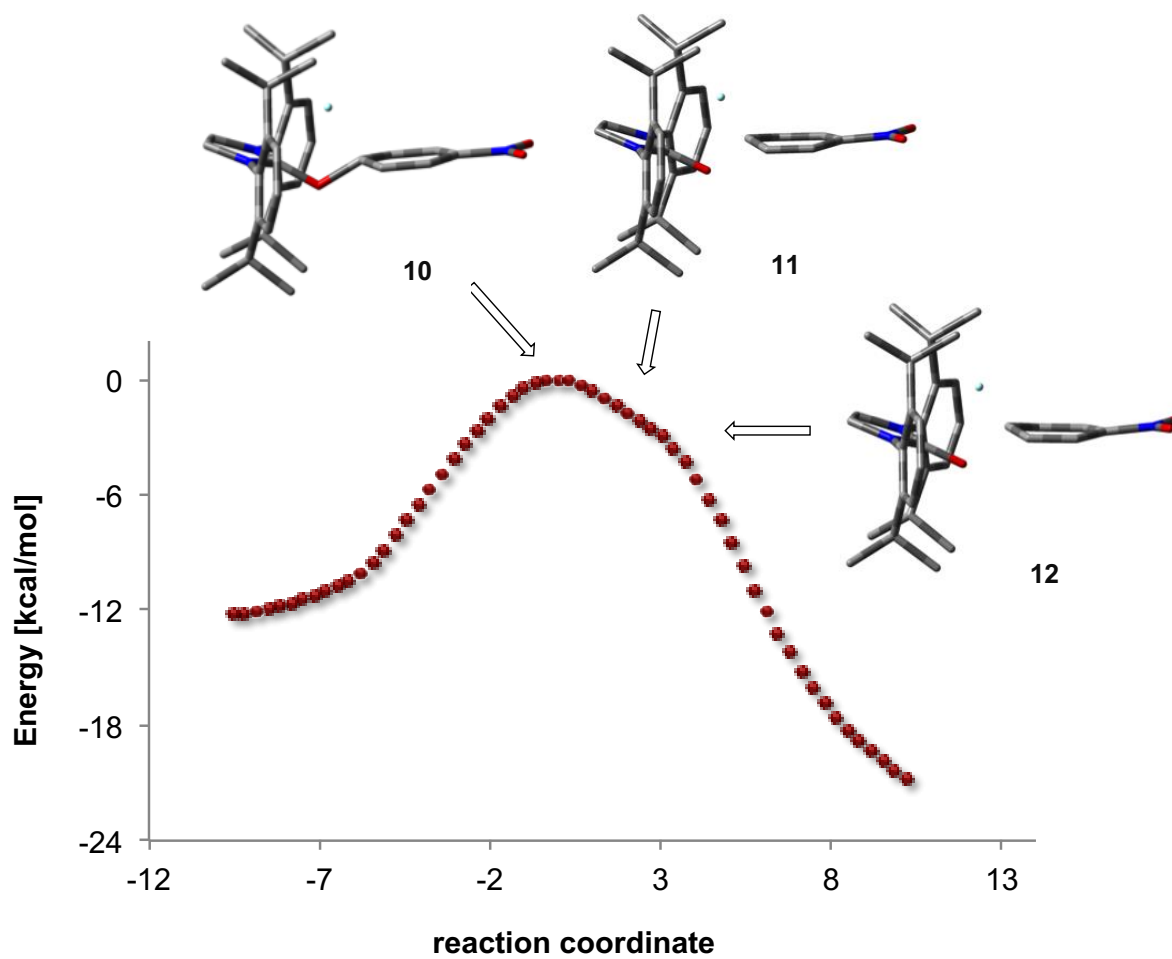
### IRC for phenol in toluene

Transition state **TS** optimized at B3LYP/6-31G(d) with a toluene continuous solvent model was subjected to an internal reaction coordinate analysis at B3LYP/6-31G(d) with a toluene continuous solvent model (Figure 60). IRC in reverse mode led to the formation of tetrahedral adduct **6** and no local minima were observed between structures **6** and **TS**. IRC in forward mode led to the formation of the reaction products, aryl fluoride and **4**. The presence of an additional local minimum and an additional transition state would have been expected for a classical  $S_NAr$  mechanism.



**Figure 60:** IRC for deoxyfluorination of phenol (B3LYP/6-31G(d), toluene continuous solvent model) and calculated reagent structures.

IRC for 4-nitrophenol in toluene:



**Figure S61:** IRC for deoxyfluorination of 4-nitrophenol (B3LYP/6-31G(d), toluene continuous solvent model).

10	11	12
C–O bond length: 1.468	C–O bond length: 1.601	C–O bond length: 1.730
C–F bond length: 1.816	C–F bond length: 1.485	C–F bond length: 1.433

IRC for 4-nitrophenol in DMSO:

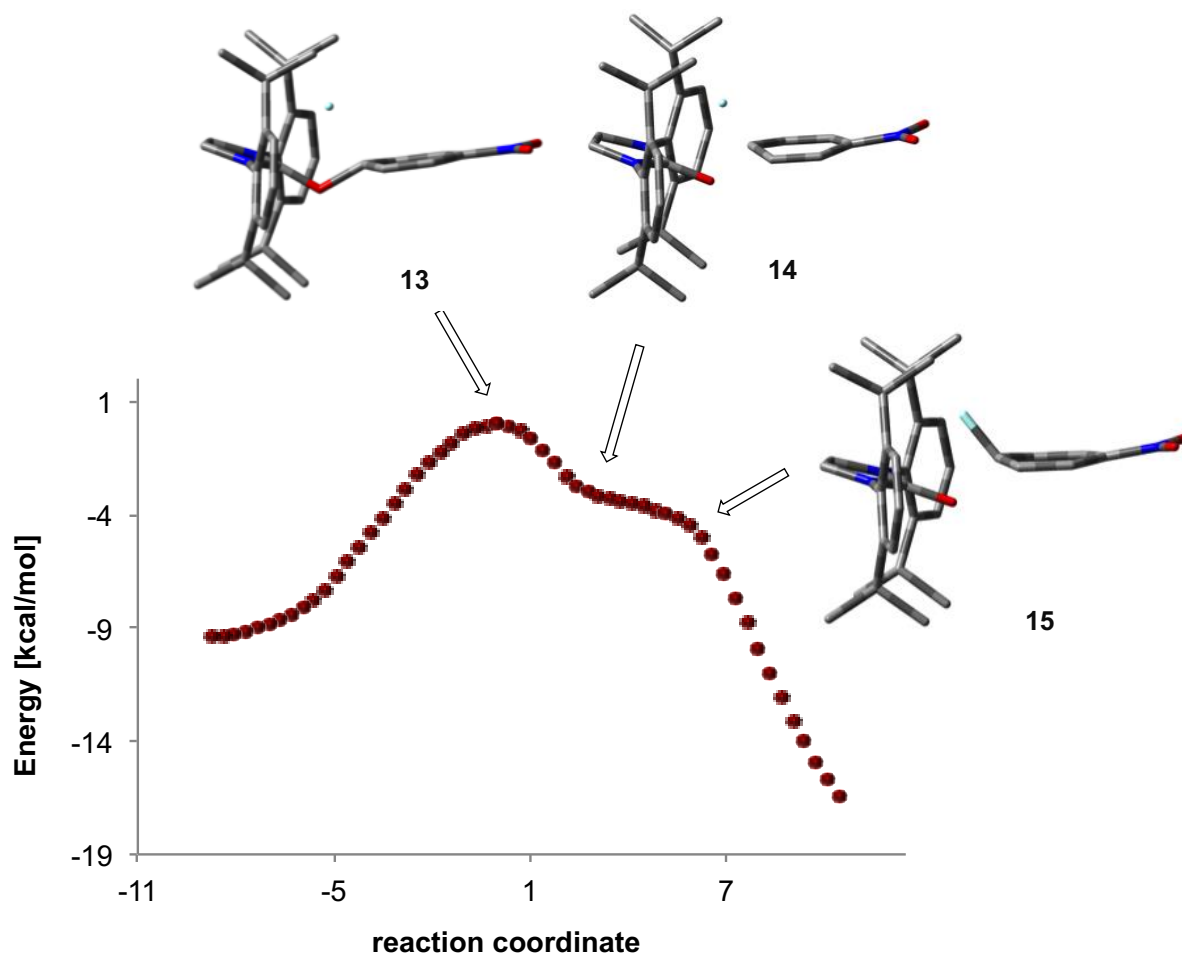


Figure 62: IRC for deoxyfluorination of 4-nitrophenol (B3LYP/6-31G(d), DMSO continuous solvent model).

13	14	15
C–O bond length: 1.442	C–O bond length: 1.565	C–O bond length: 1.693
C–F bond length: 1.896	C–F bond length: 1.459	C–F bond length: 1.421

Comparison of Figures 60, 61 and 62 reveals that both the replacement of toluene with the more polar solvent DMSO and the presence of an electron-withdrawing substituent on the phenol lead to C–O cleavage occurring later in the reaction progress. C–O bond elongation in the transition state is most pronounced for electron-rich phenol substrates in an apolar solvent model. The deoxyfluorination of 4-nitrophenol in DMSO approaches the classical regime of  $S_NAr$  reactions where C–LG bond cleavage occurs in a separate step. Commonly,

C–LG bond cleavage is associated with a separate barrier, but due to the good leaving group utilized in the deoxyfluorination, this step is barrier-less. Not only does Figure 62 reveal that the apolar solvent used in the deoxyfluorination is an important factor for the observance of a concerted transformation, but also that loss of the leaving group is sufficiently facile that this step is unlikely to contribute to the reaction barrier of the concerted displacement. Classical  $S_NAr$  reactions proceed via a stepwise mechanism with only the nucleophile attack and disruption of aromaticity contributing to the first reaction barrier and leaving group loss is associated with a second barrier. Since the barrier for the overall reaction is, in the majority of cases, dominated by the initial barrier corresponding to nucleophile attack, the ease of leaving group loss is not an important contributor to the reaction barrier. In fact, the order of halide leaving groups for  $S_NAr$  reactions is  $F > Cl > Br$ , despite C–F bonds displaying a higher bond strength than C–Cl bonds. For a concerted transformation, loss of the leaving group occurs concomitantly with nucleophilic attack and leaving group loss contributes to the overall reaction barrier. The use of a good leaving group is therefore vital for  $CS_NAr$  reactions with a low barrier.

## CHAPTER 2: A COMPUTATIONAL APPROACH TOWARDS AN IMPROVED DEOXYFLUORINATING REAGENT

In order to improve the activity of the PhenoFluor deoxyfluorination reagent, a variety of derivatives were examined. Given the significant time commitment required to synthesize different reagent scaffolds, we decided to investigate a wide range of derivatives using density functional theory and correlate those results with experimental data for a number of derivatives to verify the reliability of the computational model used. Early modifications to the PhenoFluor scaffold were selected to establish which features of the reagent are required to achieve successful deoxyfluorination. Based on experimental data available at the time we anticipated that an unsaturated imidazolium core was a crucial structural feature and similarly that N-aryl rather than N-alkyl substituents on the imidazole core were needed to achieve aromatic deoxyfluorination. Analysis of reagent derivatives was focused both on understanding the origin of the importance of particular structural features as well as the discovery of a more active reagent. For each scaffold, a tetrahedral adduct, an uronium intermediate and a transition state structure were optimized and single-point energy calculations were performed at a higher level of theory (B3LYP, 6-311++G(d,p), toluene solvent model) to obtain an accurate estimate for the experimental reaction barrier. The preference of a concerted reaction pathway proceeding *via* a fluoride rather than a bifluoride nucleophile was thoroughly established in the case of PhenoFluor, but the generality of this mechanistic pathway was verified for a number of derivatives. Without exception, a fluoride mediated concerted displacement was the lowest energy pathway found in all examined cases. Frequency calculations were performed for all optimized structures to identify them as ground – or transition state structures.

### **Computational reaction barriers for modified PhenoFluor scaffolds**

Filippo Sladojevich and Teppei Fujimoto synthesized a variety of PhenoFluor derivatives and tested their ability to effect the deoxyfluorination of phenols. Most of the early



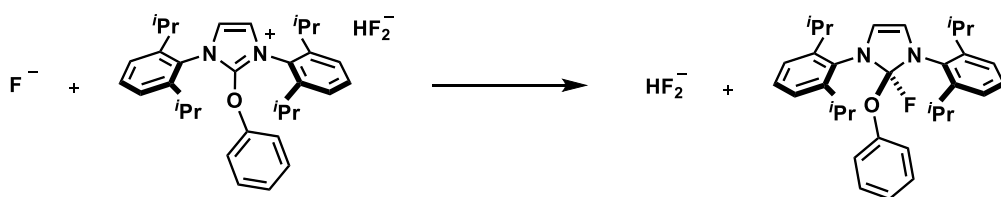
experimental work was carried out before computational data was available and correlation with experimental data was used to verify computational results and select appropriate basis sets and levels of theory. None of the PhenoFluor derivatives synthesized at the start of this work was superior to the original PhenoFluor reagent and most proved to be inactive for the deoxyfluorination of unactivated phenols. Given the low success rate and complex synthesis for new derivatives, it was decided to use computational experiments to disentangle the effects of reagent substitution patterns on various steps of the desired transformation.

During the initial analysis, it became clear that the presence of N-aryl rather than N-alkyl substituents on the imidazolium nitrogen is vital to obtaining a deoxyfluorination barrier below 30 kcal/mol. Furthermore, at least one ortho substituent has to be present on both N-aryl groups to facilitate the C–F bond formation step. In the absence of bulky ortho substituents, the N-aryl groups flatten out towards the imidazolium plane to maximize delocalization between the aromatic systems. It appears, that the flattening out of the structure stabilizes the uronium bifluoride and uronium fluoride intermediates relative to the C–F bond forming transition state to such an extent that the deoxyfluorination becomes untenable. When electron-rich heterocycles bearing bulky substituents are attached to the imidazolium core, the barriers are also found to be above 30 kcal/mol due to a less favorable electronic influence of the heterocyclic compared to the carbocyclic substituents. The incorporation of electron withdrawing substituents on the backbone of the imidazolium also leads to an increase of the reaction barrier. Electron withdrawing substituents on the imidazolium core stabilize the neutral tetrahedral adduct **6** relative to the transition state, in which the imidazolium core carries a partial positive charge.

### **Controlling the equilibrium between tetrahedral adduct and uronium bifluoride**

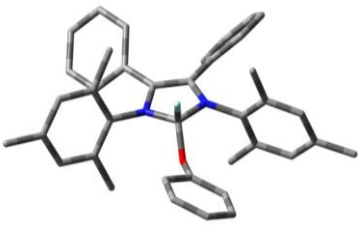
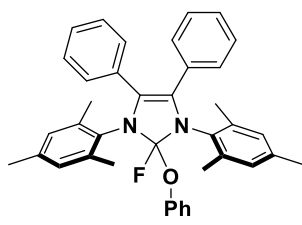
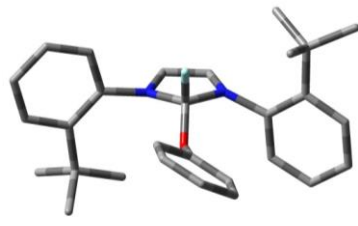
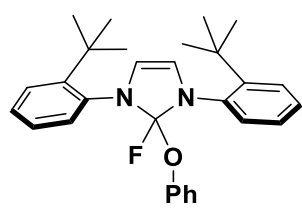
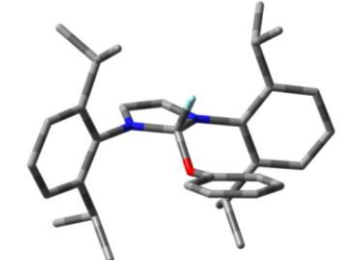
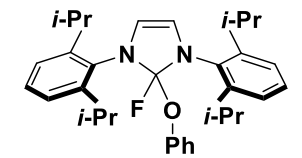
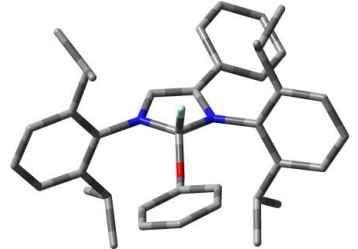
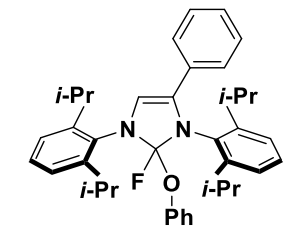
A vital step in the mechanism of PhenoFluor-mediated deoxyfluorination is the abstraction of HF from the bifluoride counteranion of uronium **5** to form tetrahedral adduct **6**

and mechanistic analysis revealed that CsF can effect this reaction step. A fluoride anion in toluene solution is used as a computational model for CsF in toluene. Given the oversimplification of a naked fluoride anion only stabilized by toluene solvent molecules, the driving force for uronium bifluoride to tetrahedral adduct interconversion (Figure 63) will be overestimated in this computational model. Consequently, the absolute energy values obtained by DFT are not reliable, but the trend observed for different PhenoFluor derivatives is unlikely to be affected by the simplified approach.

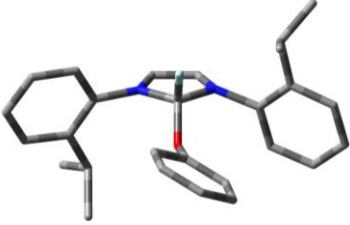
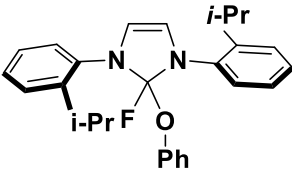
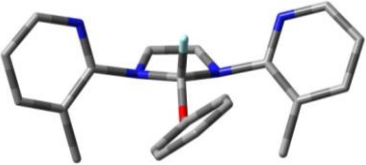
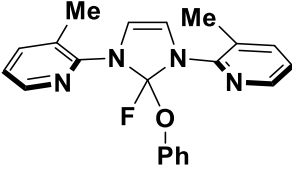
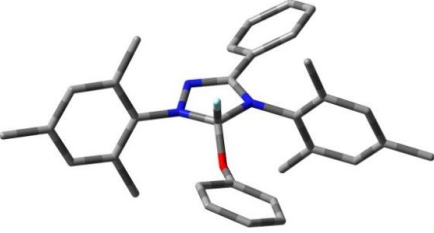
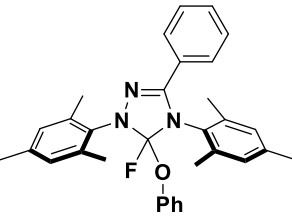
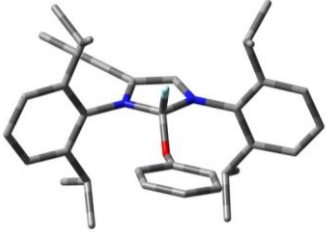
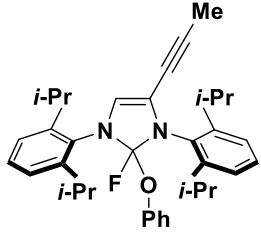

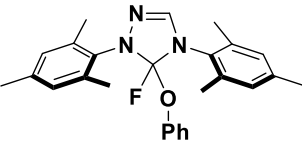

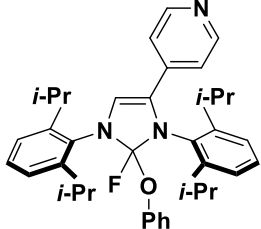


**Figure 63:** Definition for the computational energy difference between the tetrahedral adduct and the uronium fluoride. A negative value for the energy difference between the tetrahedral adduct and the uronium fluoride indicates that formation of the tetrahedral adduct in the presence of basic fluoride salts is energetically favorable.

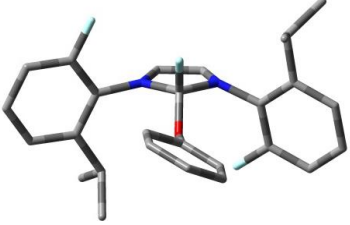
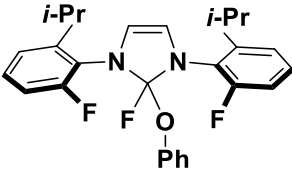
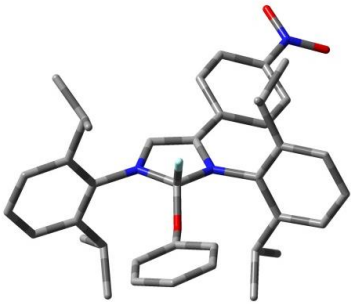
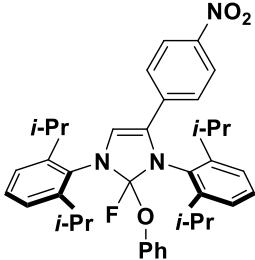
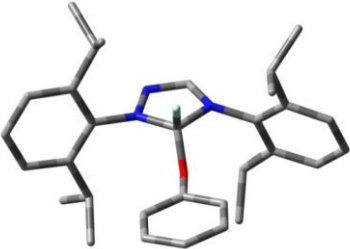
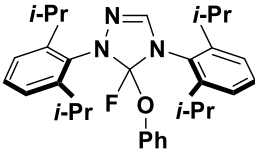
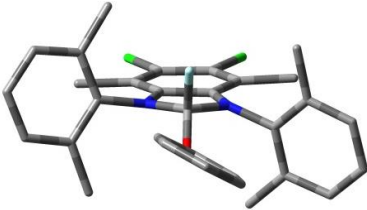
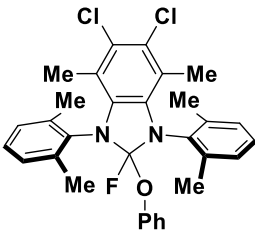
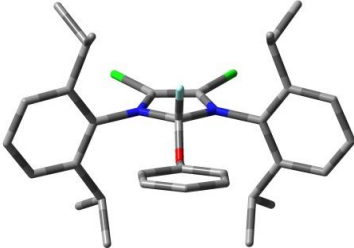
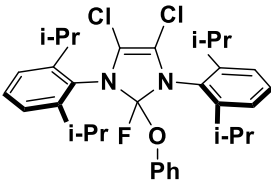
**Table 5:** DFT activation barriers for PhenoFluor derivatives and energy differences between the uronium fluoride and tetrahedral adduct structure in kcal/mol (Figure 63). All structures were optimized using B3LYP/6-31G(d) and a toluene solvent model; activation barriers were derived from single point energy calculations using B3LYP/6-311++G(d,p) and a toluene solvent model.

DFT structure of the tetrahedral adduct	Activation barrier	Chemical structure of the PhenoFluor derivative	Energy (Figure 63)
	23.4 kcal/mol		
	24.1 kcal/mol		-15.1
	24.3 kcal/mol		
PhenoFluor			
	24.4 kcal/mol		

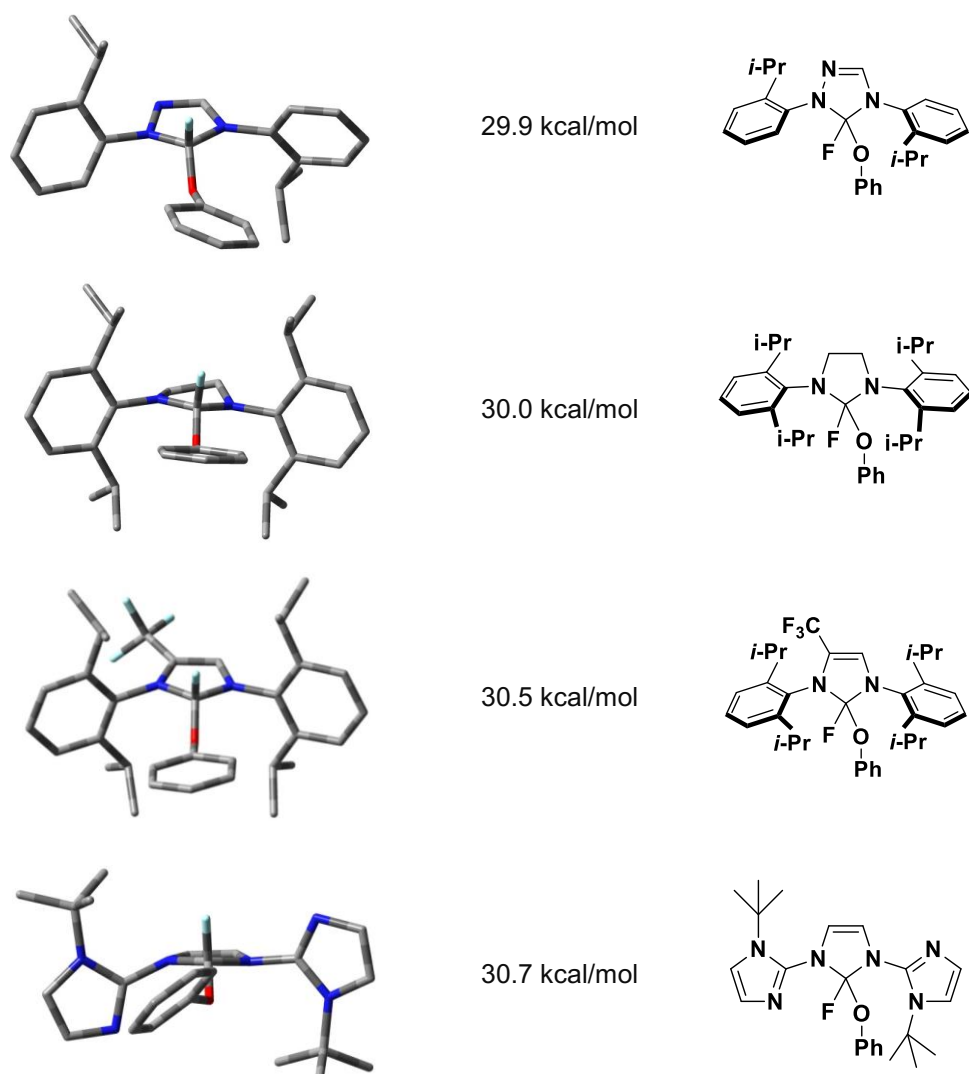
**Table 5 continued:** DFT activation barriers for PhenoFluor derivatives and energy differences between the uronium fluoride and tetrahedral adduct structure (Figure 63).

	24.8 kcal/mol		-16.3
	24.9 kcal/mol		-12.4
	25.9 kcal/mol		
	26.2 kcal/mol		
	26.3 kcal/mol		
	26.7 kcal/mol		

**Table 5 continued:** DFT activation barriers for PhenoFluor derivatives and energy differences between the uronium fluoride and tetrahedral adduct structure (Figure 63).

	26.8 kcal/mol		-17.9
	27.8 kcal/mol		- 19.5
	29.1 kcal/mol		
	29.3 kcal/mol		- 23.2
	29.4 kcal/mol		- 27.5

**Table 5 continued:** DFT activation barriers for PhenoFluor derivatives and energy differences between the uronium fluoride and tetrahedral adduct structure (Figure 63).



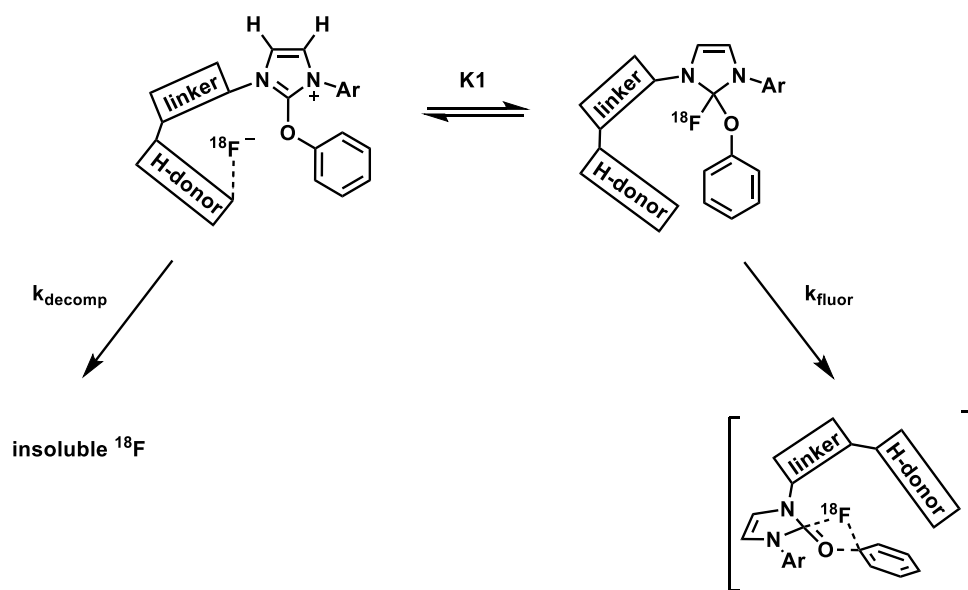
Despite extensive efforts on the computational as well as experimental front, no derivative with a substantially improved barrier was found in the initial round of exploration of PhenoFluor derivatives. Computational work did result in an understanding about how to control the equilibrium constant between the tetrahedral adduct and the uronium bifluoride structure. Electron-donating substituents located on the imidazolium ring will stabilize the uronium structures and render HF abstraction from the bifluoride counteranion of uronium bifluoride **5** unfavorable. This step will thus contribute to the activation energy and increase

the overall barrier (the contribution of uronium bifluoride to tetrahedral adduct transformation is not included in the activation barriers listed in table 5, which refer to the energy difference between the tetrahedral adduct and the transition state (Figure 63)). Electron-withdrawing substituents on the imidazolium core ensure facile formation of the tetrahedral adduct but destabilize the partially positively charged transition state relative to the tetrahedral adduct, which leads to larger activation energies for these derivatives.

### Controlling the energy difference between the tetrahedral adduct and the transition state

The deoxyfluorination of phenols with  $^{19}\text{F}$ -fluoride proceeds efficiently with PhenoFluor and, given the challenges associated with the development of an improved reagent, further investigation of PhenoFluor derivatives appeared to be futile. Following the development of an  $^{18}\text{F}$ -deoxyfluorination protocol, however, interest in novel PhenoFluor derivatives was re-awakened. Owing to detailed mechanistic studies, we had a reasonable hypothesis as to where the short-comings of the radio-deoxyfluorination reaction originated: Electron-rich phenol substrates increase the equilibrium concentration of the uronium fluoride **9** relative to the tetrahedral adduct structure **6**, exposing the fluoride counteranion in **9** to unproductive side reactions.

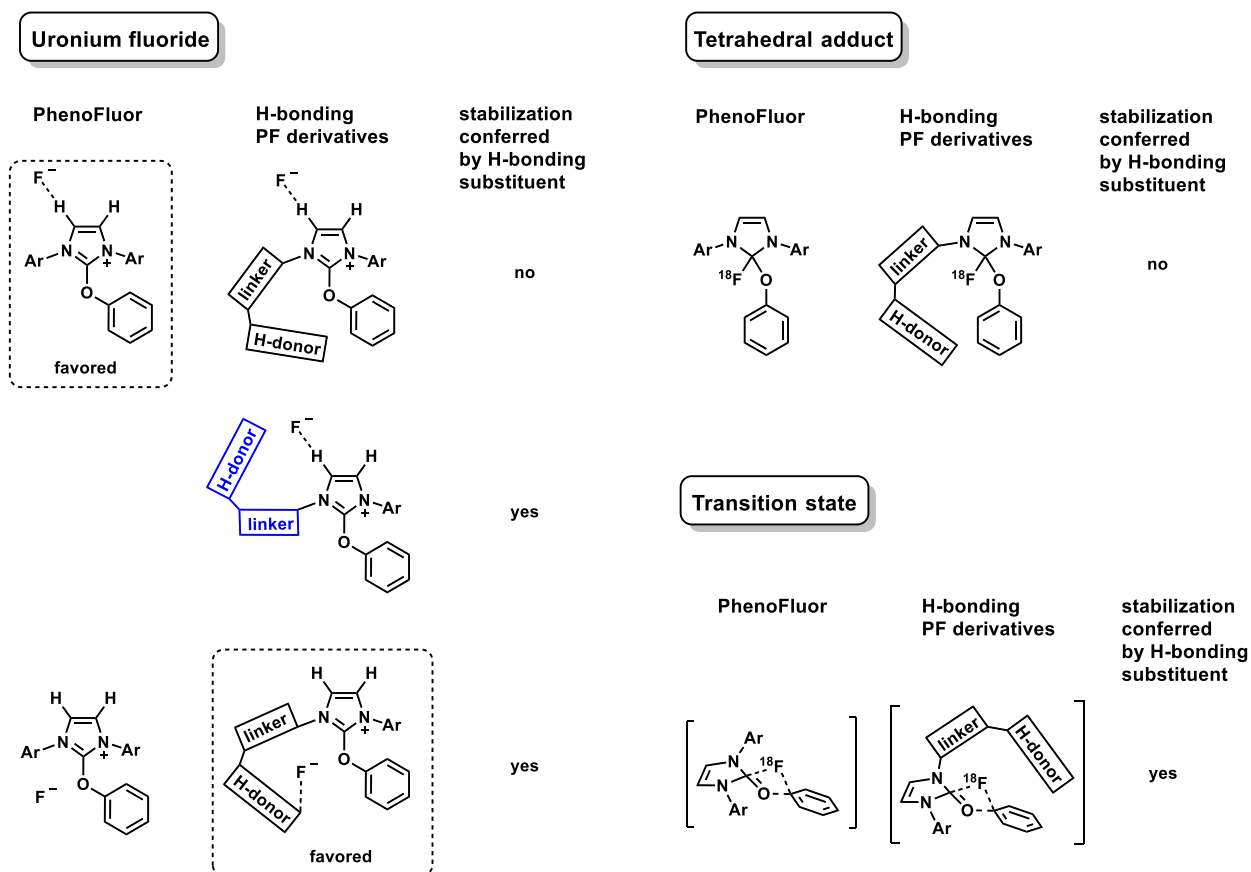
We hypothesized that the incorporation of an N-aryl substituent capable of forming a hydrogen bond to fluoride could stabilize the transition state for the deoxyfluorination. A lower fluorination barrier would increase  $k_{\text{fluor}}$  and the stabilization of the fluoride anion would also decrease  $k_{\text{decomp}}$  (Figure 64). Care has to be taken with this approach so as not to stabilize uronium fluoride **9** too much relative to tetrahedral adduct **6** since such a stabilization would raise the overall barrier for deoxyfluorination.



**Figure 64:** The effect of an N-aryl substituent capable of hydrogen-bonding the fluoride

On the outset, the proposed approach of lowering the overall fluorination barrier for electron-rich phenols through introduction of an H-bonding substituent is made possible by the location of the fluoride anion in the uronium fluoride structure of the original PhenoFluor reagent. Fluoride only carries a partial negative charge in the transition state and a full negative charge in the uronium fluoride structure. The uronium fluoride structure is consequently stabilized to a greater extent upon introduction of an H-bonding substituent capable of interacting with fluoride. Given that only the higher energy conformer is stabilized (where fluoride does not form a hydrogen bond to the imidazolium core), a weak H-bond donor can lower the energy of the transition state more than it lowers the energy of the uronium fluoride (Figure 65). Preferential transition state stabilization necessitates that the stabilization energy for the TS is greater than the sum of the stabilization energy of the uronium fluoride and the energy difference between the two possible uronium fluoride conformers (fluoride located close to the backbone and fluoride located close to the central imidazolium carbon). Such a scenario furthermore requires the use of a linker that is sufficiently inflexible that the H-bonding substituent cannot interact with the fluoride anion when the fluoride anion is hydrogen-bonded to the imidazolium backbone (Figure 65).

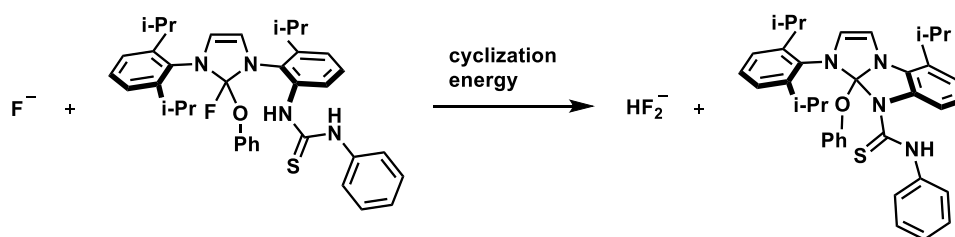




**Figure 65:** Effect on the energy of uronium fluoride, tetrahedral adduct and transition state structures resulting from the introduction of an H-bonding substituent. The use of an inflexible linker would preclude the formation of the conformer highlighted in blue.

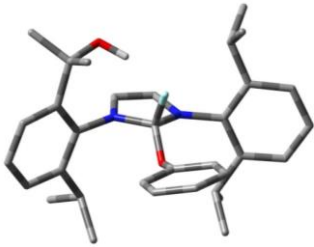
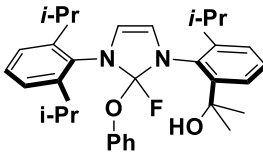

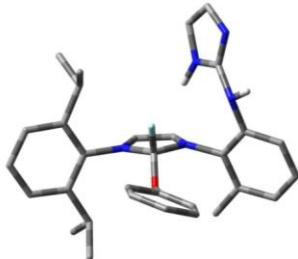
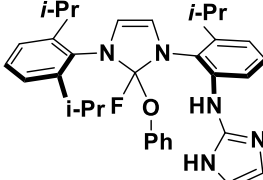
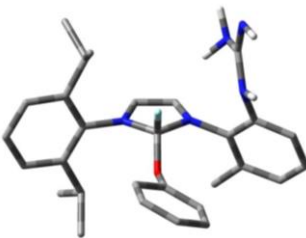
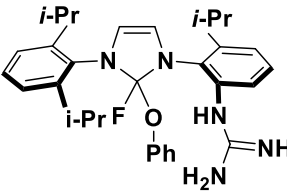


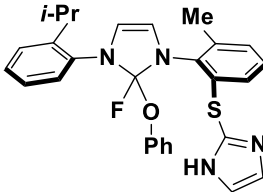
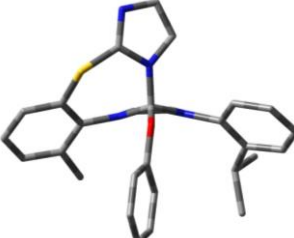
Based on initial computational data that verified that the energy difference between the tetrahedral adduct and the transition state (activation barrier in table 6) can be decreased by a substantial amount, Hassan Beyzavi and Debashis Mandal set out to synthesize hydrogen-bonding PhenoFluor derivatives. Computational data also indicated that in the presence of a single hydrogen-bond-donor on the N-aryl substituent, the uronium fluoride structure is not stabilized to a problematic extent compared to the tetrahedral adduct – no new energy minimum on the reaction pathway was introduced. Experimentally it was found, however, that the tetrahedral adduct structure reacted with external bases to form a cyclized structure (Figure 66). A computational model for the cyclization pathway was consequently developed and the proclivity of various H-bonding motifs and linkers towards base-induced

cyclization was studied.

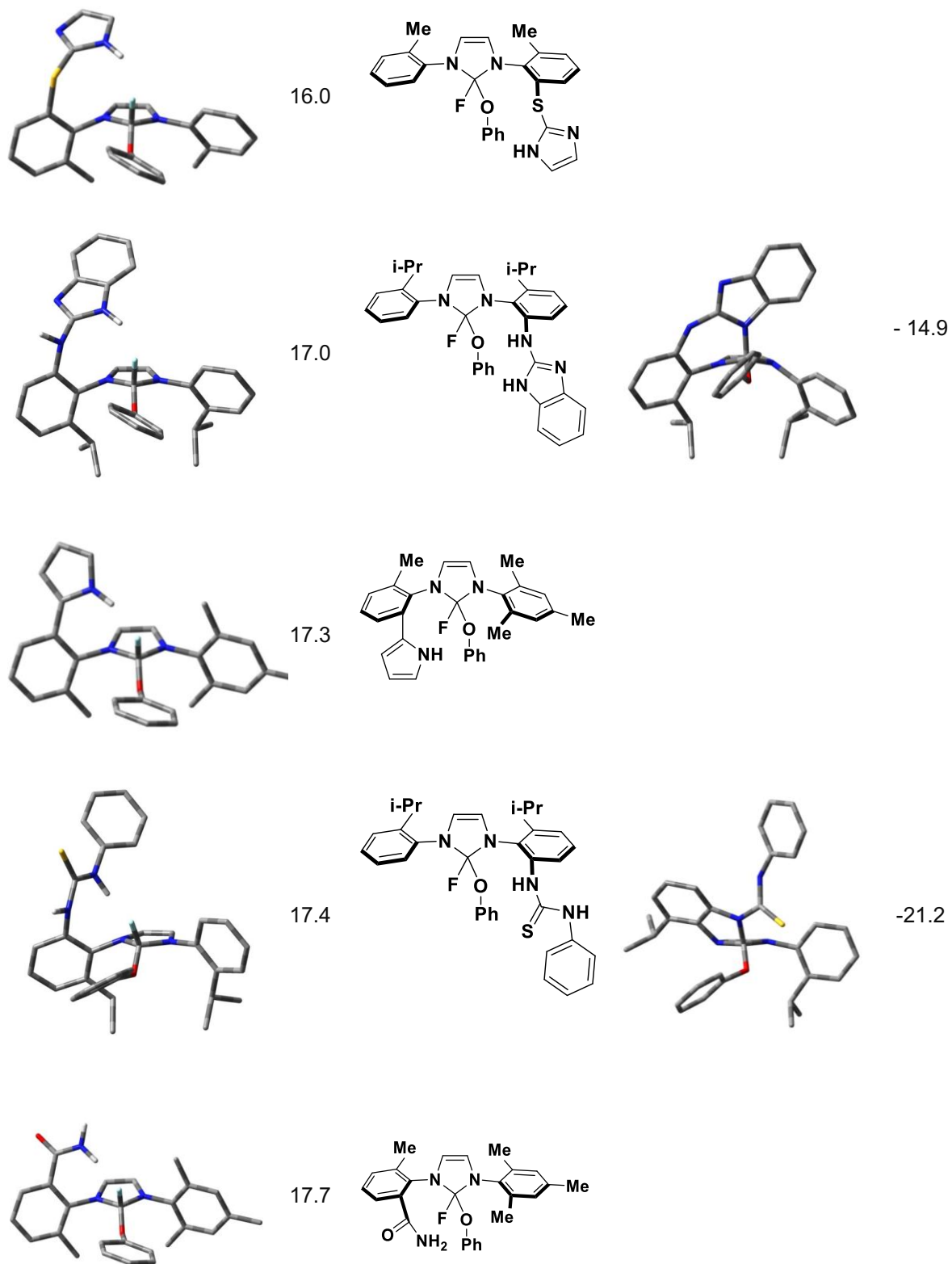


**Figure 66:** The cyclization energy listed in table 6 is defined as the DFT energy difference between fluoride and the tetrahedral adduct on the one hand and bifluoride and the cyclized product on the other hand. A negative cyclization energy implies that the formation of the cyclized product is energetically favored.

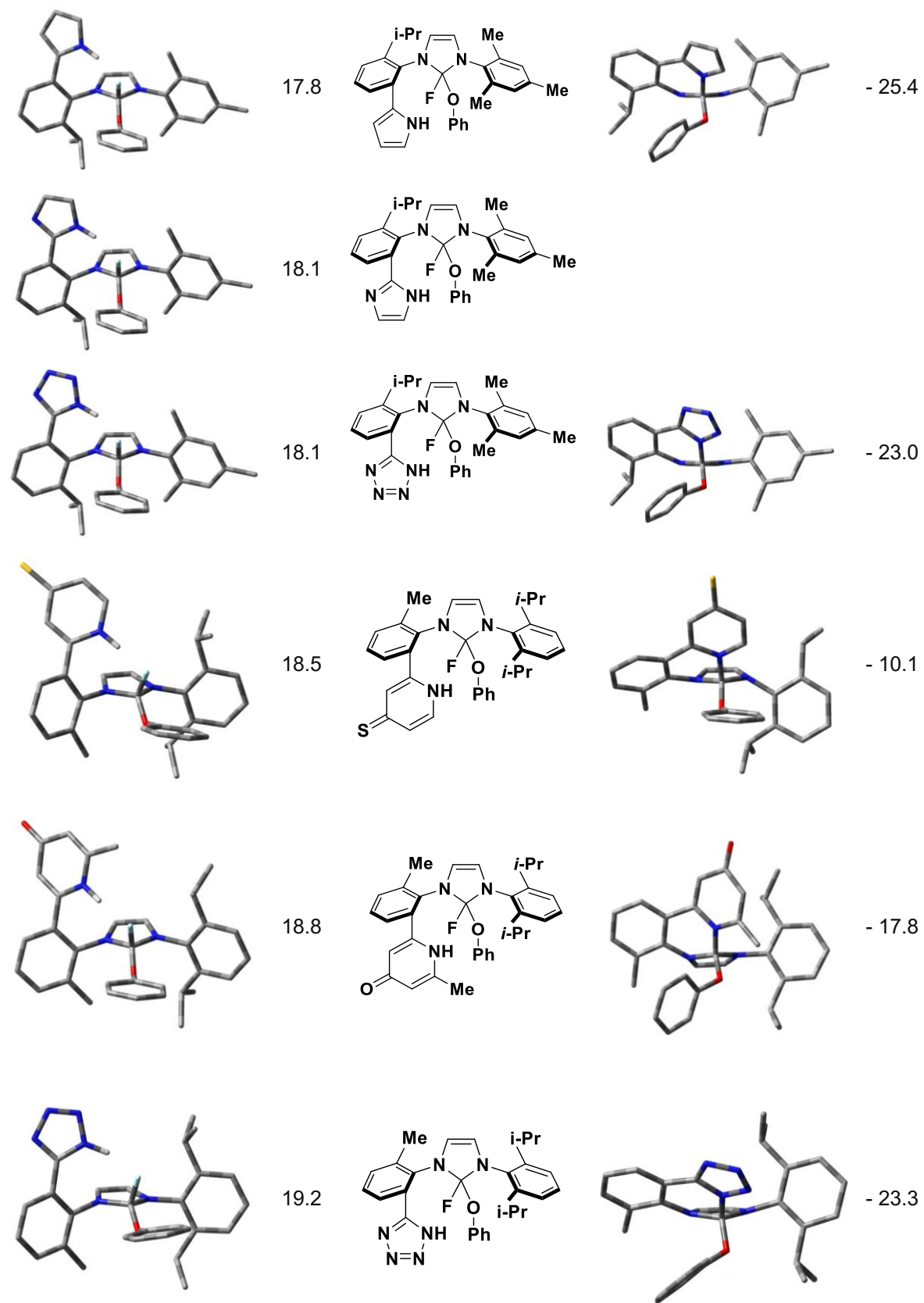
**Table 6:** Activation barriers in kcal/mol for PhenoFluor derivatives featuring N-aryl substituents that are capable of hydrogen bonding to fluoride. In the right hand column the cyclization energy (defined according to Figure 60) in kcal/mol is listed. All structures were optimized using B3LYP/6-31G(d) and a toluene solvent model; activation barriers were derived from single point energy calculations using B3LYP/6-311++G(d,p) and a toluene solvent model.

	Activation barrier		Cyclized product	Cyclization energy
	3.8			-30.5
	10.8			
	14.0			-26.2
	15.6			-13.6

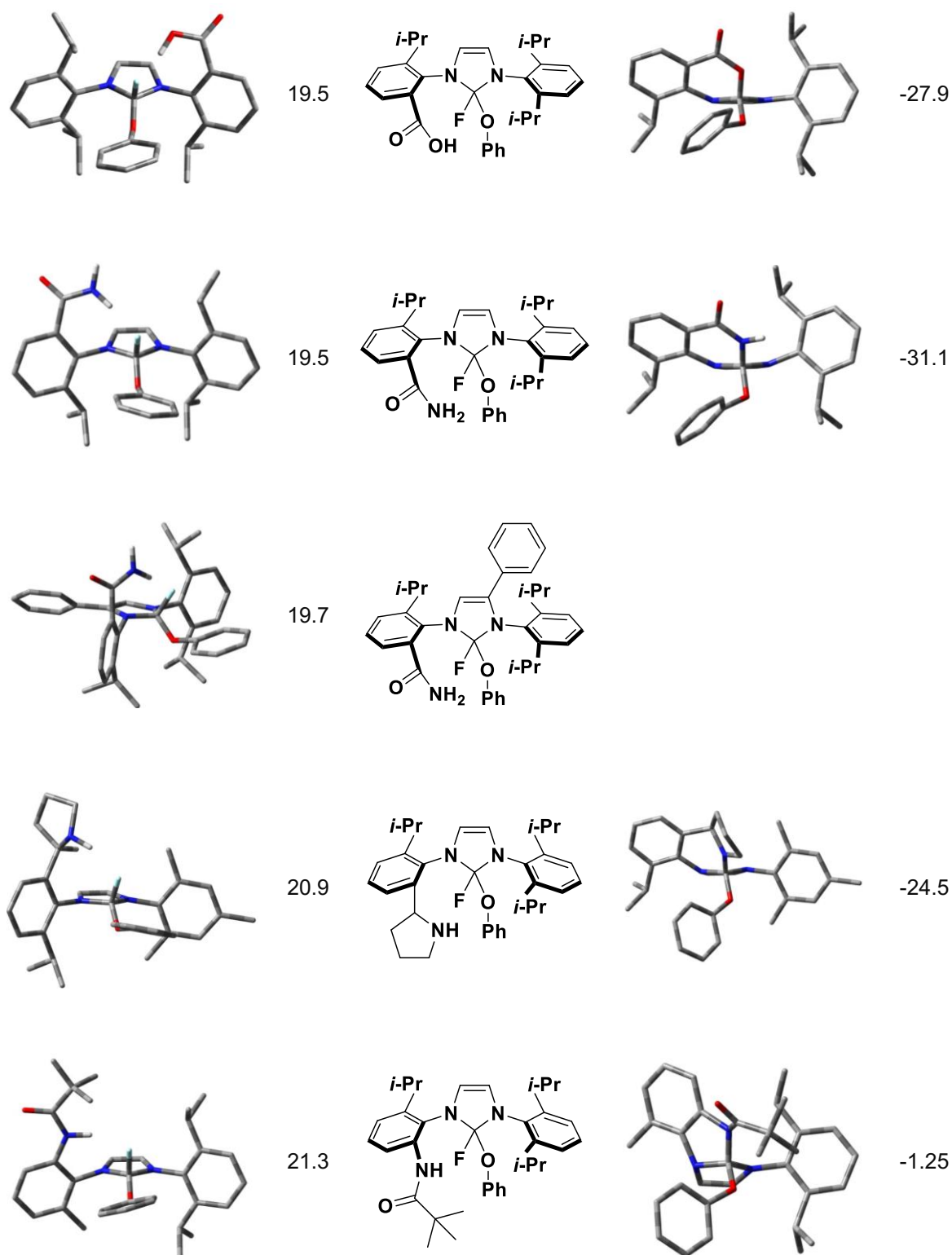
**Table 6 continued:** Activation barriers for PhenoFluor derivatives with hydrogen-bonding substituents.



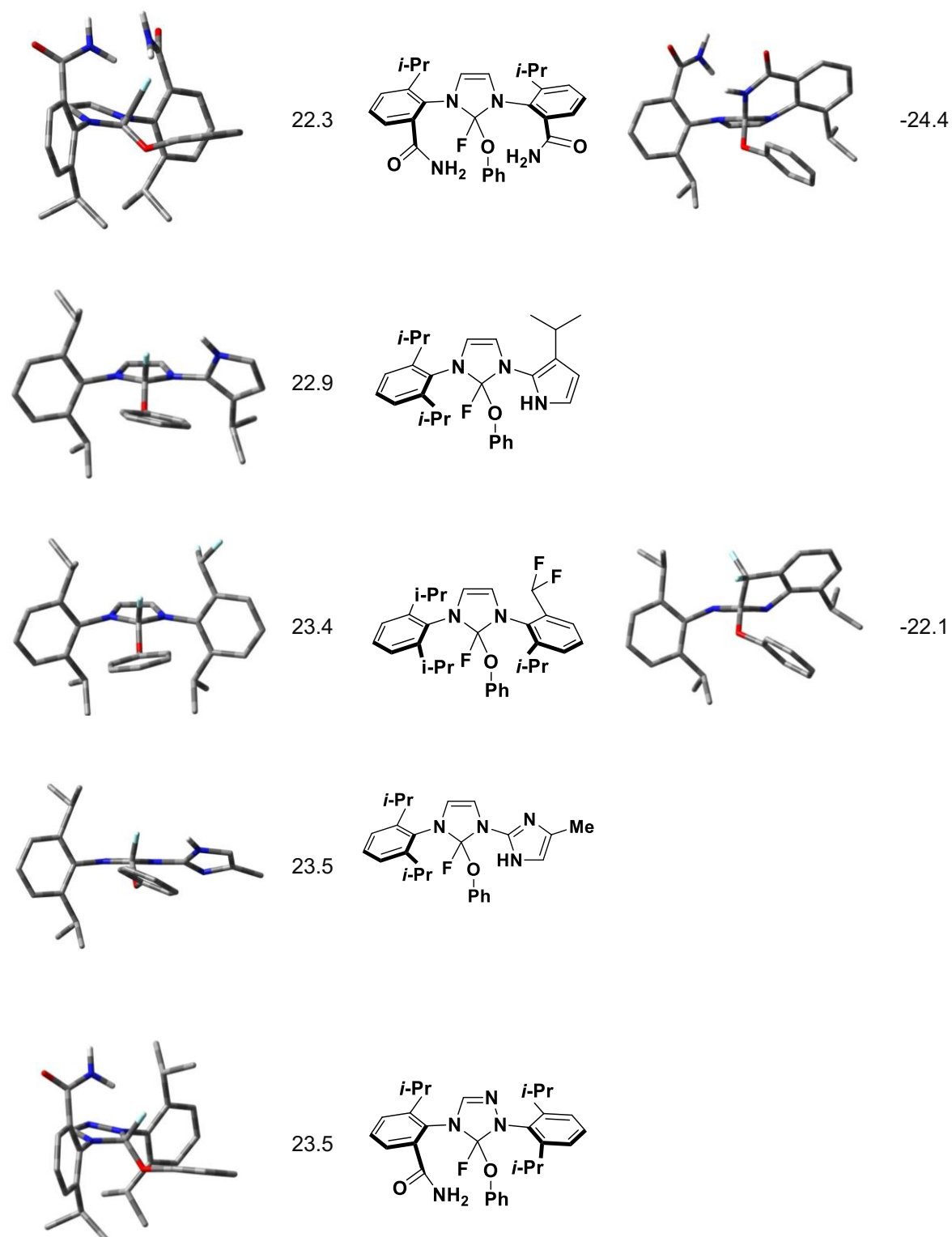
**Table 6 continued:** Activation barriers for PhenoFluor derivatives with hydrogen-bonding substituents.



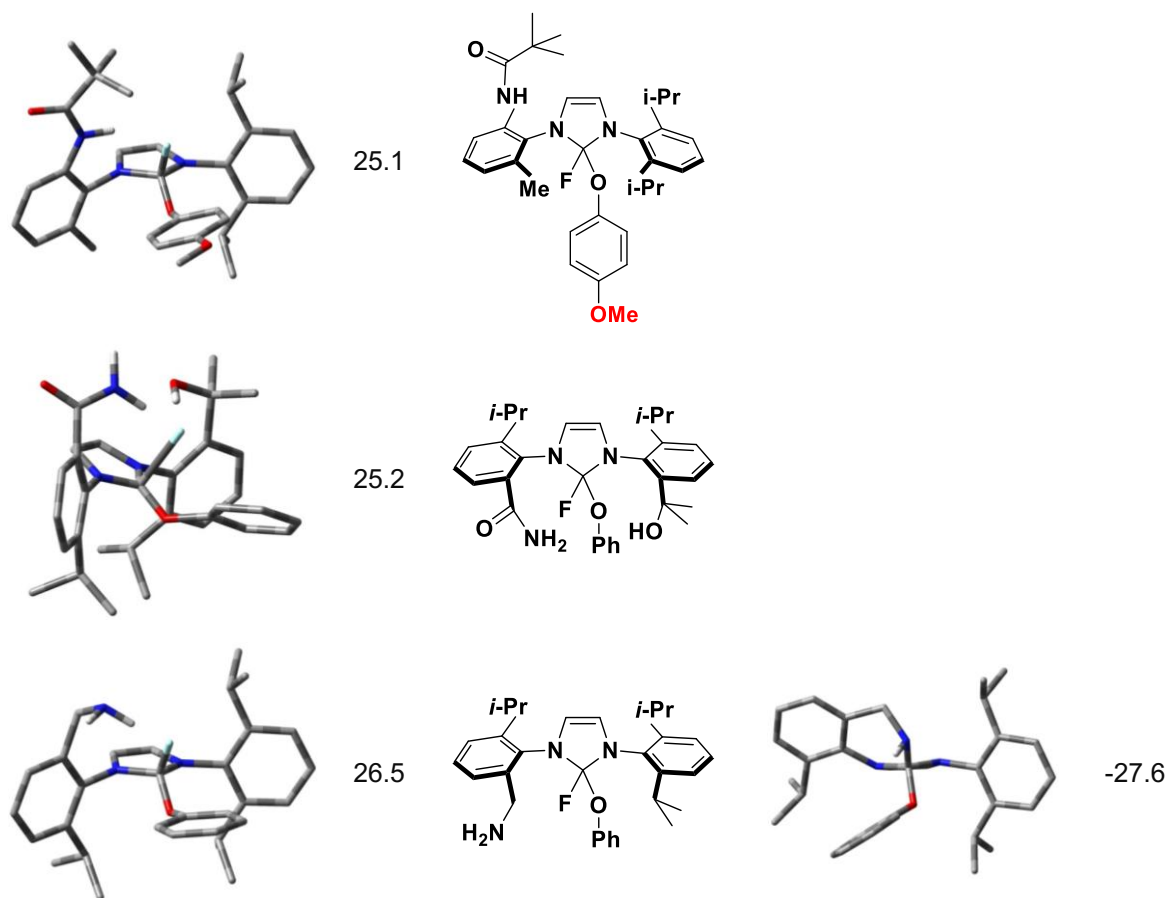
**Table 6 continued:** Activation barriers for PhenoFluor derivatives with hydrogen-bonding substituents.



**Table 6 continued:** Activation barriers for PhenoFluor derivatives with hydrogen-bonding substituents.



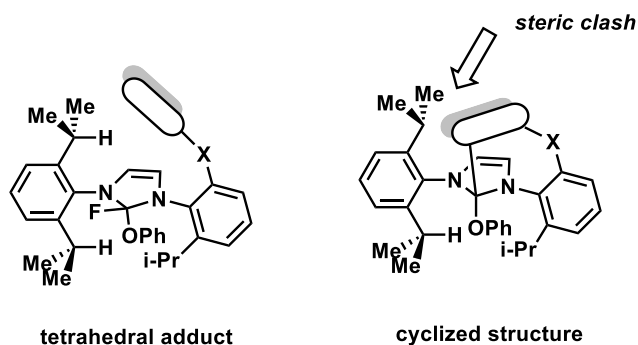
**Table 6 continued:** Activation barriers for PhenoFluor derivatives with hydrogen-bonding substituents.



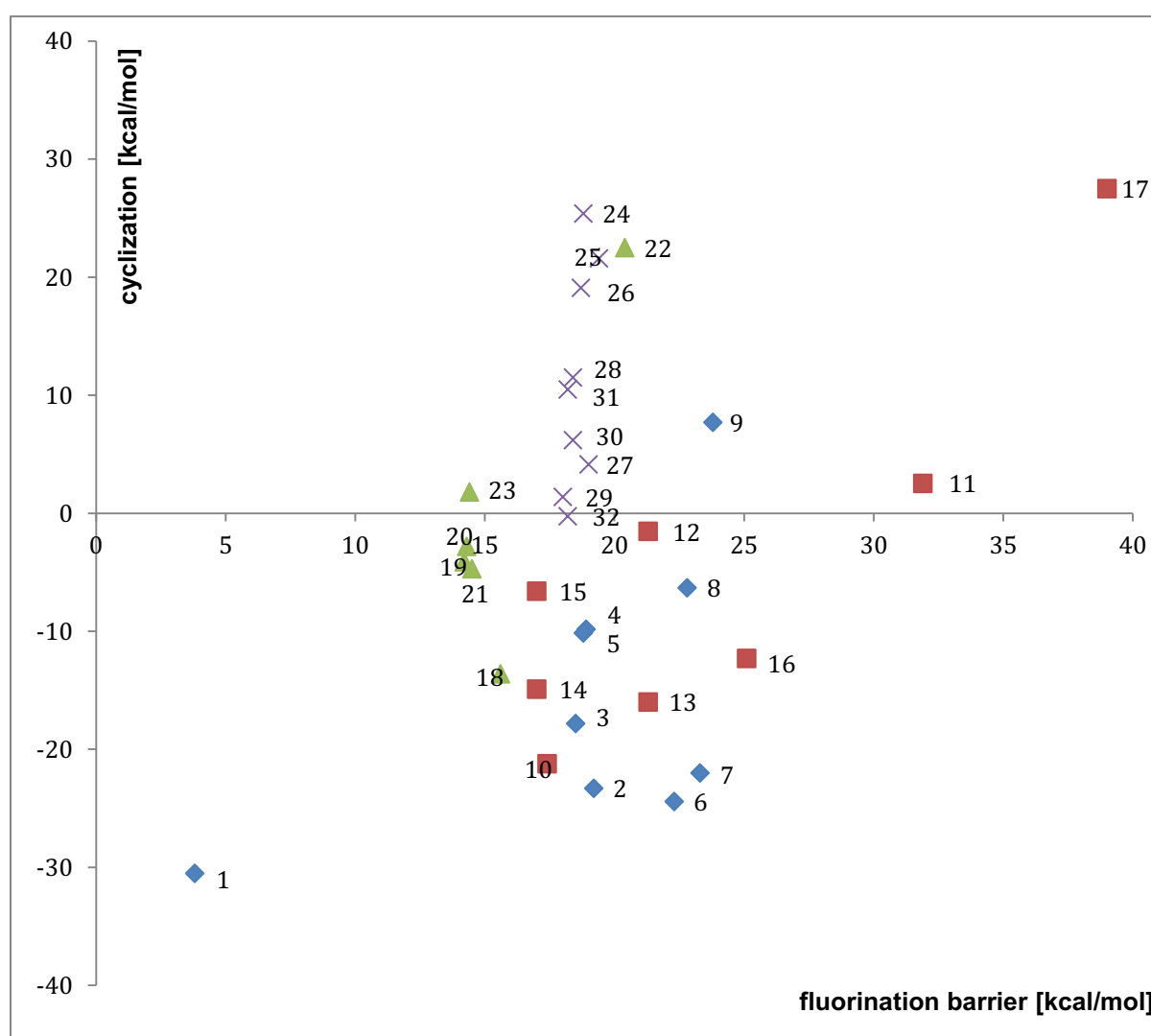
### Controlling the equilibrium between the tetrahedral adduct and the cyclized product

Analysis of the data in table 6 led us the hypothesis that a build-up of steric hindrance between the hydrogen-bonding substituent and the isopropyl group of the diisopropylphenyl group on the other nitrogen atom could be used to disfavor cyclization. Sterically hindered H-donor moieties were attached to a number of linkers and the resulting PhenoFluor derivatives were subjected to computational analysis. A two dimensional correlation was used to facilitate analysis of the data. No electronic trend in the proclivity of various derivatives towards cyclization could be discerned.

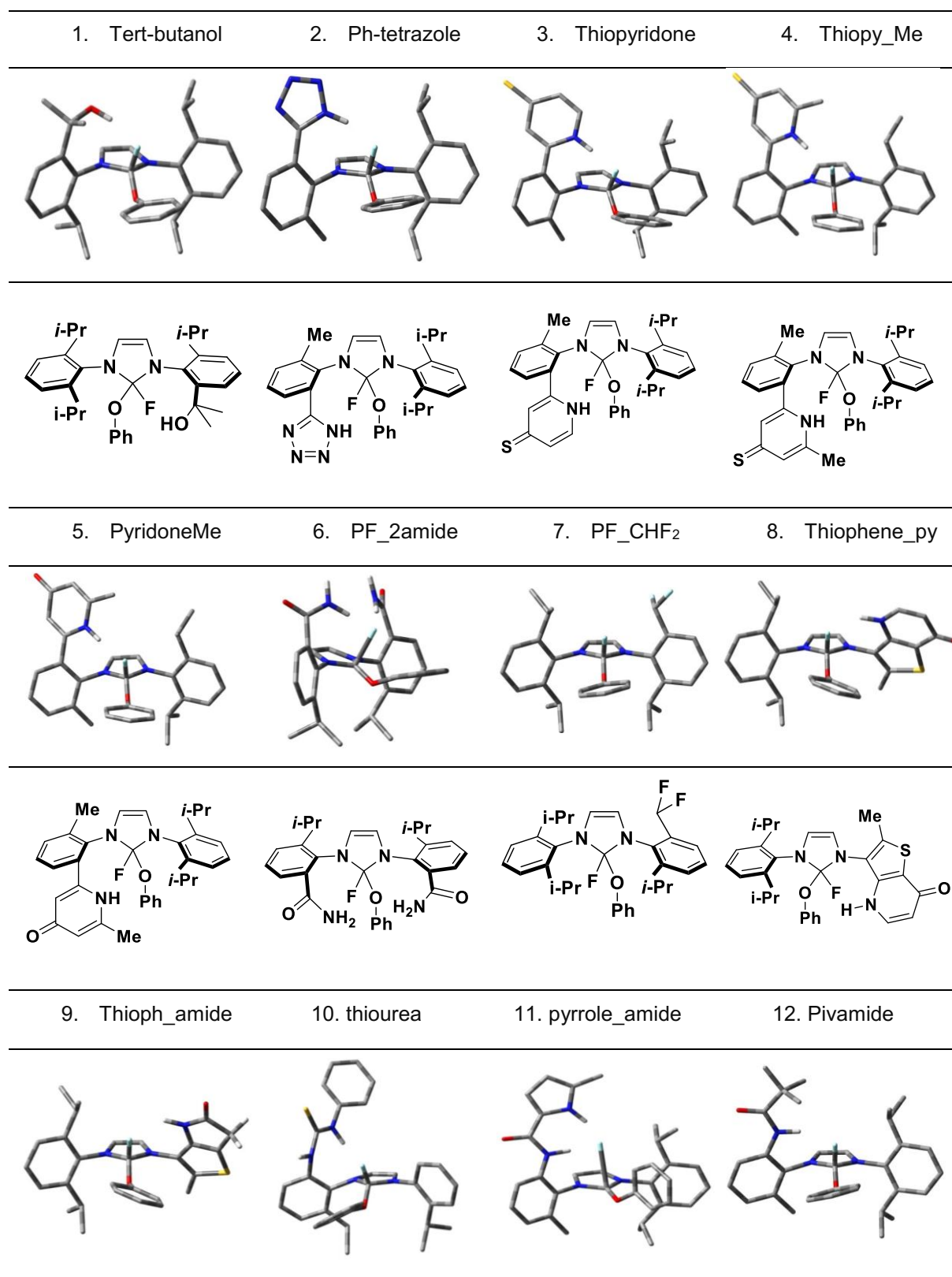




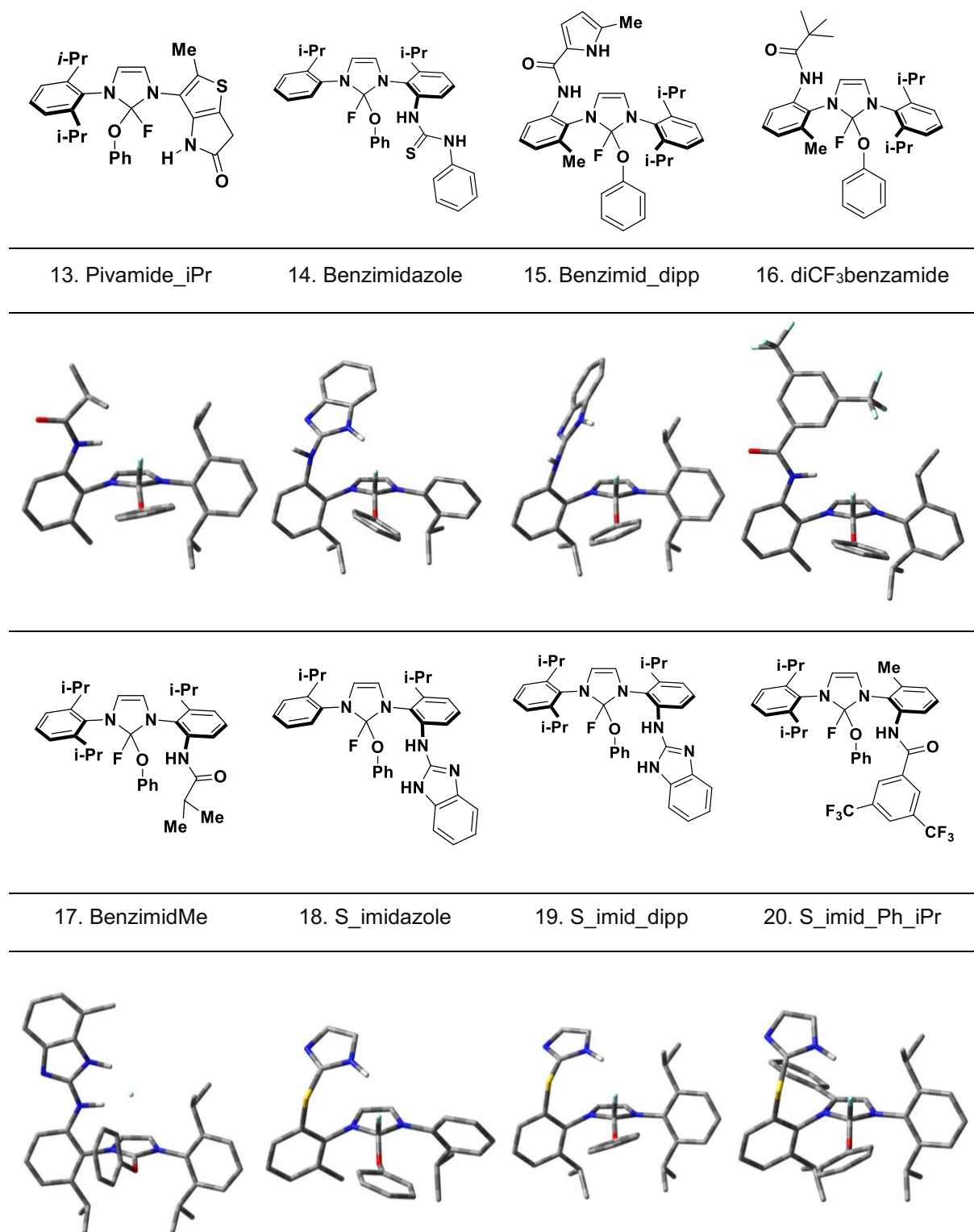
**Figure 67:** Steric hindrance between the isopropyl substituent and the H-bonding moiety is exacerbated upon cyclization. Bulky substituents henceforth disfavor cyclization.



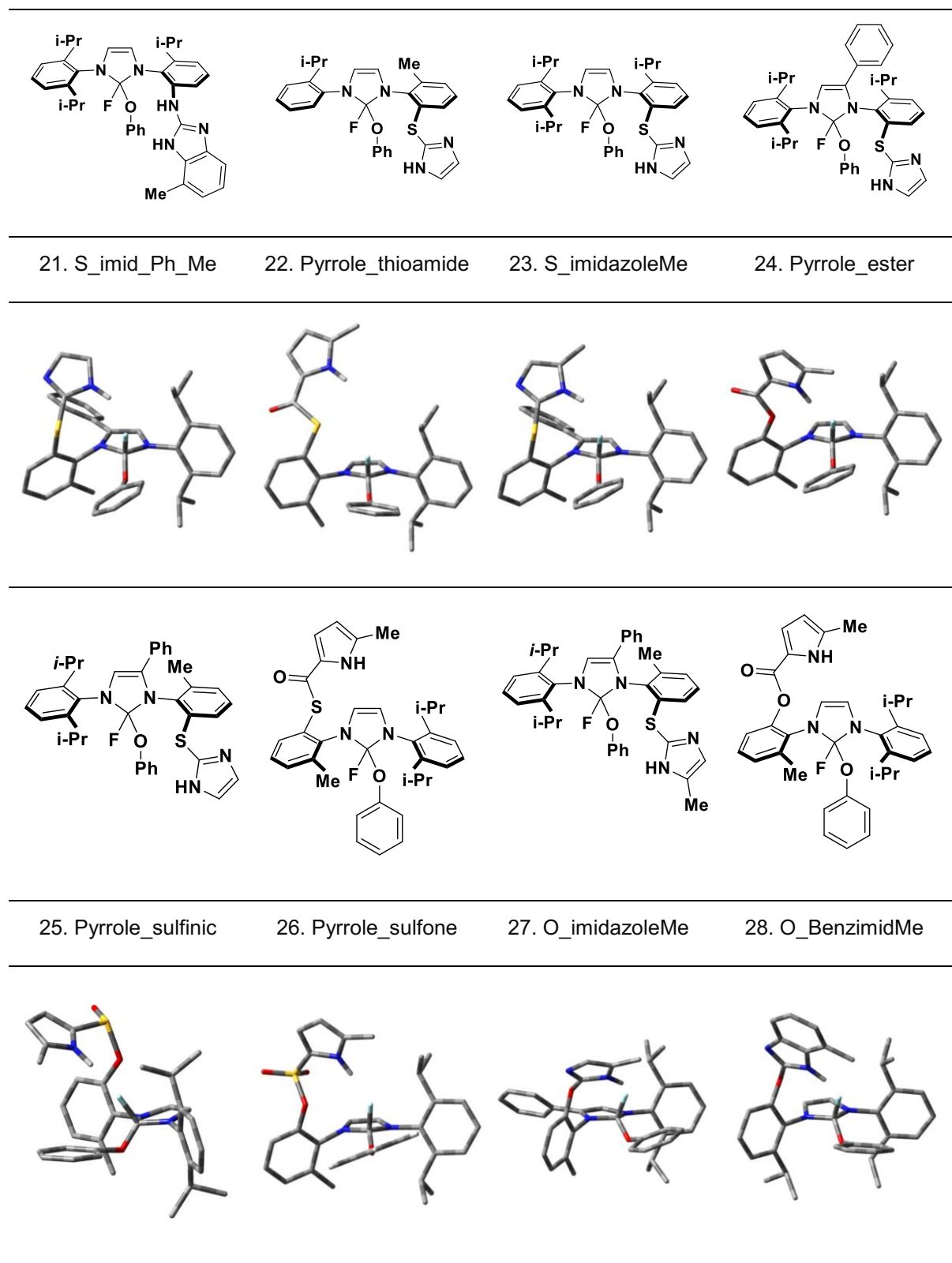
**Figure 68:** Two-dimensional correlation of the activation barrier and the cyclization energy for various PhenoFluor derivatives with H-bonding substituents. Color coding: green for X = S, grey for X = O, blue for X = CH<sub>2</sub> and red for X = NH (see Figure 67).



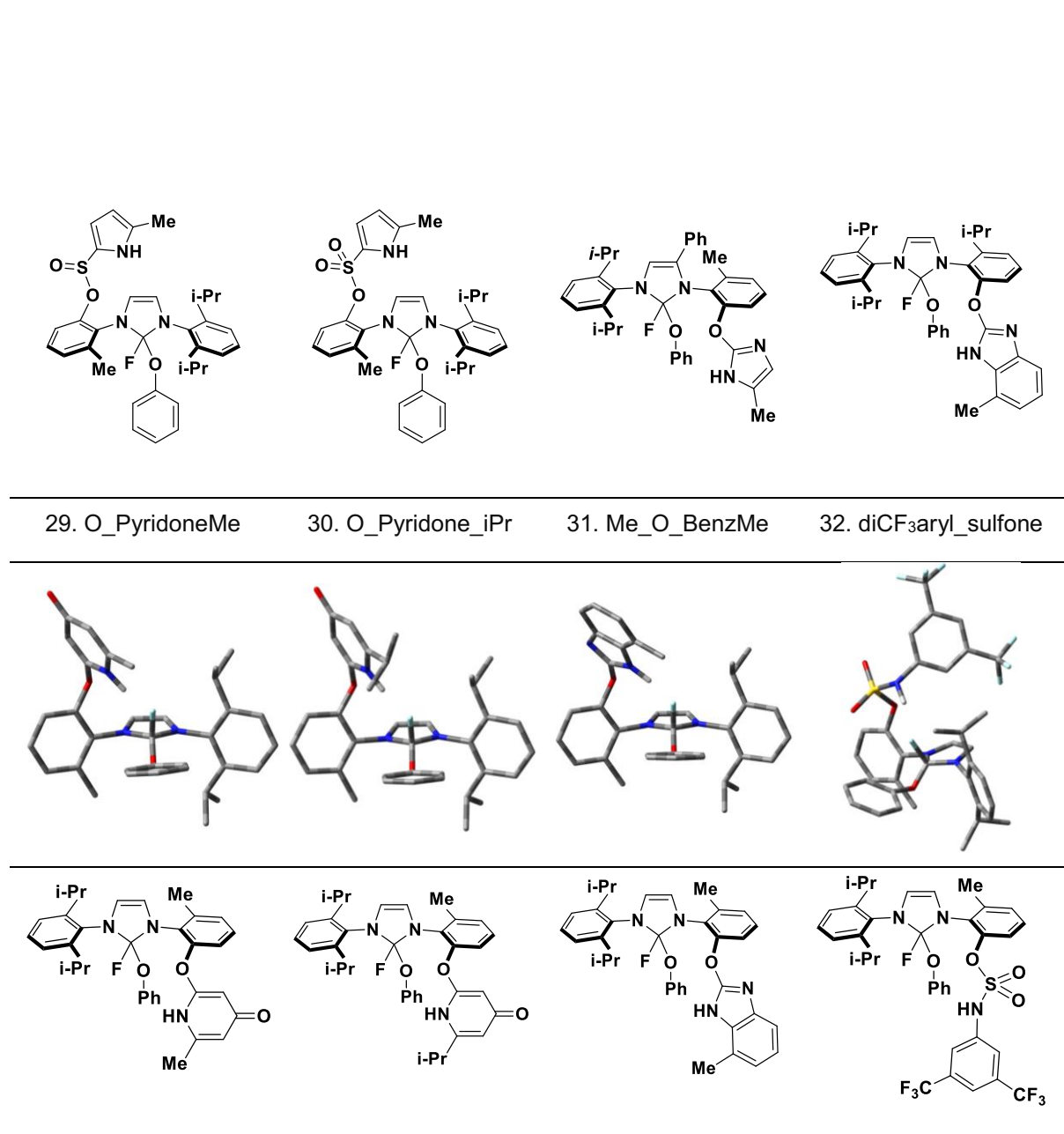
**Figure 68 continued:** Two-dimensional correlation of the activation barrier and the cyclization energy for various PhenoFluor derivatives with H-bonding substituents.



**Figure 68 continued:** Two-dimensional correlation of the activation barrier and the cyclization energy for various PhenoFluor derivatives with H-bonding substituents.



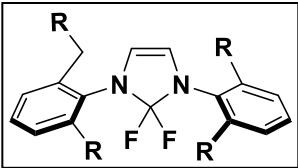
**Figure 68 continued:** Two-dimensional correlation of the activation barrier and the cyclization energy for various PhenoFluor derivatives with H-bonding substituents.



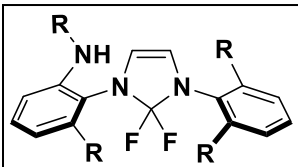
**Figure 68 continued:** Two-dimensional correlation of the activation barrier and the cyclization energy for various PhenoFluor derivatives with H-bonding substituents.

Analysis of Figure 68 revealed that the activation barrier observed shows a pronounced dependence on the linker atom. Data points in Figure 68 are color-coded to reflect the identity of the linker atom and especially in the case of oxygen and sulfur linkers, the activation barriers for all investigated derivatives fall within a narrow range. Cyclization energies largely depend on the steric environment and thus vary widely within a series with the same linker atom (see Tables 7, 8, 9 and 10). Oxygen-based derivatives featuring bulky H-donor moieties were identified as the most promising derivatives and work to synthesize and test such derivatives experimentally is in currently progress.

**Table 7:** Deoxyfluorination activation barriers and cyclization energies in kcal/mol for PhenoFluor derivatives featuring a carbon linker and a hydrogen-bonding motif.

		Activation barrier	Cyclization E	
	<b>1</b>	Tert-butanol	3.8	- 30.5
	<b>2</b>	Ph-tetrazole	19.2	- 22.3
	<b>3</b>	Thiopyridone	18.5	- 17.8
	<b>4</b>	ThiopyridoneMe	18.9	- 9.8
	<b>5</b>	PyridoneMe	18.8	- 10.1
	<b>6</b>	PF_2amide	22.3	- 24.4
	<b>7</b>	PF_CHF <sub>2</sub>	23.3	- 22.0
	<b>8</b>	Thiophene_pyridone	22.8	- 6.3
	<b>9</b>	Thiophene_amide	23.8	7.7

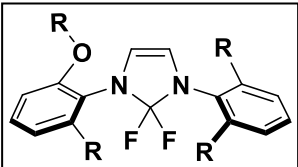
**Table 8:** Deoxyfluorination activation barriers and cyclization energies in kcal/mol for PhenoFluor derivatives featuring a nitrogen linker and a hydrogen-bonding motif.

	<b>10</b>	Thiourea	17.4	- 21.2
	<b>11</b>	Pyrrole_amide	31.9	2.5
	<b>12</b>	Pivamide	21.3	- 1.5
	<b>13</b>	Pivamide_iPr	21.3	- 16.0
	<b>14</b>	Benzimidazole	17.0	- 14.9
	<b>15</b>	Benzimidazole_iPr	17.0	- 6.6
	<b>16</b>	diCF <sub>3</sub> _benzamide	25.1	- 12.3
	<b>17</b>	BenzimidMe	39	27.5

**Table 9:** Deoxyfluorination activation barriers and cyclization energies in kcal/mol for PhenoFluor derivatives featuring a sulfur linker and a hydrogen-bonding motif.

	<b>18</b>	S_imidazole	15.6	- 13.6
	<b>19</b>	S_imidazole_dipp	14.2	- 4.1
	<b>20</b>	S_imidazole_Ph_iPr	14.3	- 2.8
	<b>21</b>	S_imidazole_Ph_Me	14.5	- 4.7
	<b>22</b>	Pyrrole_thioamide	20.4	22.5
	<b>23</b>	S_imidazoleMe	14.4	1.8

**Table 10:** Deoxyfluorination activation barriers and cyclization energies in kcal/mol for PhenoFluor derivatives featuring an oxygen linker and a hydrogen-bonding motif.

	<b>24</b>	Pyrrole_ester	18.8	25.4
	<b>25</b>	Pyrrole_sulfinic	19.4	21.6
	<b>26</b>	Pyrrole_sulfonic	18.7	19.1
	<b>27</b>	O_imidazoleMe	19.0	4.2
	<b>28</b>	O_BenzimidazoleMe	18.4	11.5
	<b>29</b>	O_PyridoneMe	18.0	1.4
	<b>30</b>	O_Pyrdone_iPr	18.4	6.2
	<b>31</b>	Me_O_BenzMe	18.2	10.5
	<b>32</b>	diCF <sub>3</sub> aryl_sulfone	18.2	- 0.25

The data presented in Figure 67 shows that a range of derivatives featuring hydrogen-bonding substituents could be identified that have deoxyfluorination barriers below that of the original PhenoFluor reagent (24.3 kcal/mol). The challenge consists in the identification of derivatives with a low reaction barrier that do not have a proclivity to cyclize under the basic reaction conditions used for deoxyfluorination with  $^{19}\text{F}$  or  $^{18}\text{F}$ -fluoride. In order for significant stabilization of the transition state structure to take place, the linker must position the hydrogen-bond donor moiety close to the location of fluoride in the transition state. Unfortunately, however, this arrangement positions the hydrogen bond donor moiety close to the imidazolium core, favoring cyclization. We found that upon cyclization the hydrogen bonding moiety moves closer towards the isopropyl groups on the adjacent nitrogen-aryl substituent (Figure 67). This observation could be used to impede the cyclization reaction without compromising the favorable alignment of the hydrogen-bonding moiety which incurs transition state stabilization. The use of bulky hydrogen-bonding moieties disfavors cyclization: Structure 19 has a significantly lower proclivity towards cyclization than structure 18 due to the presence of the diisopropyl substituents on the adjacent N-aryl substituent. The same trend was observed for the larger iPr substituent in substituent 20 compared to the methyl substituent in structure 21. Comparison of structure 29 and structure 30 shows that a slight increase in the steric bulk of the hydrogen donor moiety can bring about a destabilization of the cyclized structure. Both structure 10 and structure 12 have been synthesized by Hassan Beyzavi and their reactivity has been studied. While the labeling precursors based on compound 10 were difficult to prepare and underwent cyclization under a variety of reaction conditions, labeling precursors based on compound 12 proved to be considerably more stable. Radiodeoxyfluorination with labeling precursors based on structure 12 was unsuccessful, which we attributed to cyclization taking place under the basic reaction conditions of the labeling experiment. The experimental results are in line with the computational predictions with a cyclization energy of  $-21.3$  kcal/mol for structure 10 and  $-1.5$  kcal/mol for structure 12. Computational as well as experimental results suggest that the



problem of cyclization was not sufficiently addressed by the steric bulk introduced by the tert-butyl group in structure 12. We subsequently found that pyrrole- and benzimidazole based hydrogen bond donor motifs and be utilized to generate derivatives that are not predicted to cyclize under basic conditions. Structures 24, 25 and 26 exhibit low deoxyfluorination barriers while cyclization is disfavored by around 20 kcal/mol under basic conditions (Table 10). All three structures employ a pyrrole hydrogen bonding motif that is attached to the ortho position of the N-aryl substituent by an ester (24), sulfinic acid ester (25) or sulfonic acid ester (26). The two closely related derivatives structure 28 and structure 31 are based on benzimidazole hydrogen-bonding motifs attached *via* an oxygen linker. Both structures are associated with deoxyfluorination barriers below 19 kcal/mol and large positive cyclization energies and are thus viable candidates for an improved deoxyfluorination reagent. Substituted pyridones also are potentially interesting hydrogen-bonding motifs but sterically bulky substituents on the pyridone ring are required to disfavor cyclization since the presence of a methyl substituent (structure 29) results in a cyclization energy that is only slightly positive (Table 10). The larger isopropyl substituent in the pyridone-based structure 30, on the other hand, is associated with a more promising cyclization energy of 6.2 kcal/mol.

In addition to interesting candidates for synthetic exploration found in the oxygen-linker series (structures 24, 25, 26, 28, 30, 31 in table 10), structure 22 and structure 23, which feature a sulfur-based linker, were also considered (Table 9). The computed cyclization energy for 23 is only 1.8 kcal/mol and cyclization of the structure under the basic reaction conditions is feasible. Cyclization is unlikely to occur for structure 22, but this derivative has a predicted deoxyfluorination barrier of 20.4 kcal/mol, which is higher than those for the candidates selected from the oxygen series. Furthermore, we were concerned that under the basic reaction conditions of the deoxyfluorination, nucleophilic groups present on the reaction substrate could react with structure 22 to induce cleavage of the thioester.

We found that structural elements bearing a single H-bond donor suitably arranged to interact with fluoride in the transition state is preferable to structural elements bearing two H-bond donors: Structure 11 and structure 17, for which both the N-H linker and the H-bond donor moiety form hydrogen bonds to fluoride, are associated with high deoxyfluorination barriers (Table 8). For structures with two hydrogen bonds the uronium fluoride structure becomes stabilized to such an extent that a new energy minimum is introduced. Additional hydrogen bond donors will lower the energy of the transition state compared to a transition state structure stabilized by a single hydrogen bond. The additional stabilization brought about by the presence of a second hydrogen bond is far larger in the case of the uronium fluoride structure, however, leading to an increase in the reaction barrier (Figure 65).

The conclusion drawn from the computational analysis was that derivatives featuring an oxygen linker attached to a bulky hydrogen-bonding motif bearing a single hydrogen-bond donor are the most promising candidates for the development of an improved deoxyfluorination reagent. Synthetic efforts towards compounds such as structure 24, 25, 26, 28, 30 and 31 are currently underway.

## CHAPTER 3: EXPERIMENTAL METHODS

### General methods

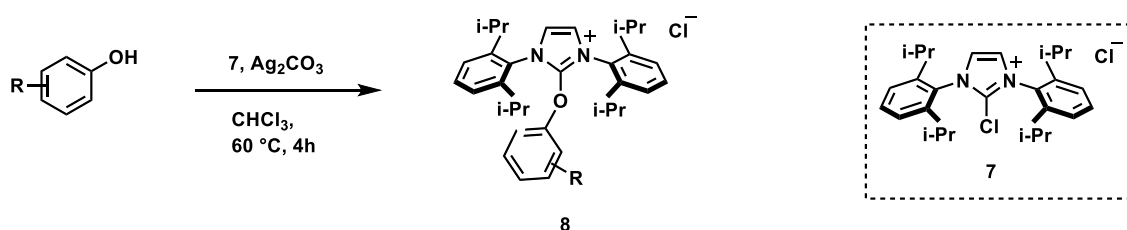
No-carrier-added  $^{18}\text{F}$ -fluoride was produced from water 97% enriched in  $^{18}\text{O}$  (Sigma-Aldrich®) by the nuclear reaction  $^{18}\text{O}(\text{p},\text{n})^{18}\text{F}$  using a Siemens Eclipse HP cyclotron and a silver-bodied target at MGH Athinoula A. Martinos Center for Biomedical Imaging. The produced  $^{18}\text{F}$ -fluoride in water was transferred from the cyclotron target by helium push. Liquid chromatographic analysis (LC) was performed with Agilent 1100 series HPLCs connected to a Carol and Ramsey Associates Model 105-S radioactivity detector. An Agilent Eclipse XDB-C18, 5  $\mu\text{m}$ , 4.6 x 150 mm HPLC column was used for analytical analysis and an Agilent Eclipse XDB-C18, 5  $\mu\text{m}$ , 9.4 x 250 mm HPLC column was used for preparative HPLC. Analytical and preparative HPLC used the following mobile phases: 0.1%  $\text{CF}_3\text{CO}_2\text{H}$  in water (A) 0.1%  $\text{CF}_3\text{CO}_2\text{H}$  in acetonitrile (B). Program: 5% (B) for 1 minutes then a gradient 5–95% (B) over 9 minutes followed by 2 minutes of 95% (B). In the analysis of the  $^{18}\text{F}$ -labeled compounds, isotopically unmodified reference substances were used for identification. Radioactivity was measured in a Capintec, Inc. CRC-25PET ion chamber. Solvents and reagents for radiochemical experiments: 2-Butanone (ACS reagent, >99.0%), Ethanol (absolute, >99.8%), Chloroform (ACS reagent, >99.8%) and Tributylamine (>98.5%) were purchased from SigmaAldrich® and used as received. Water was obtained from a Millipore Milli-Q Integral Water Purification System. Potassium bicarbonate ( $\geq 99\%$ ) was purchased from SigmaAldrich® and used as received.

$^{18}\text{F}$ -Fluoride solution obtained from a cyclotron was loaded onto a Macherey-Nagel SPE Chromafix 30-PS- $\text{HCO}_3$  cartridge. After loading, the cartridge was washed with 2-butanone : EtOH = 10:1 (1 mL).  $^{18}\text{F}$ -Fluoride was eluted with a solution of labeling precursor (5.0 mg) in dissolved in 2-butanone : EtOH = 10 :1 (0.5 mL) into a 1 dram borosilicate vial containing either  $\text{NBU}_3$  (25  $\mu\text{mol}$ ) or  $\text{KHCO}_3$  (5 mg). The reaction vial was sealed with a teflon-lined cap

and left to stir at 130 °C for 20 minutes.

All  $^{18}\text{F}$ -labeled molecules were characterized by comparing the radioactivity HPLC trace of the crude reaction mixture to the HPLC UV trace of authentic reference sample. Note: radioactivity chromatographs are offset by 0.15 min on account of the delay introduced by the spatial separation between the diode array detector and the radioactivity detector.

### Preparation of labeling precursors



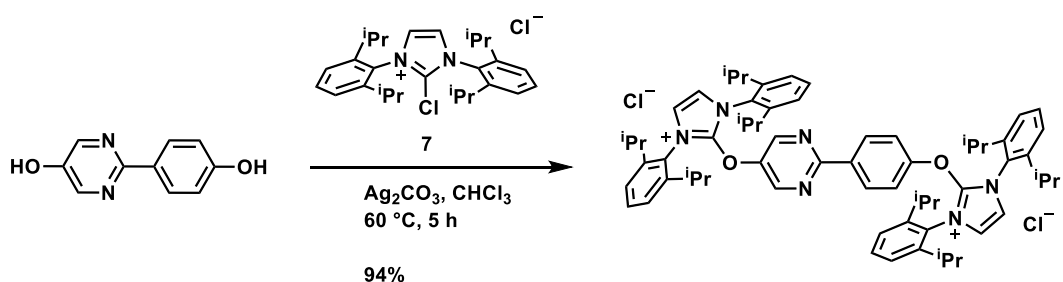
**Figure 69:** Synthesis of labeling precursors from **7** and  $\text{Ag}_2\text{CO}_3$ .

To a 20 ml vial containing **7** (1.00 equiv),  $\text{Ag}_2\text{CO}_3$  (0.50 equiv) and phenol (1.00 equiv), chloroform (2 mL/mmol phenol) was added and the resulting suspension left to stir at  $60\text{ }^\circ\text{C}$  for 4 hours. The precipitate was removed by filtration and the filtrate was concentrated to obtain the labeling precursor, which was used without further purification.

### Labeling precursors bearing additional hydroxyl groups

Selective mono-deoxyfluorination of substrates containing multiple aromatic hydroxyl groups can be achieved if the two hydroxyl groups are sufficiently electronically differentiated.  $^{18}\text{F}$ -deoxyfluorination on a heteroarene could be effected in the presence of a phenol through temporary derivatization of the phenolic hydroxyl group. The labelling precursor was prepared using two equivalents of **7** and subjected to  $^{18}\text{F}$ -deoxyfluorination. The imidazolium protecting group on the phenol is hydrolyzed under the reaction conditions and the reaction mixture can be subjected to HPLC purification without additional steps. Alcohols, unlike phenols, do not form stable uronium salts with **7** and no additional reagent has to be used if aliphatic hydroxyl groups are present in the substrate. Ethanol is used as a

co-solvent in the reaction, which indicates that the presence of aliphatic hydroxyl groups does not interfere with the  $^{18}\text{F}$ -deoxyfluorination reaction.



**Figure 70:** Synthesis of bis-uronium compounds.

2-(4-Hydroxyphenyl)pyrimidin-5-ol (32.7 mg, 160  $\mu\text{mol}$ , 1.00 equiv), **7** (150 mg, 320  $\mu\text{mol}$ , 2.00 equiv),  $\text{Ag}_2\text{CO}_3$  (44.1 mg, 160  $\mu\text{mol}$ , 1.00 equiv) and chloroform (10 mL) were added to a 20 ml borosilicate vial and the resulting suspension was stirred at 60  $^\circ\text{C}$  for 4 hours. Recrystallization from chloroform afforded 160 mg of the title compound as a colorless solid (94% yield).

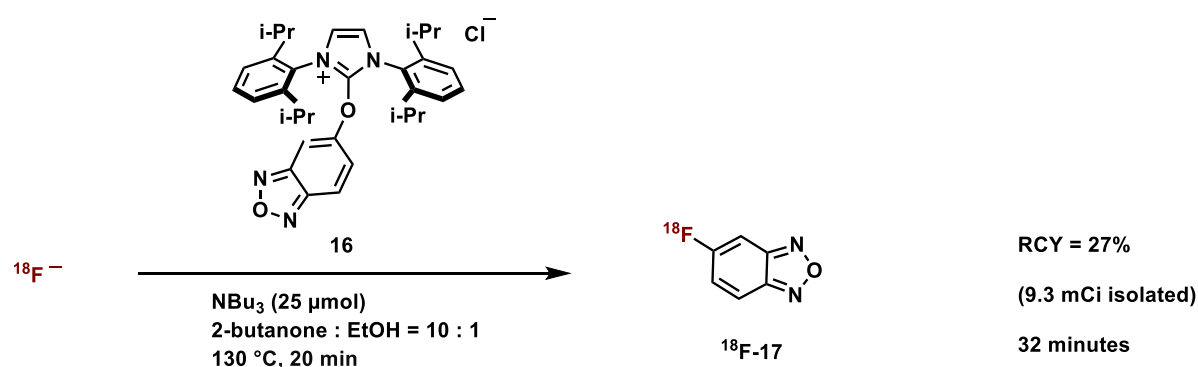
#### NMR Spectroscopy:

$^1\text{H}$  NMR (400 MHz,  $\text{DMSO-}d_6$ , 23  $^\circ\text{C}$ ,  $\delta$ ): 8.55 (s, 4H), 8.50 (s, 2H), 8.02 (d,  $J = 6.8$  Hz, 2H), 7.62 (t,  $J = 6.4$  Hz, 2H), 7.59 (t,  $J = 6.4$  Hz, 2H), 7.46 (d,  $J = 6.4$  Hz, 2H), 7.44 (d,  $J = 6.4$  Hz, 2H), 6.96 (d,  $J = 6.8$  Hz, 2H), 2.50–2.62 (m, 8H), 1.19–1.26 (m, 48H) ppm.

$^{13}\text{C}$  NMR (100 MHz,  $\text{DMSO-}d_6$ , 23  $^\circ\text{C}$ ,  $\delta$ ): 159.5, 155.0, 147.4, 147.3, 145.1, 145.0, 143.6, 143.5, 133.5, 132.5, 132.3, 130.4, 127.0, 126.9, 125.2, 125.1, 122.8, 117.3, 28.8, 28.7, 25.1, 25.0, 22.6, 22.4 ppm.

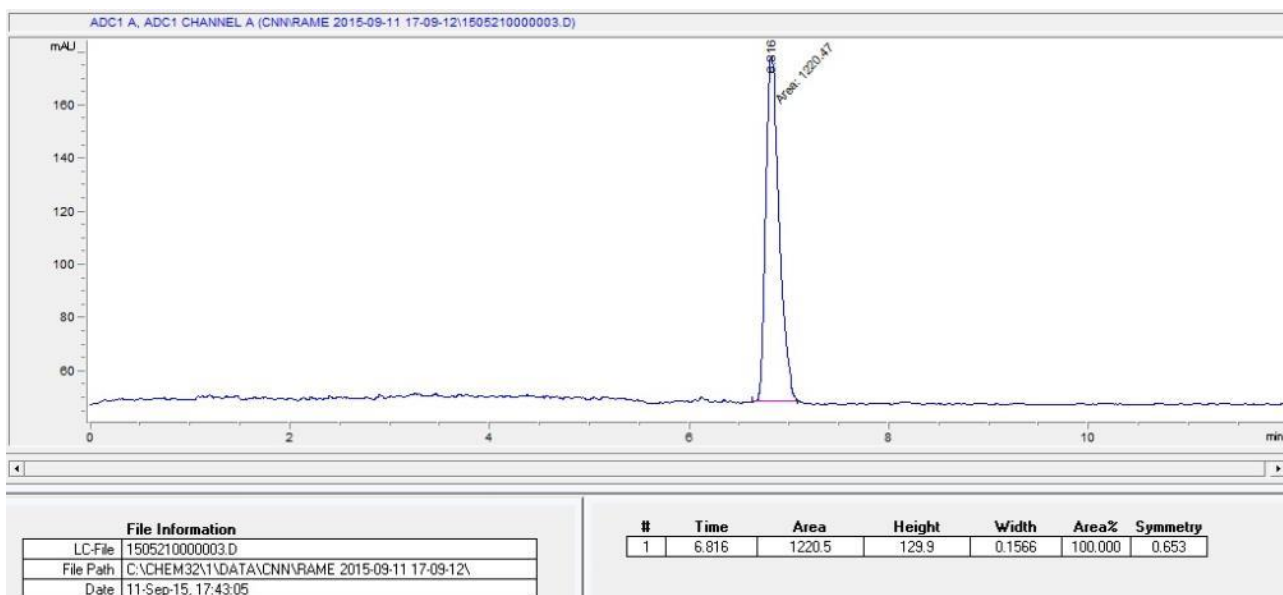
**HRMS-FIA(m/z)** calc'd for  $\text{C}_{13}\text{H}_8\text{FNS}$   $[\text{M}-2\text{Cl}^-/2]^+$ , 481.30905; found, 481.3092.

## <sup>18</sup>F-Fluorination of the labeling precursor

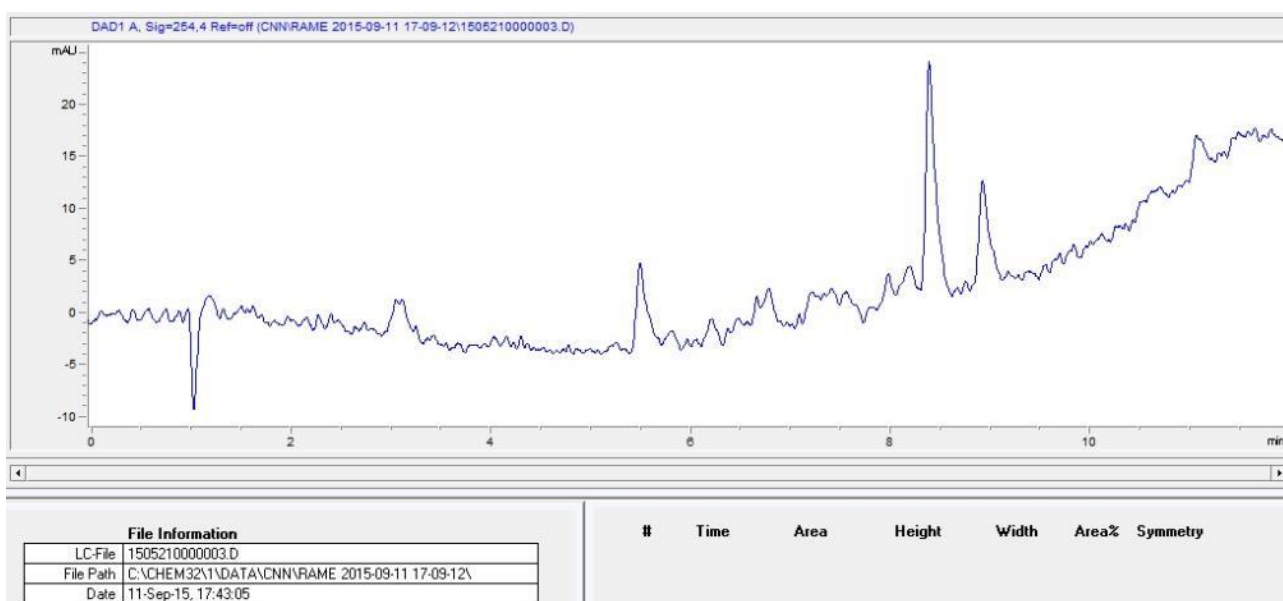


**Figure 71:** Reaction scheme for the preparation of **<sup>18</sup>F-17**.

<sup>18</sup>F-Fluoride solution (0.6 ml, 34.0 mCi) was loaded onto an anion exchange cartridge (Chromafix 30-PS-HCO<sub>3</sub>) with >99% trapping efficiency, and the cartridge was washed with 2-butanone : EtOH = 10:1 (1 mL). In order to maximize elution efficiency, the cartridge was inverted and fitted with a female × female luer adapter (Cole-Palmer, Nylon, EW-45502-22) to connect the top end of the inverted cartridge to a 1 ml plastic syringe containing a solution of the labeling precursor (8.0 mg of **16** dissolved in 2-butanone : EtOH : NBu<sub>3</sub> = 10 : 1 : 0.1 (1.0 mL)). The eluent was trapped in a 4 mL borosilicate vial and was measured to contain 21 mCi (62% of the total activity used). The reaction vial was sealed with a teflon-lined cap and left to stir at 130 °C for 17 minutes. The reaction mixture was allowed to cool down for 1 minute before being subjected to purification by semi-preparative HPLC. The fraction corresponding to radiolabeled product **<sup>18</sup>F-17** was collected and was measured to contain 9.3 mCi (27% of the initial activity). The isolated, non-decay corrected yield was 27% and the synthesis and purification time was 32 minutes from the time <sup>18</sup>F was obtained from the cyclotron.



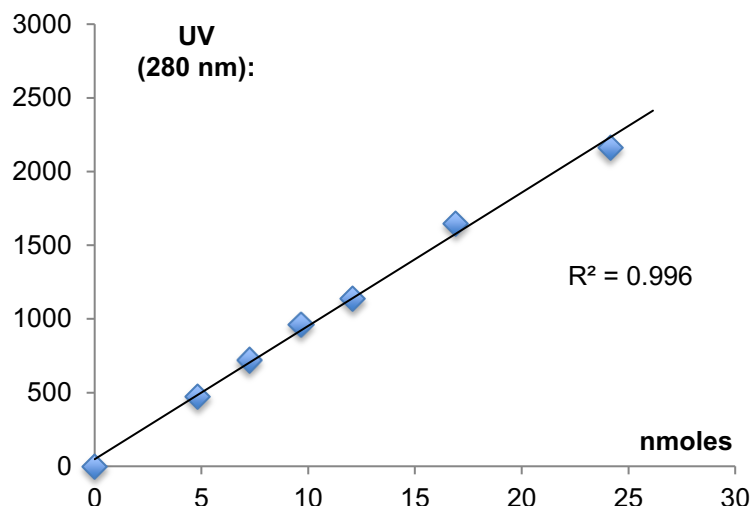
**Figure 72:** Analytical HPLC radiotracer of HPLC purified material.



**Figure 73:** UV trace (254 nm) of HPLC purified material.

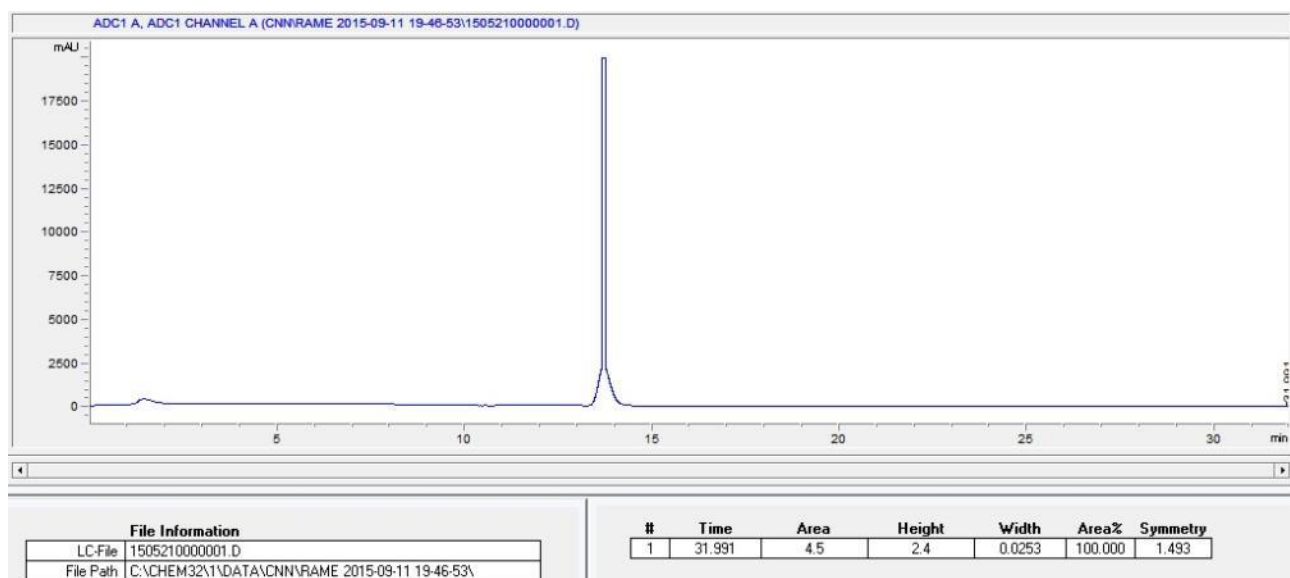
### Specific Activity

Using the authentic reference material **17** a standard curve was generated by integration of the UV absorbance signal (at 280 nm) of 6 different known amounts (Figure 74).



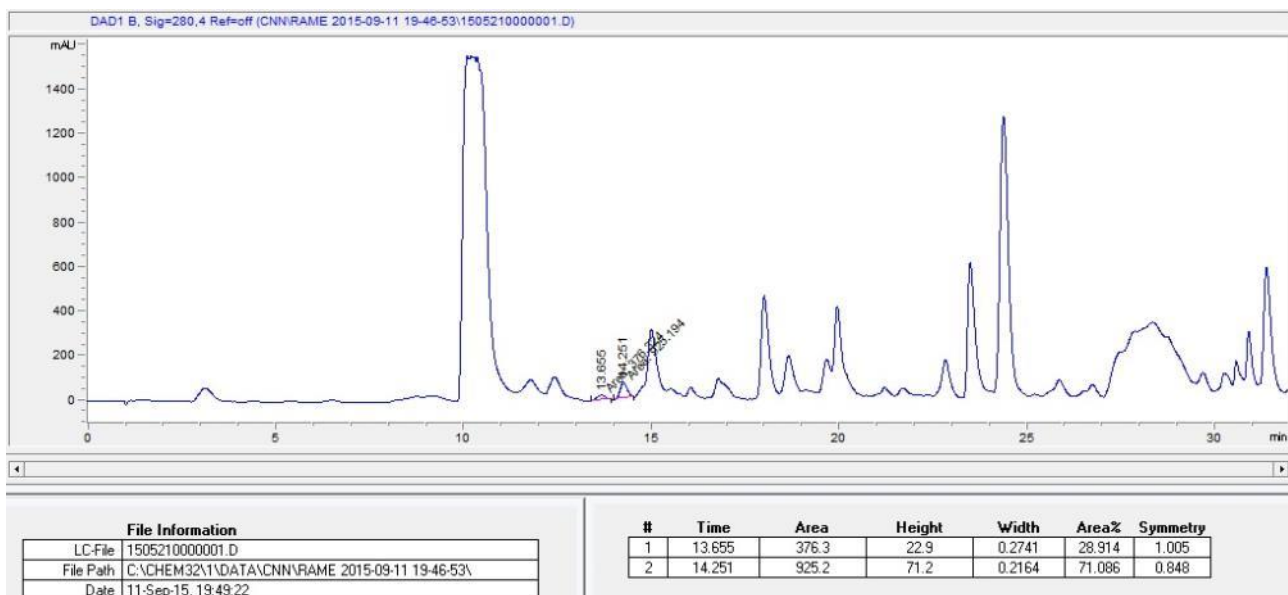
**Figure 74:** Standard curve of the UV absorbance vs amount of the authentic reference material **17**.

The synthesis of 22 mCi  $^{18}\text{F}$ -**17** was performed and the reaction mixture left to decay for 2 hours to reduce radiation exposure to the researcher. The reaction mixture was concentrated and dissolved in 100  $\mu\text{L}$  ethanol and transferred into an HPLC vial. 50  $\mu\text{L}$  (corresponding to 11 mCi decay-corrected product) was analyzed by analytical HPLC.



**Figure 75:** Radiotracer of the sample showing a peak that corresponds to  $^{18}\text{F}$ -**17**.

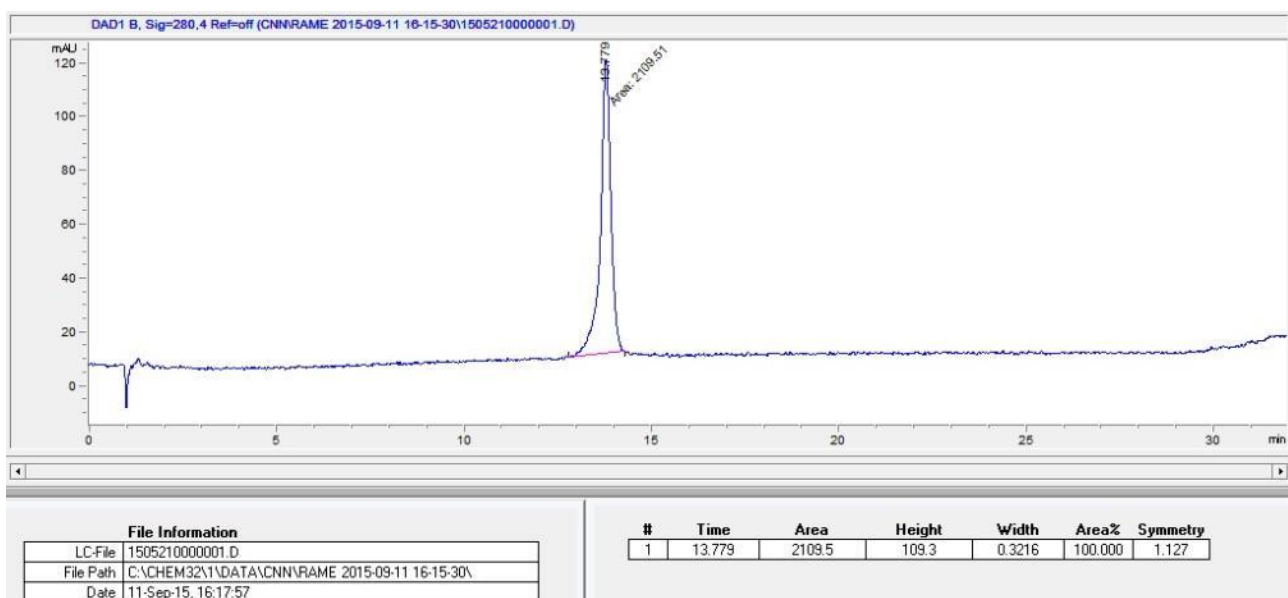




**Figure 76:** UV (280 nm) trace of the sample.

⇒ 376.3 absorbance (280 nm)

By comparison with the standard curve (Figure 77), it was determined that 50  $\mu\text{L}$  of reaction mixture corresponding to 11 mCi activity contained 3.63 nmoles **17**. The specific activity of the sample was  $3.03 \text{ Ci} \times \mu\text{mol}^{-1}$ .



**Figure 77:** Reference material **17** UV (280 nm) trace.

## REFERENCES

- 1 Differding, E. & Lang, R. W. New fluorinating reagents - I. The first enantioselective fluorination reaction. *Tetrahedron Lett.* **29**, 6087-6090, (1988).
- 2 Differding, E. & Lang, R. W. New fluorinating reagents. Part II. Preparation and Synthetic Application of a Saccharin Derived N-Fluorosultam. *Helv. Chim. Acta* **72**, 1248-1252, (1989).
- 3 Differding, E. & Ofner, H. N-Fluorobenzenesulfonimide: A Practical Reagent For Electrophilic Fluorinations. *Synlett* **1991**, 187-189, (1991).
- 4 Barnette, W. E. N-Fluoro-N-alkylsulfonamides: useful reagents for the fluorination of carbanions. *J. Am. Chem. Soc.* **106**, 452-454, (1984).
- 5 Davis, F. A. & Han, W. N-fluoro-o-benzenedisulfonimide: a useful new fluorinating reagent. *Tetrahedron Lett.* **32**, 1631-1634, (1991).
- 6 Davis, F. A., Zhou, P. & Murphy, C. K. Asymmetric fluorination of enolates with N-fluoro 2,10-(3,3-dichlorocamphorsultam). *Tetrahedron Lett.* **34**, 3971-3974, (1993).
- 7 Resnati, G. & DesMarteau, D. D. N-fluorobis[(trifluoromethyl)sulfonyl]imide: an efficient reagent for the alpha-fluorination of functionalized carbonyl compounds. *J. Org. Chem.* **56**, 4925-4929, (1991).
- 8 Banks, R. E. Selectfluor™ reagent F-TEDA-BF<sub>4</sub> in action: tamed fluorine at your service. *J. Fluorine Chem.* **87**, 1-17, (1998).
- 9 Banks, R. E., Besheesh, M. K., Mohialdin-Khaffaf, S. N. & Sharif, I. 1-Alkyl-4-fluoro-1,4-diazoniabicyclo[2.2.2]octane salts: user-friendly site-selective electrophilic fluorinating agents of the N-fluoroammonium class. *J. Chem. Soc., Perkin Trans. 1*, 2069-2076, (1996).
- 10 Banks, R. E., Du Boisson, R. A. & Tsiliopoulos, E. Electrophilic fluorination with N-fluoroquinuclidinium fluoride. *J. Fluorine Chem.* **32**, 461-466, (1986).
- 11 Banks, R. E., Mohialdin-Khaffaf, S. N., Lal, G. S., Sharif, I. & Syvret, R. G. 1-Alkyl-4-fluoro-1,4-diazoniabicyclo[2.2.2]octane salts: a novel family of electrophilic fluorinating agents. *J. Chem. Soc., Chem. Commun.*, 595-596, (1992).
- 12 Banks, R. E. & Sharif, I. N-Fluoroquinuclidinium salts - synthesis and use as electrophilic fluorinating agents. *J. Fluorine Chem.* **55**, 207-214, (1991).
- 13 Tomita, K., Kawada, K. & Umemoto, T. Use and application of new fluorinating agents, N-fluoropyridinium triflate and its derivatives. *J. Fluorine Chem.* **35**, 52, (1987).
- 14 Umemoto, T. *et al.* Power- and structure-variable fluorinating agents. The N-

- fluoropyridinium salt system. *J. Am. Chem. Soc.* **112**, 8563-8575, (1990).
- 15 Umemoto, T., Harasawa, K., Tomizawa, G., Kawada, K. & Tomita, K. Syntheses and Properties of N-Fluoropyridinium Salts. *Bull. Chem. Soc. Jpn.* **64**, 1081-1092, (1991).
- 16 Umemoto, T., Kawada, K. & Tomita, K. N-fluoropyridinium triflate and its derivatives: Useful fluorinating agents. *Tetrahedron Lett.* **27**, 4465-4468, (1986).
- 17 Bi, X. Deoxo-Fluor [Bis(2-methoxyethyl)aminosulfur Trifluoride]: An Advanced Nucleophilic Fluorinating Reagent in Organic Synthesis. *Synlett* **2006**, 2515-2516, (2006).
- 18 S. Lal, G., P. Pez, G., J. Pesaresi, R. & M. Prozonic, F. Bis(2-methoxyethyl)aminosulfur trifluoride: a new broad-spectrum deoxofluorinating agent with enhanced thermal stability. *Chem. Commun.*, 215-216, (1999).
- 19 Messina, P. A., Mange, K. C. & Middleton, W. J. Aminosulfur trifluorides: relative thermal stability. *J. Fluorine Chem.* **42**, 137-143, (1989).
- 20 Mange, K. C. & Middleton, W. J. Fluorination of cyclohexanols with 4-morpholinosulfur trifluoride. *J. Fluorine Chem.* **43**, 405-413, (1989).
- 21 Markovskij, L. N., Pashinnik, V. E. & Kirsanov, A. V. Application of Dialkylaminosulfur Trifluorides in the Synthesis of Fluoroorganic Compounds. *Synthesis* **1973**, 787-789, (1973).
- 22 Sheppard, W. A. Alkyl- and Arylsulfur Trifluorides. *J. Am. Chem. Soc.* **84**, 3058-3063, (1962).
- 23 Kim, D. W. *et al.* A New Class of S<sub>N</sub>2 Reactions Catalyzed by Protic Solvents: Facile Fluorination for Isotopic Labeling of Diagnostic Molecules. *J. Am. Chem. Soc.* **128**, 16394-16397, (2006).
- 24 Bucsi, I. *et al.* Stable Dialkyl Ether/Poly(Hydrogen Fluoride) Complexes: Dimethyl Ether/Poly(Hydrogen Fluoride), A New, Convenient, and Effective Fluorinating Agent. *J. Am. Chem. Soc.* **124**, 7728-7736, (2002).
- 25 Olah, G. A., Li, X.-Y., Wang, Q. & Surya Prakash, G. K. Poly-4-vinylpyridinium Poly(Hydrogen Fluoride): A Solid Hydrogen Fluoride Equivalent Reagent. *Synthesis* **1993**, 693-699, (1993).
- 26 Olah, G. A. *et al.* Pyridinium poly(hydrogen fluoride) (30% pyridine-70% hydrogen fluoride): a convenient reagent for organic fluorination reactions. *J. Org. Chem.* **44**, 3872-3881, (1979).
- 27 York, C., Surya Prakash, G. K. & Olah, G. A. Desulfurative fluorination using nitrosonium tetrafluoroborate and pyridinium poly(hydrogen fluoride). *Tetrahedron* **52**, 9-14, (1996).
- 28 Haufe, G. Triethylamine Trishydrofluoride in Synthesis. *J. Prakt. Chem. /Chem-Ztg*

- 338**, 99-113, (1996).
- 29 Yoshiyama, T. & Fuchigami, T. Anodic gem-Difluorination of Dithioacetals. *Chem. Lett.* **21**, 1995-1998, (1992).
- 30 Fuchigami, T. & Fujita, T. The First Electrosynthesis of Hypervalent Iodobenzene Difluoride Derivatives and Its Application to Indirect Anodic gem-Difluorination. *J. Org. Chem.* **59**, 7190-7192, (1994).
- 31 Sun, H. & DiMugno, S. G. Anhydrous Tetrabutylammonium Fluoride. *J. Am. Chem. Soc.* **127**, 2050-2051, (2005).
- 32 Grushin, V. V. The Organometallic Fluorine Chemistry of Palladium and Rhodium: Studies toward Aromatic Fluorination. *Acc. Chem. Res.* **43**, 160-171, (2010).
- 33 Grushin, V. V. Thermal Stability, Decomposition Paths, and Ph/Ph Exchange Reactions of [(Ph<sub>3</sub>P)<sub>2</sub>Pd(Ph)X] (X = I, Br, Cl, F, and HF<sub>2</sub>). *Organometallics* **19**, 1888-1900, (2000).
- 34 Grushin, V. V. & Marshall, W. J. Ar-F Reductive Elimination from Palladium(II) Revisited. *Organometallics* **26**, 4997-5002, (2007).
- 35 Zhao, S.-B., Becker, J. J. & Gagné, M. R. Steric Crowding Makes Challenging Csp<sup>3</sup>-F Reductive Eliminations Feasible. *Organometallics* **30**, 3926-3929, (2011).
- 36 Zhao, S.-B., Wang, R.-Y., Nguyen, H., Becker, J. J. & Gagne, M. R. Electrophilic fluorination of cationic Pt-aryl complexes. *Chem. Commun.* **48**, 443-445, (2012).
- 37 Cochrane, N. A., Nguyen, H. & Gagne, M. R. Catalytic Enantioselective Cyclization and C3-Fluorination of Polyenes. *J. Am. Chem. Soc.* **135**, 628-631, (2013).
- 38 Yandulov, D. V. & Tran, N. T. Aryl-Fluoride Reductive Elimination from Pd(II): Feasibility Assessment from Theory and Experiment. *J. Am. Chem. Soc.* **129**, 1342-1358, (2007).
- 39 Dubinsky-Davidchik, I. S., Potash, S., Goldberg, I., Vigalok, A. & Vedernikov, A. N. Electrophilic Fluorination of Organoplatinum(II) Iodides: Iodine and Platinum Atoms as Competing Fluorination Sites. *J. Am. Chem. Soc.* **134**, 14027-14032, (2012).
- 40 Kaspi, A. W., Yahav-Levi, A., Goldberg, I. & Vigalok, A. Xenon Difluoride Induced Aryl Iodide Reductive Elimination: a Simple Access to Difluoropalladium(II) Complexes. *Inorg. Chem.* **47**, 5-7, (2008).
- 41 Vigalok, A. Metal-Mediated Formation of Carbon-Halogen Bonds. *Chem. Eur. J.* **14**, 5102-5108, (2008).
- 42 Vigalok, A. Electrophilic Fluorination of Group 10 Organometallic Complexes: Chemistry beyond Oxidative Addition. *Organometallics* **30**, 4802-4810, (2011).
- 43 Furuya, T. *et al.* Mechanism of C-F Reductive Elimination from Palladium(IV) Fluorides. *J. Am. Chem. Soc.* **132**, 3793-3807, (2010).

- 44 Furuya, T. & Ritter, T. Carbon–Fluorine Reductive Elimination from a High-Valent Palladium Fluoride. *J. Am. Chem. Soc.* **130**, 10060-10061, (2008).
- 45 Lee, H. G., Milner, P. J. & Buchwald, S. L. An Improved Catalyst System for the Pd-Catalyzed Fluorination of (Hetero)Aryl Triflates. *Org. Lett.* **15**, 5602-5605, (2013).
- 46 Maimone, T. J. *et al.* Evidence for in Situ Catalyst Modification during the Pd-Catalyzed Conversion of Aryl Triflates to Aryl Fluorides. *J. Am. Chem. Soc.* **133**, 18106-18109, (2011).
- 47 Noël, T., Maimone, T. J. & Buchwald, S. L. Accelerating Palladium-Catalyzed C–F Bond Formation: Use of a Microflow Packed-Bed Reactor. *Angew. Chem. Int. Ed.* **50**, 8900-8903, (2011).
- 48 Watson, D. A. *et al.* Formation of ArF from LPdAr(F): Catalytic Conversion of Aryl Triflates to Aryl Fluorides. *Science* **325**, 1661-1664, (2009).
- 49 Milner, P. J., Kinzel, T., Zhang, Y. & Buchwald, S. L. Studying Regioisomer Formation in the Pd-Catalyzed Fluorination of Aryl Triflates by Deuterium Labeling. *J. Am. Chem. Soc.* **136**, 15757-15766, (2014).
- 50 Hull, K. L., Anani, W. Q. & Sanford, M. S. Palladium-Catalyzed Fluorination of Carbon–Hydrogen Bonds. *J. Am. Chem. Soc.* **128**, 7134-7135, (2006).
- 51 Brown, J. M. & Gouverneur, V. Transition-Metal-Mediated Reactions for Csp<sup>2</sup>–F Bond Construction: The State of Play. *Angew. Chem. Int. Ed.* **48**, 8610-8614, (2009).
- 52 Brown, J. M. & Gouverneur, V. Übergangsmetall-vermittelte Reaktionen zum Aufbau von Csp<sup>2</sup>–F-Bindungen. *Angew. Chem.* **121**, 8762-8766, (2009).
- 53 Campbell, M. G. & Ritter, T. Late-Stage Fluorination: From Fundamentals to Application. *Org. Process Res. Dev.* **18**, 474-480, (2014).
- 54 Cresswell, A. J., Davies, S. G., Roberts, P. M. & Thomson, J. E. Beyond the Balz–Schiemann Reaction: The Utility of Tetrafluoroborates and Boron Trifluoride as Nucleophilic Fluoride Sources. *Chem. Rev.* **115**, 566-611, (2015).
- 55 Furuya, T., Kamlet, A. S. & Ritter, T. Catalysis for fluorination and trifluoromethylation. *Nature* **473**, 470-477, (2011).
- 56 Furuya, T., Klein, J. E. & Ritter, T. C–F Bond Formation for the Synthesis of Aryl Fluorides. *Synthesis* **2010**, 1804-1821, (2010).
- 57 Hagmann, W. K. The Many Roles for Fluorine in Medicinal Chemistry. *J. Med. Chem.* **51**, 4359-4369, (2008).
- 58 Hollingworth, C. & Gouverneur, V. Transition metal catalysis and nucleophilic fluorination. *Chem. Commun.* **48**, 2929-2942, (2012).
- 59 Jiang, X., Liu, H. & Gu, Z. Carbon–Halogen Bond Formation by the Reductive Elimination of PdII Species. *Asian J. Org. Chem.* **1**, 16-24, (2012).

- 60 Kirk, K. L. Fluorination in Medicinal Chemistry: Methods, Strategies, and Recent Developments. *Org. Process Res. Dev.* **12**, 305-321, (2008).
- 61 Liang, T., Neumann, C. N. & Ritter, T. Introduction of Fluorine and Fluorine-Containing Functional Groups. *Angew. Chem. Int. Ed.* **52**, 8214-8264, (2013).
- 62 Liang, T., Neumann, C. N. & Ritter, T. Einführung von Fluor und fluorhaltigen funktionellen Gruppen. *Angew. Chem.* **125**, 8372-8423, (2013).
- 63 Lin, A., Huehls, C. B. & Yang, J. Recent advances in C–H fluorination. *Org. Chem. Front.* **1**, 434-438, (2014).
- 64 Liu, G. Transition metal-catalyzed fluorination of multi carbon-carbon bonds: new strategies for fluorinated heterocycles. *Org. Biomol. Chem.* **10**, 6243-6248, (2012).
- 65 Purser, S., Moore, P. R., Swallow, S. & Gouverneur, V. Fluorine in medicinal chemistry. *Chem. Soc. Rev.* **37**, 320-330, (2008).
- 66 Tang, P., Furuya, T. & Ritter, T. Silver-Catalyzed Late-Stage Fluorination. *J. Am. Chem. Soc.* **132**, 12150-12154, (2010).
- 67 Xu, T. & Liu, G. Silver-Catalyzed Fluorination Reactions. *Synlett* **23**, 955-958, (2012).
- 68 Ichiishi, N. *et al.* Copper-Catalyzed [<sup>18</sup>F]Fluorination of (Mesityl)(aryl)iodonium Salts. *Org. Lett.* **16**, 3224-3227, (2014).
- 69 Akana, J. A., Bhattacharyya, K. X., Müller, P. & Sadighi, J. P. Reversible C–F Bond Formation and the Au-Catalyzed Hydrofluorination of Alkynes. *J. Am. Chem. Soc.* **129**, 7736-7737, (2007).
- 70 Furuya, T., Strom, A. E. & Ritter, T. Silver-Mediated Fluorination of Functionalized Aryl Stannanes. *J. Am. Chem. Soc.* **131**, 1662-1663, (2009).
- 71 Ye, Y. & Sanford, M. S. Mild Copper-Mediated Fluorination of Aryl Stannanes and Aryl Trifluoroborates. *J. Am. Chem. Soc.* **135**, 4648-4651, (2013).
- 72 Furuya, T. & Ritter, T. Fluorination of Boronic Acids Mediated by Silver(I) Triflate. *Org. Lett.* **11**, 2860-2863, (2009).
- 73 Ye, Y., Schimler, S. D., Hanley, P. S. & Sanford, M. S. Cu(OTf)<sub>2</sub>-Mediated Fluorination of Aryltrifluoroborates with Potassium Fluoride. *J. Am. Chem. Soc.* **135**, 16292-16295, (2013).
- 74 Fier, P. S., Luo, J. & Hartwig, J. F. Copper-Mediated Fluorination of Arylboronate Esters. Identification of a Copper(III) Fluoride Complex. *J. Am. Chem. Soc.* **135**, 2552-2559, (2013).
- 75 Mazzotti, A. R., Campbell, M. G., Tang, P., Murphy, J. M. & Ritter, T. Palladium(III)-Catalyzed Fluorination of Arylboronic Acid Derivatives. *J. Am. Chem. Soc.* **135**, 14012-14015, (2013).
- 76 Tang, P., Wang, W. & Ritter, T. Deoxyfluorination of Phenols. *J. Am. Chem. Soc.*

- 133**, 11482-11484, (2011).
- 77 Fujimoto, T., Becker, F. & Ritter, T. PhenoFluor: Practical Synthesis, New Formulation, and Deoxyfluorination of Heteroaromatics. *Org. Process Res. Dev.* **18**, 1041-1044, (2014).
- 78 Fier, P. S. & Hartwig, J. F. Selective C–H Fluorination of Pyridines and Diazines Inspired by a Classic Amination Reaction. *Science* **342**, 956-960, (2013).
- 79 Stavber, S., Jereb, M. & Zupan, M. Direct  $\alpha$ -Fluorination of Ketones Using N–F Reagents. *Synthesis* **2002**, 2609-2615, (2002).
- 80 Marigo, M., Fielenbach, D., Braunton, A., Kjærsgaard, A. & Jørgensen, K. A. Enantioselective Formation of Stereogenic Carbon–Fluorine Centers by a Simple Catalytic Method. *Angew. Chem. Int. Ed.* **44**, 3703-3706, (2005).
- 81 Steiner, D. D., Mase, N. & Barbas, C. F. Direct Asymmetric  $\alpha$ -Fluorination of Aldehydes. *Angew. Chem. Int. Ed.* **44**, 3706-3710, (2005).
- 82 Beeson, T. D. & MacMillan, D. W. C. Enantioselective Organocatalytic  $\alpha$ -Fluorination of Aldehydes. *J. Am. Chem. Soc.* **127**, 8826-8828, (2005).
- 83 Paull, D. H., Scerba, M. T., Alden-Danforth, E., Widger, L. R. & Lectka, T. Catalytic, Asymmetric  $\alpha$ -Fluorination of Acid Chlorides: Dual Metal–Ketene Enolate Activation. *J. Am. Chem. Soc.* **130**, 17260-17261, (2008).
- 84 Stavber, G., Zupan, M. & Stavber, S. Micellar-System-Mediated Direct Fluorination of Ketones in Water. *Synlett* **2009**, 589-594, (2009).
- 85 Kalow, J. A., Schmitt, D. E. & Doyle, A. G. Synthesis of  $\beta$ -Fluoroamines by Lewis Base Catalyzed Hydrofluorination of Aziridines. *J. Org. Chem.* **77**, 4177-4183, (2012).
- 86 Katcher, M. H. & Doyle, A. G. Palladium-Catalyzed Asymmetric Synthesis of Allylic Fluorides. *J. Am. Chem. Soc.* **132**, 17402-17404, (2010).
- 87 Katcher, M. H., Norrby, P.-O. & Doyle, A. G. Mechanistic Investigations of Palladium-Catalyzed Allylic Fluorination. *Organometallics* **33**, 2121-2133, (2014).
- 88 Braun, M.-G. & Doyle, A. G. Palladium-Catalyzed Allylic C–H Fluorination. *J. Am. Chem. Soc.* **135**, 12990-12993, (2013).
- 89 Hollingworth, C. *et al.* Palladium-Catalyzed Allylic Fluorination. *Angew. Chem. Int. Ed.* **50**, 2613-2617, (2011).
- 90 Topczewski, J. J., Tewson, T. J. & Nguyen, H. M. Iridium-Catalyzed Allylic Fluorination of Trichloroacetimidates. *J. Am. Chem. Soc.* **133**, 19318-19321, (2011).
- 91 Yin, F., Wang, Z., Li, Z. & Li, C. Silver-Catalyzed Decarboxylative Fluorination of Aliphatic Carboxylic Acids in Aqueous Solution. *J. Am. Chem. Soc.* **134**, 10401-10404, (2012).

- 92 Barker, T. J. & Boger, D. L. Fe(III)/NaBH<sub>4</sub>-Mediated Free Radical Hydrofluorination of Unactivated Alkenes. *J. Am. Chem. Soc.* **134**, 13588-13591, (2012).
- 93 Shigehisa, H., Nishi, E., Fujisawa, M. & Hiroya, K. Cobalt-Catalyzed Hydrofluorination of Unactivated Olefins: A Radical Approach of Fluorine Transfer. *Org. Lett.* **15**, 5158-5161, (2013).
- 94 Emer, E., Pfeifer, L., Brown, J. M. & Gouverneur, V. cis-Specific Hydrofluorination of Alkenylarenes under Palladium Catalysis through an Ionic Pathway. *Angew. Chem. Int. Ed.* **53**, 4181-4185, (2014).
- 95 Sladojevich, F., Arlow, S. I., Tang, P. & Ritter, T. Late-Stage Deoxyfluorination of Alcohols with PhenoFluor. *J. Am. Chem. Soc.* **135**, 2470-2473, (2013).
- 96 Bloom, S. *et al.* A Polycomponent Metal-Catalyzed Aliphatic, Allylic, and Benzylic Fluorination. *Angew. Chem. Int. Ed.* **51**, 10580-10583, (2012).
- 97 Liu, W., Huang, X. & Groves, J. T. Oxidative aliphatic C–H fluorination with manganese catalysts and fluoride ion. *Nat. Protocols* **8**, 2348-2354, (2013).
- 98 Benedetto, E. *et al.* Regio- and stereoretentive synthesis of branched, linear (E)- and (Z)-allyl fluorides from allyl carbonates under Ir-catalysis. *Chem. Sci.* **4**, 89-96, (2013).
- 99 Grushin, V. V. Palladium Fluoride Complexes: One More Step toward Metal-Mediated C–F Bond Formation. *Chem. Eur. J.* **8**, 1006-1014, (2002).
- 100 Grushin, V. V. & Marshall, W. J. Fluorination of Nonactivated Haloarenes via Arynes under Mild Conditions, Resulting from Further Studies toward Ar–F Reductive Elimination from Palladium(II). *Organometallics* **27**, 4825-4828, (2008).
- 101 Fagnou, K. & Lautens, M. Halide Effects in Transition Metal Catalysis. *Angew. Chem. Int. Ed.* **41**, 26-47, (2002).
- 102 Fagnou, K. & Lautens, M. Der Einfluss von Halogenidionen in der Übergangsmetallkatalyse. *Angew. Chem.* **114**, 26-49, (2002).
- 103 Fier, P. S. & Hartwig, J. F. Synthesis and Late-Stage Functionalization of Complex Molecules through C–H Fluorination and Nucleophilic Aromatic Substitution. *J. Am. Chem. Soc.* **136**, 10139-10147, (2014).
- 104 Emsley, J. Very strong hydrogen bonding. *Chem. Soc. Rev.* **9**, 91-124, (1980).
- 105 Chen, X. & Brauman, J. I. Hydrogen Bonding Lowers Intrinsic Nucleophilicity of Solvated Nucleophiles. *J. Am. Chem. Soc.* **130**, 15038-15046, (2008).
- 106 Liotta, C. L. & Harris, H. P. Chemistry of naked anions. I. Reactions of the 18-crown-6 complex of potassium fluoride with organic substrates in aprotic organic solvents. *J. Am. Chem. Soc.* **96**, 2250-2252, (1974).
- 107 Clark, J. H. Fluoride ion as a base in organic synthesis. *Chem. Rev.* **80**, 429-452,



- (1980).
- 108 Mezzetti, A. & Becker, C. Swimming against the Stream? A Discussion of the Bonding in d6 and d8 Fluoro Complexes and Its Consequences for Catalytic Applications. *Helv. Chim. Acta* **85**, 2686-2703, (2002).
- 109 Dong, J., Krasnova, L., Finn, M. G. & Sharpless, K. B. Sulfur(VI) Fluoride Exchange (SuFEx): Another Good Reaction for Click Chemistry. *Angew. Chem. Int. Ed.* **53**, 9430-9448, (2014).
- 110 Dong, J., Krasnova, L., Finn, M. G. & Sharpless, K. B. Schwefel(VI)-fluorid-Austausch (SuFEx): Eine weitere gute Anwendung für die Click-Chemie. *Angew. Chem.* **126**, 9584-9603, (2014).
- 111 Kim, D. W., Jeong, H.-J., Lim, S. T. & Sohn, M.-H. Tetrabutylammonium Tetra(tert-Butyl Alcohol)-Coordinated Fluoride as a Facile Fluoride Source. *Angew. Chem. Int. Ed.* **47**, 8404-8406, (2008).
- 112 Ralf, S., Carmen, W. & Esther, S. Recent Developments and Trends in <sup>18</sup>F-Radiochemistry: Syntheses and Applications. *Mini-Reviews in Organic Chemistry* **4**, 317-329, (2007).
- 113 Shinde, S. S., Lee, B. S. & Chi, D. Y. Synergistic Effect of Two Solvents, tert-Alcohol and Ionic Liquid, in One Molecule in Nucleophilic Fluorination. *Org. Lett.* **10**, 733-735, (2008).
- 114 Kim, D. W., Song, C. E. & Chi, D. Y. New Method of Fluorination Using Potassium Fluoride in Ionic Liquid: Significantly Enhanced Reactivity of Fluoride and Improved Selectivity. *J. Am. Chem. Soc.* **124**, 10278-10279, (2002).
- 115 Hintermann, L., Läng, F., Maire, P. & Togni, A. Interactions of Cationic Palladium(II)- and Platinum(II)- $\eta^3$ -Allyl Complexes with Fluoride: Is Asymmetric Allylic Fluorination a Viable Reaction? *Eur. J. Inorg. Chem.* **2006**, 1397-1412, (2006).
- 116 Milner, P. J. *et al.* Investigating the Dearomative Rearrangement of Biaryl Phosphine-Ligated Pd(II) Complexes. *J. Am. Chem. Soc.* **134**, 19922-19934, (2012).
- 117 Sather, A. C. *et al.* A Fluorinated Ligand Enables Room-Temperature and Regioselective Pd-Catalyzed Fluorination of Aryl Triflates and Bromides. *J. Am. Chem. Soc.* **137**, 13433-13438, (2015).
- 118 Eustáquio, A. S., O'Hagan, D. & Moore, B. S. Engineering Fluorometabolite Production: Fluorinase Expression in *Salinispora tropica* Yields Fluorosalinisporamide. *J. Nat. Prod.* **73**, 378-382, (2010).
- 119 Dong, C. *et al.* Crystal structure and mechanism of a bacterial fluorinating enzyme. *Nature* **427**, 561-565, (2004).
- 120 Li, X.-G., Domarkas, J. & O'Hagan, D. Fluorinase mediated chemoenzymatic

- synthesis of [<sup>18</sup>F]-fluoroacetate. *Chem. Commun.* **46**, 7819-7821, (2010).
- 121 Walker, M. C. *et al.* Expanding the Fluorine Chemistry of Living Systems Using Engineered Polyketide Synthase Pathways. *Science* **341**, 1089-1094, (2013).
- 122 Ma, J.-A. & Cahard, D. Update 1 of: Asymmetric Fluorination, Trifluoromethylation, and Perfluoroalkylation Reactions. *Chem. Rev.* **108**, PR1-PR43, (2008).
- 123 Lin, J.-H. & Xiao, J.-C. Recent advances in asymmetric fluorination and fluoroalkylation reactions via organocatalysis. *Tetrahedron Lett.* **55**, 6147-6155, (2014).
- 124 Valero, G., Companyó, X. & Rios, R. Enantioselective Organocatalytic Synthesis of Fluorinated Molecules. *Chem. Eur. J.* **17**, 2018-2037, (2011).
- 125 Hennecke, U. A New Approach towards the Asymmetric Fluorination of Alkenes Using Anionic Phase-Transfer Catalysts. *Angew. Chem. Int. Ed.* **51**, 4532-4534, (2012).
- 126 Hennecke, U. Eine neue Strategie für asymmetrische Fluorierungen von Alkenen auf Basis anionischer Phasentransferkatalysatoren. *Angew. Chem.* **124**, 4608-4610, (2012).
- 127 Struble, M. D., Scerba, M. T., Siegler, M. & Lectka, T. Evidence for a Symmetrical Fluoronium Ion in Solution. *Science* **340**, 57-60, (2013).
- 128 Ishimaru, T. *et al.* Cinchona Alkaloid Catalyzed Enantioselective Fluorination of Allyl Silanes, Silyl Enol Ethers, and Oxindoles. *Angew. Chem. Int. Ed.* **47**, 4157-4161, (2008).
- 129 Lozano, O. *et al.* Organocatalyzed Enantioselective Fluorocyclizations. *Angew. Chem. Int. Ed.* **50**, 8105-8109, (2011).
- 130 Hintermann, L. & Togni, A. Catalytic Enantioselective Fluorination of  $\beta$ -Ketoesters. *Angew. Chem. Int. Ed.* **39**, 4359-4362, (2000).
- 131 Hintermann, L. & Togni, A. Katalytische enantioselektive Fluorierung von  $\beta$ -Ketoestern. *Angew. Chem.* **112**, 4530-4533, (2000).
- 132 Honjo, T., Phipps, R. J., Rauniyar, V. & Toste, F. D. A Doubly Axially Chiral Phosphoric Acid Catalyst for the Asymmetric Tandem Oxyfluorination of Enamides. *Angew. Chem. Int. Ed.* **51**, 9684-9688, (2012).
- 133 Phipps, R. J., Hiramatsu, K. & Toste, F. D. Asymmetric Fluorination of Enamides: Access to  $\alpha$ -Fluoroimines Using an Anionic Chiral Phase-Transfer Catalyst. *J. Am. Chem. Soc.* **134**, 8376-8379, (2012).
- 134 Phipps, R. J. & Toste, F. D. Chiral Anion Phase-Transfer Catalysis Applied to the Direct Enantioselective Fluorinative Dearomatization of Phenols. *J. Am. Chem. Soc.* **135**, 1268-1271, (2013).

- 135 Rauniyar, V., Lackner, A. D., Hamilton, G. L. & Toste, F. D. Asymmetric Electrophilic Fluorination Using an Anionic Chiral Phase-Transfer Catalyst. *Science* **334**, 1681-1684, (2011).
- 136 Wu, J. *et al.* A combination of directing groups and chiral anion phase-transfer catalysis for enantioselective fluorination of alkenes. *Proc. Natl. Acad. Sci. USA* **110**, 13729-13733, (2013).
- 137 Zi, W., Wang, Y.-M. & Toste, F. D. An In Situ Directing Group Strategy for Chiral Anion Phase-Transfer Fluorination of Allylic Alcohols. *J. Am. Chem. Soc.* **136**, 12864-12867, (2014).
- 138 Bergman, J. & Solin, O. Fluorine-18-labeled fluorine gas for synthesis of tracer molecules. *Nucl. Med. Biol.* **24**, 677-683.
- 139 Cai, L., Lu, S. & Pike, V. W. Chemistry with [<sup>18</sup>F]Fluoride Ion. *Eur. J. Org. Chem.* **2008**, 2853-2873, (2008).
- 140 Hummer, G., Pratt, L. R. & García, A. E. Free Energy of Ionic Hydration. *J. Phys. Chem.* **100**, 1206-1215, (1996).
- 141 Cabarcos, O. M., Weinheimer, C. J., Lisy, J. M. & Xantheas, S. S. Microscopic hydration of the fluoride anion. *J. Chem. Phys.* **110**, 5-8, (1999).
- 142 Ametamey, S. M., Honer, M. & Schubiger, P. A. Molecular imaging with PET. *Chem. Rev.* **108**, 1501-1516, (2008).
- 143 Teare, H. *et al.* Radiosynthesis and Evaluation of [<sup>18</sup>F]Selectfluor bis(triflate). *Angew. Chem. Int. Ed.* **49**, 6821-6824, (2010).
- 144 Lee, H. G., Milner, P. J. & Buchwald, S. L. Pd-Catalyzed Nucleophilic Fluorination of Aryl Bromides. *J. Am. Chem. Soc.* **136**, 3792-3795, (2014).
- 145 Cardinale, J. *et al.* Carrier-effect on palladium-catalyzed, nucleophilic <sup>18</sup>F-fluorination of aryl triflates. *J. Labelled Compd. Radiopharm.* **55**, 450-453, (2012).
- 146 Pike, V. W. & Aigbirhio, F. I. Reactions of cyclotron-produced [<sup>18</sup>F]fluoride with diaryliodonium salts-a novel single-step route to no-carrier-added [<sup>18</sup>F]fluoroarenes. *J. Chem. Soc., Chem. Commun.*, 2215-2216, (1995).
- 147 Ross, T. L., Ermert, J., Hocke, C. & Coenen, H. H. Nucleophilic <sup>18</sup>F-Fluorination of Heteroaromatic Iodonium Salts with No-Carrier-Added [<sup>18</sup>F]Fluoride. *J. Am. Chem. Soc.* **129**, 8018-8025, (2007).
- 148 Tredwell, M. *et al.* A General Copper-Mediated Nucleophilic <sup>18</sup>F Fluorination of Arenes. *Angew. Chem. Int. Ed.* **53**, 7751-7755, (2014).
- 149 Gao, Z. *et al.* Metal-Free Oxidative Fluorination of Phenols with [<sup>18</sup>F]Fluoride. *Angew. Chem. Int. Ed.* **51**, 6733-6737, (2012).
- 150 Lee, E. *et al.* A Fluoride-Derived Electrophilic Late-Stage Fluorination Reagent for

- PET Imaging. *Science* **334**, 639-642, (2011).
- 151 Furuya, T., Kaiser, H. M. & Ritter, T. Palladium-Mediated Fluorination of Arylboronic Acids. *Angew. Chem. Int. Ed.* **47**, 5993-5996, (2008).
- 152 Kamlet, A. S. *et al.* Application of Palladium-Mediated <sup>18</sup>F-Fluorination to PET Radiotracer Development: Overcoming Hurdles to Translation. *PLoS ONE* **8**, e59187, (2013).
- 153 *European Medicines Agency*,  
<[www.ema.europa.eu/docs/en\\_GB/document\\_library/Scientific\\_guideline/2009/09/WC500003587.pdf](http://www.ema.europa.eu/docs/en_GB/document_library/Scientific_guideline/2009/09/WC500003587.pdf)>
- 154 Lee, E., Hooker, J. M. & Ritter, T. Nickel-Mediated Oxidative Fluorination for PET with Aqueous [<sup>18</sup>F] Fluoride. *J. Am. Chem. Soc.* **134**, 17456-17458, (2012).
- 155 Stenhagen, I. S. R. *et al.* [<sup>18</sup>F]Fluorination of an arylboronic ester using [<sup>18</sup>F]selectfluor bis(triflate): application to 6-[<sup>18</sup>F]fluoro-I-DOPA. *Chem. Commun.* **49**, 1386-1388, (2013).
- 156 Tredwell, M. & Gouverneur, V. <sup>18</sup>F Labeling of Arenes. *Angew. Chem. Int. Ed.* **51**, 11426-11437, (2012).
- 157 Tredwell, M. & Gouverneur, V. <sup>18</sup>F-Markierung von Arenen. *Angew. Chem.* **124**, 11590-11602, (2012).
- 158 Fernández, I., Frenking, G. & Uggerud, E. Rate-Determining Factors in Nucleophilic Aromatic Substitution Reactions. *J. Org. Chem.* **75**, 2971-2980, (2010).
- 159 Terrier, F. *Modern nucleophilic aromatic substitution*. (Wiley-VCH, 2013).
- 160 Cheron, N., El Kaim, L., Grimaud, L. & Fleurat-Lessard, P. Evidences for the key role of hydrogen bonds in nucleophilic aromatic substitution reactions. *Chem. Eur. J.* **17**, 14929-14934, (2011).
- 161 Picazo, E., Houk, K. N. & Garg, N. K. Computational predictions of substituted benzyne and indolyne regioselectivities. *Tetrahedron Lett.* **56**, 3511-3514, (2015).
- 162 Crampton, M. R. in *Organic Reaction Mechanisms · 2010* 175-190 (John Wiley & Sons, Ltd, 2012).
- 163 Lloyd-Jones, G. C., Moseley, J. D. & Renny, J. S. Mechanism and Application of the Newman-Kwart O→S Rearrangement of O-Aryl Thiocarbamates. *Synthesis* **2008**, 661-689, (2008).
- 164 Glukhovtsev, M. N., Bach, R. D. & Laiter, S. Single-Step and Multistep Mechanisms of Aromatic Nucleophilic Substitution of Halobenzenes and Halonitrobenzenes with Halide Anions: Ab Initio Computational Study. *J. Org. Chem.* **62**, 4036-4046, (1997).
- 165 Fry, S. E. & Pienta, N. J. Effects of molten salts on reactions. Nucleophilic aromatic substitution by halide ions in molten dodecyltributylphosphonium salts. *J. Am. Chem.*

- Soc. **107**, 6399-6400, (1985).
- 166 Hunter, A. *et al.* Stepwise versus Concerted Mechanisms at Trigonal Carbon: Transfer of the 1,3,5-Triazinyl Group between Aryl Oxide Ions in Aqueous Solution. *J. Am. Chem. Soc.* **117**, 5484-5491, (1995).
- 167 Renfrew, A. H. M., Taylor, J. A., Whitmore, J. M. J. & Williams, A. A single transition state in nucleophilic aromatic substitution: reaction of phenolate ions with 2-(4-nitrophenoxy)-4,6-dimethoxy-1,3,5-triazine in aqueous solution. *J. Chem. Soc. Perk. Trans. 2*, 1703-1704, (1993).
- 168 Renfrew, A. H. M., Taylor, J. A., Whitmore, J. M. J. & Williams, A. Nucleophilic aromatic substitution in heterocycles: alcoholysis and hydrolysis of 2-anilino-4,6-dichloro-1,3,5-triazines. *J. Chem. Soc. Perk. Trans. 2*, 2389-2393, (1994).
- 169 Renfrew, A. H. M., Taylor, J. A., Whitmore, J. M. J. & Williams, A. Timing of bonding changes in fundamental reactions in solutions: pyridinolysis of a triazinylpyridinium salt. *J. Chem. Soc. Perk. Trans. 2*, 2383-2384, (1994).
- 170 Dub, P. A. *et al.* C–F Bond Breaking through Aromatic Nucleophilic Substitution with a Hydroxo Ligand Mediated via Water Bifunctional Activation. *Bull. Chem. Soc. Jpn.* **86**, 557-568, (2013).
- 171 Goryunov, L. I. *et al.* Di- and Trifluorobenzenes in Reactions with Me<sub>2</sub>EM (E = P, N; M = SiMe<sub>3</sub>, SnMe<sub>3</sub>, Li) Reagents: Evidence for a Concerted Mechanism of Aromatic Nucleophilic Substitution. *Eur. J. Org. Chem.* **2010**, 1111-1123, (2010).
- 172 Nawaz, F. *et al.* Temporary Intramolecular Generation of Pyridine Carbenes in Metal-Free Three-Component C–H Bond Functionalisation/Aryl-Transfer Reactions. *Chem. Eur. J.* **19**, 17578-17583, (2013).
- 173 Sawyer, C. B. & Kirsch, J. F. Kinetic isotope effects for reactions of methyl formate-methoxyl-18O. *J. Am. Chem. Soc.* **95**, 7375-7381, (1973).
- 174 Lasne, M.-C. *et al.* in *Contrast Agents II* Vol. 222 *Topics in Current Chemistry* (ed Werner Krause) Ch. 7, 201-258 (Springer Berlin Heidelberg, 2002).
- 175 Matsson, O. & MacMillan, S. Isotope effects for fluorine-18 and carbon-11 in the study of reaction mechanisms. *J. Labelled Compd. Radiopharm.* **50**, 982-988, (2007).
- 176 Yamabe, S., Minato, T. & Kawabata, Y. The importance of the  $\sigma^*-\pi^*$  orbital mixing for the nucleophilic displacement on the unsaturated carbon. *Can. J. Chem.* **62**, 235-240, (1984).
- 177 Bronner, S. M., Goetz, A. E. & Garg, N. K. Overturning Indolyne Regioselectivities and Synthesis of Indolactam V. *J. Am. Chem. Soc.* **133**, 3832-3835, (2011).
- 178 Mu, L. *et al.* <sup>18</sup>F-Radiolabeling of Aromatic Compounds Using Triarylsulfonium Salts.

- Eur. J. Org. Chem.* **2012**, 889-892, (2012).
- 179 Neumann, C. N. & Ritter, T. Late-Stage Fluorination: Fancy Novelty or Useful Tool? *Angew. Chem. Int. Ed.* **54**, 3216-3221, (2015).
- 180 Hammett, L. P. The Effect of Structure upon the Reactions of Organic Compounds. Benzene Derivatives. *J. Am. Chem. Soc.* **59**, 96-103, (1937).
- 181 Hansch, C., Leo, A. & Taft, R. W. A survey of Hammett substituent constants and resonance and field parameters. *Chem. Rev.* **91**, 165-195, (1991).
- 182 Krygowski, T. M. & Stępień, B. T. Sigma- and Pi-Electron Delocalization: Focus on Substituent Effects. *Chem. Rev.* **105**, 3482-3512, (2005).
- 183 Chodera, J. D. & Mobley, D. L. Entropy-Enthalpy Compensation: Role and Ramifications in Biomolecular Ligand Recognition and Design. *Annu. Rev. Biophys. Biomol. Struct.* **42**, 121-142, (2013).
- 184 Liu, L. & Guo, Q.-X. Isokinetic Relationship, Isoequilibrium Relationship, and Enthalpy-Entropy Compensation. *Chem. Rev.* **101**, 673-696, (2001).
- 185 Leffler, J. E. THE ENTHALPY-ENTROPY RELATIONSHIP AND ITS IMPLICATIONS FOR ORGANIC CHEMISTRY. *J. Org. Chem.* **20**, 1202-1231, (1955).
- 186 Peng, C. & Bernhard Schlegel, H. Combining Synchronous Transit and Quasi-Newton Methods to Find Transition States. *Isr. J. Chem.* **33**, 449-454, (1993).
- 187 Peng, C., Ayala, P. Y., Schlegel, H. B. & Frisch, M. J. Using redundant internal coordinates to optimize equilibrium geometries and transition states. *J. Comput. Chem.* **17**, 49-56, (1996).
- 188 Foresman, J. B., Frisch, A. E. & Gaussian, I. *Exploring chemistry with electronic structure methods.* (Gaussian, Inc., 1996).
- 189 Cyrański, M. K. Energetic Aspects of Cyclic Pi-Electron Delocalization: Evaluation of the Methods of Estimating Aromatic Stabilization Energies. *Chem. Rev.* **105**, 3773-3811, (2005).